

**THE EFFECT OF TEMPERATURE-DEPENDENT PROPERTIES
ON THE HIGH TEMPERATURE SLIDING WEAR BEHAVIOUR
OF DETONATION SPRAYED Ni-BASED COATINGS**

Thesis

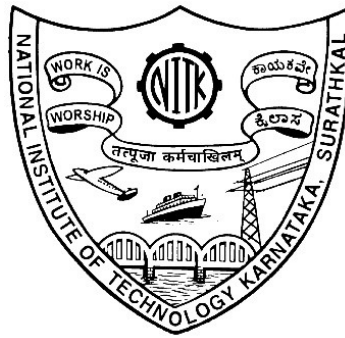
Submitted in partial fulfillment of the requirements for the degree of

DOCTOR OF PHILOSOPHY

by

N. PURUSHOTHAM

(197058MT005)



**DEPARTMENT OF METALLURGICAL AND MATERIALS
ENGINEERING**

**NATIONAL INSTITUTE OF TECHNOLOGY KARNATAKA
SURATHKAL, MANGALURU – 575025**

October, 2023

**THE EFFECT OF TEMPERATURE-DEPENDENT PROPERTIES
ON THE HIGH TEMPERATURE SLIDING WEAR BEHAVIOUR
OF DETONATION SPRAYED Ni-BASED COATINGS**

Thesis

Submitted in partial fulfillment of the requirements for the degree of

DOCTOR OF PHILOSOPHY

by

N. PURUSHOTHAM

(197058MT005)

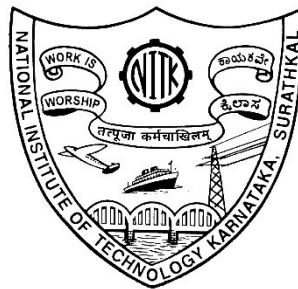
Under the guidance of

Dr. B. RAJASEKARAN

Associate Professor

Dept. of Metallurgical and Materials Engineering

NITK Surathkal



**DEPARTMENT OF METALLURGICAL AND MATERIALS
ENGINEERING**

**NATIONAL INSTITUTE OF TECHNOLOGY KARNATAKA
SURATHKAL, MANGALURU – 575025**

October, 2023

DECLARATION

By the Ph.D. Research Scholar

I hereby declare that the Research Synopsis entitled "THE EFFECT OF TEMPERATURE-DEPENDENT PROPERTIES ON THE HIGH TEMPERATURE SLIDING WEAR BEHAVIOUR OF DETONATION SPRAYED Ni-BASED COATINGS" which is being submitted to the National Institute of Technology Karnataka, Surathkal in partial fulfilment of the requirements for the award of the degree of **Doctor of Philosophy in Metallurgical and Materials Engineering** is a *bonafide report of the research work carried out by me*. The material contained in this Research Synopsis has not been submitted to any University or Institution for the award of any degree.



N. PURUSHOTHAM

Register Number: **197058MT005**

Department of Metallurgical and Materials
Engineering

Place: NITK, Surathkal

Date: 17/10/2023

CERTIFICATE

This is to *certify* that the Research Synopsis entitled " **THE EFFECT OF TEMPERATURE-DEPENDENT PROPERTIES ON THE HIGH TEMPERATURE SLIDING WEAR BEHAVIOUR OF DETONATION SPRAYED Ni-BASED COATINGS**", submitted by **N. PURUSHOTHAM** (Register Number: **197058MT005**) as the record of the research work carried out by him, is *accepted as the Research Synopsis submission* in partial fulfilment of the requirements for the award of the degree of **Doctor of Philosophy**.



Research Guide

Dr. B. Rajasekaran

Associate Professor

Department of Metallurgical and Materials Engineering



Chairman-DRPC

Department of Metallurgical and Materials Engineering

National Institute of Technology Karnataka

Surathkal, Mangalore – 575025

Chairman - DRPC
Dept. of Metallurgical and Materials Engineering
National Institute of Technology Karnataka, Surathkal
Post Srinivasnagar, Mangalore - 575 025
Karnataka, India

ACKNOWLEDGEMENT

Four years of my Ph.D. journey were filled with lots of challenges and learning moments. The experience that I am carrying out is incredible and life-changing. It has given me a new dimension in life and changed how I approach a problem. This journey could not have been completed without the support and encouragement of a few people. I would like to acknowledge you individually for all that you have done for me.

I sincerely thank my Research Guide, **Dr. B. Rajasekaran**, for accepting me into the Ph.D. program and keeping constant faith in me. He is always supportive and remarkably perceptive in advising in the right direction and correcting vital details. Without his continuous encouragement, I would still be in my Ph.D. dreams. He is a great mentor, and I learned so much from him through his long academic journey. I could not have finished my thesis in time without his untiring help in making every sentence concise and correct. I am truly blessed to have come to the National Institute of Technology Karnataka, where **Dr. B. Rajasekaran** welcomed me with open arms, and my life started on a whole new course.

I want to thank **Dr. Preetham Kumar G V** (Associate. Prof., Dept. of Metallurgical and Materials Engineering) and **Dr. Parthasarathy P** (Asst. Prof., Dept. Mechanical Engineering) for being my Research Progress Assessment Committee (RPAC) members. Very few research scholars are fortunate to get RPAC members to work in a similar research area, and I was one of those. They never gave any excuses, even in their busy schedule to share knowledge and attend my seminars. Their comment, observation, understanding, and discussion encouraged me to think beyond boundaries.

With a deep sense of regard, I wish to thank **Dr. Ravishankar K. S**, Head of the Department of Metallurgical and Materials Engineering, for the best support for successfully completing this research work.

I humbly acknowledge **Dr. G. Sivakumar** and **the Director** of the International Advanced Research Centre for Powder Metallurgy and New Materials (ARCI) for facilitating the atmospheric plasma and detonation spray coatings.

I extend my sincere thanks to **Dr. N.L. Parthasarathi**, High-temperature Materials Technology Section, Indira Gandhi Centre for Atomic Research (IGCAR) Kalpakkam, for his constrictive suggestions in improvising my research work.

I would like to thank all my colleagues, teaching and non-teaching staff of the Metallurgical and Materials Engineering department for their constant support and cooperation.

I would like to express my gratitude to my mother (**N. Alivelamma**) and father (**N. Sanjanna**) for the support they have given this long. I also thank my sister (**N. Roja**) and friends for their wishes and encouragement. I sincerely thank all my teachers who taught me for so long.

Above all, I would like to thank you for completing this thesis.

(N PURUSHOTHAM)

Place: NITK, Surathkal

Date: 17/10/2023

ABSTRACT

Overlay Ni-based thermal spray coatings are commonly used in high-temperature sectors (up to 1000 °C) to enhance component durability for various applications. The Ni-based overlay coatings, such as Ni-5%Al and Ni-20% Cr, were deposited on the IN718 substrate using detonation spray coating (DSC) with a thickness of about 250 ± 25 μm . The temperature-dependent material properties such as thermal expansion, recrystallization, and stress relieving of the coatings on the high-temperature wear resistance coating have been studied. In-situ high-temperature X-ray diffraction (HT-XRD) was used to investigate high-temperature properties such as stress relieving, recrystallization, and thermal expansion (CTEs). The dry sliding friction and wear test was performed by using a ball-on-disc tribometer by sliding velocities (0.1 m/s), varying loads (6N and 10N), and temperatures (25 °C and 850 °C) against alumina (Al_2O_3) counterpart. The Rietveld refinement method was used to calculate phase quantification, crystal orientation, and peak fitting employing pseudo voigt analytical functions with the Panalytical X'pert high plus software. The crystallite size (D) and lattice strain (ϵ) were determined by the Scherrer equation and Williamson-Hall (W-H) analysis using a uniform deformation model (UDM), employing X-ray peak profile analysis (XPPA). Field emission scanning electron microscopy (FE-SEM) with Energy-dispersive X-ray spectroscopy (EDS) was used to analyze surface morphology, cross-section, and wear maps and identify wear mechanisms and elemental composition at different conditions. A confocal optical microscope 3D profilometer was used to measure the surface roughness, depth, and width of the wear scar and further to calculate the wear volume and wear rate. Raman spectroscopy was also employed to determine the chemical phase compositional alterations by analyzing the worn surfaces of the coatings at elevated temperatures. Glow Discharge Optical Emission Spectrometry (GD-OES) was used to measure the quantitative depth profiles with different chemical compositions and the thickness of reaction zones.

The wear test results demonstrated that the as-deposited Ni-based coatings coefficient of friction (CoF) and wear rate (ω) continuously decreased as the temperature increased. The primary wear mechanism changed from abrasive (micro-

ploughing) and surface fatigue (delamination) to adhesive (material transfer) and oxidative wear (Tribo-oxidation). The impact of stress relieving, recrystallization, and forming a composite tribo-layer (Cr_2O_3 , NiO) at elevated temperatures reduced the friction and enhanced the wear resistance. In high-temperature conditions, the thermal expansion mismatch between the coating and substrate is negligible, with reduced spallation and cracking at the interface. The effect of stress relieving, recrystallization, thermal expansion, and oxidation on the wear resistance of the coating has been discussed with suitable wear mechanisms for improving the tribological properties at high temperatures.

TABLE OF CONTENTS

ABSTRACT	i
ABBREVIATION	xvii
NOMENCLATURE	xix
CHAPTER 1	1
INTRODUCTION	1
1.1 Turbine materials	3
1.2 Superalloys	4
1.2.1 Inconel718.....	5
1.3 Different coating techniques	5
1.3.1 Physical Vapor Deposition (PVD).....	6
1.3.2 Chemical Vapor Deposition (CVD).....	7
1.3.3 Thermal spray	7
1.3.3.1 Plasma spraying	8
1.3.3.2 Detonation spraying	9
1.3.3.2.1 structure and working cycle of detonation spray coating (DSC)	10
1.3.3.2.2 Process Parameters in Detonation Spray Coating.....	10
CHAPTER 2	13
LITERATURE REVIEW	13
2.1 Tribology	13
2.1.1 Wear and its classification	14
2.1.2 Factors that can influence the wear mechanisms.....	15
2.1.2.1 Hardness.....	15
2.1.2.2 Loads (N)	16

2.1.2.3 Speed and sliding distance	16
2.1.2.4 Surface roughness (S_a or R_a)	17
2.1.2.5 Temperature	17
2.1.2.6 The influence of surface films on a wear process.....	17
2.1.2.7 Lubrication.....	18
2.1.2.8 Contact area	19
2.1.2.9 Counterpart	19
2.1.2.10 Microstructure.....	19
2.1.4 High-temperature wear of materials	20
2.2 Insitu high-temperature X-ray diffraction (HT-XRD).....	24
2.2.1 Coefficient of thermal expansion.....	25
2.3 Phase diagrams.....	28
2.3.1. Ni-Al Phase diagram.....	28
2.3.2. Ni-Cr Phase diagram.....	29
2.4 Objectives and Scope of Work	30
2.4.1 Scope of proposed research work	30
2.4.2 Research gaps.....	30
2.4.3 Objectives of the proposed research Work	31
2.4.4 Limitations	31
2.4.5 Flow chart of a proposed work	32
2.5 Outline of Thesis.....	33
CHAPTER 3	34
EXPERIMENTAL PROCEDURE AND MATERIALS.....	34
3.1 Experimental procedures	34
3.1.1 Substrate.....	34
3.1.2 Feedstock material	34

3.1.3. Coating deposition techniques	35
3.2. Testing methods.....	36
3.2.1 Microhardness examination	36
3.2.2. Tribological evaluation	36
3.2.3. In-situ high temperature X-ray diffraction (HT-XRD).....	38
3.3 Surface characterization.....	40
3.4 Calculation procedure	41
3.4.1. Coefficients of thermal expansion (CTE).....	41
3.4.2. Scherrer method	42
3.4.3. Williamson–Hall (W–H) plot	42
3.4.4. Specific wear rate.....	43
CHAPTER 4.....	44
RESULTS AND DISCUSSIONS.....	44
4.1. Sliding Wear Behaviour of Ni-5%Al Coating Deposited by Detonation Spray on IN718.....	44
4.1.1. Characterization of IN718 and Ni-5%Al coated samples.....	44
4.1.2 Sliding Wear	46
4.1.3 Worn out Surface Morphology analysis by 3D profilometer	48
4.1.4. Worn surface of wear tracks	50
4.2. High temperature sliding wear behaviour of detonation sprayed Ni-5wt%Al coating	51
4.2.1. Microstructural characterization of Ni-5wt%Al coating	51
4.2.2. Microhardness.....	52
4.2.3. Dry sliding friction and wear behaviour	53
4.2.4. Topographical evolution of the worn surface of Ni-5wt%Al coatings..	55
4.2.5. Analysis of worn surface morphologies of Ni-5wt%Al	57

4.2.6. FE-SEM and Elemental mapping analysis on the worn surface of Al ₂ O ₃ ball.....	58
4.2.7 EDS analysis of the wear surface of the coating at 25 °C and 850 °C ...	60
4.2.8 Raman spectroscopy	61
4.2.9 Cross-sectional analysis of a Ni-5wt%Al coating	63
4.2.10. Peak shift and lattice parameters behaviour of Ni-5wt%Al during the high temperature	65
4.2.11. Thermal expansion behaviour of Ni-5wt%Al coating.....	66
4.2.12. Crystallite size and Lattice strain.....	67
4.2.13. Limitations of the study and scope for improvement	68
4.2.1. In-situ high temperature X-ray diffraction study on atmospheric plasma and detonation sprayed Ni-5wt%Al coatings	69
4.2.1.1. In situ high-temperature XRD	69
4.2.1.2. Peak shift behaviour of Ni-5wt%Al coating during the HT-XRD	71
4.2.1.3. Measurement of coefficient of thermal expansion (CTE)	72
4.2.1.4. Crystallite size and Lattice strain.....	73
4.2.1.5. Microstructural evolution of coatings at before and after HT-XRD...	75
4.2.1.6. EDS elemental mapping of in-situ HT-XRD Ni-5wt%Al coating	78
4.3. Effect of thermal expansion on the high temperature wear resistance of Ni-20%Cr detonation spray coating on IN718 substrate.....	82
4.3.1. In-situ high-temperature X-ray diffraction (HT-XRD).....	82
4.3.1.1. Stacking and peak shift behaviour of a Ni-20%Cr coating.....	82
4.3.1.2. Measurement of coefficient of thermal expansion (CTE)	83
4.3.1.3. Crystallite size and lattice strain	84
4.3.2. Tribological behaviour of Ni-20%Cr coating	85
4.3.2.1. Microstructural characterization of Ni-20%Cr coating	85

4.3.2.2. Microhardness evaluation of the Ni-20%Cr coating	87
4.3.2.3. Dry sliding friction and wear behaviour of Ni-20%Cr coating	88
4.3.2.4. Worn surface topography by 3D profilometer	90
4.3.2.5. Temperature-mediated wear behaviors of Ni-20%Cr coatings	91
4.3.2.6. SEM-EDS morphology of worn surfaces over Al ₂ O ₃ counter material	92
4.3.2.7. SEM/EDS elemental line analyses of worn surfaces	93
4.3.2.8. Post wear test tribo-layer analysis.....	95
4.3.2.9. Recrystallization	96
4.3.2.10. Cross-sectional analysis of a Ni-20%Cr coating	97
4.3.2.11. The effect of temperature on the wear behaviour of Ni-20%Cr	98
4.4 Dry sliding friction and wear behaviour of DSC sprayed Ni-based coatings with different compositions at elevated temperatures	100
4.4.1. Microstructural and Microhardness evolution of coatings	100
4.4.2. Dry sliding friction and wear behaviour	101
4.4.2.1. Effect of normal loads (N) on friction and wear behavior.....	102
4.4.2.2. Effect of temperature on friction and wear behaviour	102
4.4.2.3 Wear rate (ω).....	102
4.4.3. Topographical evolution of the worn surface of coatings	103
4.4.4. Temperature-mediated wear behaviors of coatings	105
4.4.5. SEM/EDS elemental mapping analyses of worn surfaces	107
4.4.6. Post-wear test tribo-layer analysis	109
4.4.7. X-ray diffraction and Recrystallization	110
4.4.8. Quantitative depth profiling analysis by glow discharge optical emission spectroscopy (GD-OES)	111
4.4.9. Counterpart analysis.....	112

4.4.10. Wear rate coefficient (ω)	114
CHAPTER 5	117
CONCLUSIONS	117
5.1 Conclusions of proposed research work	117
5.1.1 Coating characterization	117
5.1.2 Dry sliding friction and wear behaviour of coatings	118
5.1.2.1 Sliding Wear Behaviour of Ni-5%Al Coating Deposited by Detonation Spray on IN718	118
5.1.2.2 High temperature sliding wear behaviour of detonation sprayed Ni- 5wt%Al coating.	119
5.1.2.2.1 In-situ high temperature X-ray diffraction study on atmospheric plasma and detonation sprayed Ni-5wt%Al coatings	119
5.1.2.3 Effect of thermal expansion on the high-temperature wear resistance of Ni-20%Cr detonation spray coating on IN718 substrate.....	121
5.1.2.4 Dry sliding friction and wear behaviour of DSC sprayed Ni-based coatings with different compositions at elevated temperatures	121
5.2 Recommendations for future work	122
REFERENCES	123
LIST OF PUBLICATIONS	140
BIO-DATA	141

LIST OF FIGURES

Fig. 1.1. Surface modification techniques.	6
Fig. 1.2. Detonation spray coating process	9
Fig. 1.3. DSC working cycle.....	10
Fig. 2. 1. Binary Al–Ni phase diagram	28
Fig. 2. 2 Phase diagram of Ni–Cr system.....	29
Fig. 2. 3 Flow chart of a proposed activity.....	32
Fig. 3.1. Experimental setup of a ball-on-disk tribometer at two elevated temperatures. (a) Room temperature (25 °C), (b) High temperature (850 °C).....	37
Fig. 3.2. HT-XRD setup. (a) Heating program of the experiment (b) Schematic diagram of HT-XRD (c) Heating setup (d) Sample stage (Platinum heating foil).	39
Fig. 3.3. Non-contact optical scanning 3D profilometer.	41
Fig. 4.1. SEM micrographs of as-deposited Ni-5%Al coating; (a) Surface morphology of as-sprayed condition (b) Cross-section of coating.....	44
Fig. 4.2. XRD patterns of as-deposited Ni-5%Al coating.	45
Fig. 4.3. Non-contacting optical microscope 3D-profile and FE-SEM micrographs of the polished samples: (a and c) IN718 and (b and d) Ni-5%Al coating.	45
Fig. 4.4. Coefficient of friction curves of the IN718 and coating at 25 °C under 6N and 10N loads: (a and b) IN718 substrate (c and d) Ni-5%Al coating.....	46
Fig. 4.5. Non-contacting optical microscope 3D profile of wear tracks with depth profiles under 6N and 10N loads: (a and b) IN718 substrate (c and d) Ni-5%Al coating.	48
Fig. 4.6. Wear rate of IN718 and Ni-5%Al coating at 25 °C under 6N and 10N loads.	49
Fig. 4.7. SEM micrographs of the worn surface of the IN718 and Ni-5%Al coating at 6N and 10N loads: (a) IN718 substrate (b) Ni-5%Al coating.	50

Fig. 4.8. FESEM and 3D profilometry micrographs of Ni-5wt%Al coating by DSC spraying technique (a,d) As-deposited; (b,e) Polished specimens tested at 25 °C; (c,f) Polished samples tested an 850 °C".	51
Fig. 4. 9. Dry sliding friction and wear behavior of a Ni-5wt%Al coating sliding against an alumina ball in stagnant air at 25 °C and 850 °C. (a) CoF vs. sliding distance, (b) Wear rate vs. temperature.	53
Fig. 4. 10. Non-contacting optical 3D topographies of wear scars of Ni-5wt%Al coating after dry sliding wear test at 6N and 10N loads. (a-f) RT (25 °C) and (g-l) HT (850 °C).	55
Fig. 4. 11. Worn surface morphologies of Ni-5wt%Al coating (a-b) 6N (c-d) 10N loads at RT (25 °C) and (e-f) 6N (g-h) 10N loads at HT (850 °C).	57
Fig. 4. 12. FESEM micrographs and Elemental mapping on the worn surface of Al ₂ O ₃ ball at different temperatures. (a) Unworn surface of the counterpart (b and b1) 25 °C (c and c1) 850 °C.	58
Fig. 4. 13. EDS line analysis of element content on the worn surface of the coating cross-sections at (a and b) 25 °C and (c and d) 850 °C.	60
Fig. 4. 14. Raman topography of outside and inside the worn scar of Ni-5wt%Al coatings at 25 °C and 850 °C. (a-d) 25 °C (e-f) 850 °C and (a,b and e,f) outside of the worn scar (c,d, and g,h) inside of the worn scars.	61
Fig. 4.15. Raman spectra of outside and inside the worn scar of Ni-5wt%Al coatings at 25 °C and 850 °C.	62
Fig. 4. 16. Cross-sectional (sub-surface) FESEM images of the worn surface of a Ni-5wt%Al coating at 850°C under typical loads. (a-c) 6N and (d-f) 10N.	63
Fig. 4. 17. BSE micrographs and corresponding EDS element mappings of the cross-sections of the worn surface of Ni-5wt%Al coating at 850 °C. (a) 6N (b) 10N.	64
Fig. 4. 18. Shifting of the highest intensity peak of Ni in Ni-5wt%Al coating from RT (25 °C) to HT (850 °C) at in-situ HT-XRD.	65
Fig. 4. 19. Crystallite size (D) and lattice strain (ε) with the elevated temperature of Ni-5wt%Al coatings.	67
Fig. 4. 20. Stacking and Difference plots for the fit patterns of in-situ HT-XRD of Ni-5wt%Al coating after Rietveld refinement; (a) APS, and (b) DSC.	69

Fig. 4. 21. Peak Shift phenomenon during HT-XRD, (a) APS, and (b) DSC, and the insert indicates the thermal expansion-induced peak shifting phenomena.....	71
Fig. 4. 22. (a) Lattice parameters and (b) CTE of APS and DSC sprayed Ni-5wt%Al coatings.	72
Fig. 4. 23. Crystallite size and Lattice strain of APS and DSC sprayed Ni-5wt%Al coatings using Williamson-Hall analysis through UDM.	73
Fig. 4. 24. As-deposited cross-section and Surface morphology of Ni-5wt%Al coatings; (a and c) APS and (b and d) DSC.	75
Fig. 4. 25. Surface morphology and cross-section of Ni-5wt%Al coatings after HT-XRD condition at 1150 °C; (a and c) APS and (b and d) DSC.....	76
Fig. 4. 26. EDS mapping analyses of element content on the Ni-5wt%Al coating surface and cross-section at as-deposited condition; (a&c) APS and (c&d) DSC.	78
Fig. 4. 27. EDS mapping analyses of element content on the Ni-5wt%Al coating surface and cross-section after the in situ high-temperature XRD at 1150 °C; (a&c) APS and (c&d).	79
Fig. 4. 28. Stacking and Peak Shift During HT-XRD and the inset depicts the thermal expansion caused peak shifting phenomenon. (a) Diffraction peak stacking (b) Peak Shift phenomenon.	82
Fig. 4. 29. Lattice parameters and CTE vs. temperatures of DSC sprayed Ni-20%Cr coatings.	83
Fig. 4. 30. Variation of crystallite size (D) and lattice strain (ϵ) with annealing temperature of Ni-20%Cr coatings.	84
Fig. 4. 31. 3D topographical and FESEM micrographs of Ni-20%Cr coating; (a, d) As-deposited (b, e) After polishing and 25 °C (c, f) after the wear test at 850 °C.	85
Fig. 4. 32. Elemental mapping analysis of Ni-20%Cr coating; (a) As-deposited (b and c) After the Wear at 25 °C and 850 °C.....	86
Fig. 4. 33. Depicts the dry sliding friction and wear behaviour of a Ni-20%Cr coating sliding against a ball in stagnant air evaluated at RT (25 °C) and HT (850 °C). (a) CoF vs. sliding distance (b) Wear rate vs. temperature.	88

Fig. 4. 34. Non-contacting optical 3D profilometry of the 3D and 2D topographies of wear traces of Ni-20%Cr coating after dry sliding under different 6N and 10N loads. (a, b) RT (25 °C) and (c, d) HT (850 °C).	90
Fig. 4. 35. Worn surface morphologies of Ni-20%Cr coating (a, c) 6N (b, d) 10N loads at 25 °C and 850 °C.	91
Fig. 4. 36. FESEM micrographs and Elemental mapping on the worn surface of Al ₂ O ₃ ball at different temperatures. (a and c) 25 °C (b and d) 850 °C.	92
Fig. 4. 37. EDS line analysis of element content on the coating cross-sections at (a, c) 25 °C and (b, d) 850 °C for Ni-20%Cr coating.	93
Fig. 4. 38. Post wear track of Ni-20%Cr coatings after the ball-on-disc sliding test at 25 °C and 850 °C. (a) Raman spectra, (b) XRD analysis.	95
Fig. 4. 39. BSE micrographs and corresponding EDS element mappings of the cross-sections of the worn surface of Ni-20%Cr coating at 850 °C. (a) 6N (b) 10N.	97
Fig. 4. 40. Schematic diagram of tribological evolution of Ni-20%Cr coating at 25 °C&850 °C.	98
Fig. 4. 41. 3D profilometry topographs of DSC sprayed Ni-5wt%Al and Ni-20%Cr coatings. (a&d) As-deposited, (b&e) Polished surfaces, (c&f) After the wear test at 850 °C.	100
Fig. 4. 42. Depicts the dry sliding friction and wear behaviour of Ni-5wt%Al and Ni-20%Cr coatings under the 6N and 10N loads at 25 °C and 850 °C. (a) CoF vs. sliding distance; (b) Wear rate vs. temperature.	101
Fig. 4. 43. 3D topographies and depth profiles of wear tracks of the coatings after dry sliding friction and wear under different 6N and 10N loads. (a&b) 25 °C and (c&d) 850 °C.	103
Fig. 4. 44. Worn surface morphologies of coatings (a-b) 6N (c-d) 10N loads at 25 °C and (e-f) 6N (g-h) 10N loads at 850 °C.	105
Fig. 4. 45. EDS line analysis of element composition on coating cross-sections at (a, c) 25 °C and (b, d) 850 °C.	107
Fig. 4. 46. Raman spectra of wear tracks after the ball-on-disc sliding wear at different temperatures. (a and b) 25 °C, (c and d) 850 °C.	109

Fig. 4. 47. Stacking of XRD diffraction patterns at various temperatures. (a&b) Ni-5wt%Al, (c&d) Ni-20%Cr at 25 °C and 850 °C.....	110
Fig. 4. 48. Quantitative elemental depth profiles of Ni-based coatings at various temperatures. (a and b) 25 °C, (c and d) 850 °C.....	111
Fig. 4. 49. Worn surface morphologies of Al ₂ O ₃ counter material. (a & b) 25 °C and (c & d) 850 °C.....	112
Fig. 4. 50. EDS element mapping analysis of counter material at 850 °C.....	113
Fig. 4. 51. Wear rate vs. CV of Ni-based coatings at different temperatures. (b & d) 25 °C, (a & c) 850 °C.	114
Fig. 4. 52. A schematic representation of the tribological behavior of Ni-based coatings under various loads (6N & 10N).....	115

LIST OF TABLES

Table 3.1. Chemical composition of nickel-based superalloy (IN718).	34
Table 3.2. Nominal chemical composition of feedstock powder used.	35
Table 3.3. Spraying parameters for APS and DSC coatings.....	35
Table 3.4. Test parameters for dry sliding friction and wear experiments.	38
Table 3.5. Test parameters for in-situ HT-XRD.	39
Table 4.1. Mechanical properties of substrate and coating.....	46
Table 4.2. Coefficient of friction of IN718 and Ni-5%Al coating at 25 °C temperatures under 6N and 10N loads.	47
Table 4.3. Depth, width, and volume loss of the IN718 and Ni-5%Al coating at different loads.	50
Table 4. 4. Surface roughness and Elemental distribution of feedstock powder and as-deposited Ni-5wt%Al coating.....	52
Table 4. 5. Vickers microhardness of Ni-5wt%Al coating and counterpart at 25 °C and 850 °C.....	53
Table 4. 6. Sliding wear behaviour of Ni-5wt%Al coatings at 25 °C and 850 °C.....	55
Table 4. 7. Dimensions and roughness parameters of the wear tracks with standard deviations of Ni-5wt%Al coating at 25 °C and 850 °C.....	56
Table 4. 8. EDS line analysis of the elemental composition of Ni-5wt%Al coating at different temperatures.	61
Table 4. 9. Shows an elemental mapping analysis of a Ni-5wt%Al coating at 850 °C using FESEM-EDS.	65
Table 4. 10. Thermal expansion coefficient and lattice parameters of Ni-5wt%Al coating at different temperatures.	67
Table 4. 11. Rietveld analysis for in-situ HT-XRD pattern of Ni-5wt%Al coatings...	71
Table 4. 12. XRD analysis – Crystallite size (nm) and lattice-strain (%) of Ni-5wt%Al coatings using Williamson-Hall analysis through UDM.	75
Table 4. 13. Porosity of APS and DSC sprayed Ni-5wt%Al coating.....	78

Table 4. 14. Element contents (wt%) of APS and DSC sprayed Ni-5wt%Al coating.	81
Table 4. 15. Surface roughness and EDS analysis of DSC sprayed Ni-20%Cr coating.	87
Table 4. 16. Microhardness values and standard deviations of Ni-20%Cr coatings after the wear test at 25 °C and 850 °C.....	88
Table 4. 17. Wear data with standard deviations of Ni-20%Cr coating at 25 °C and 850 °C temperatures.....	90
Table 4. 18. EDS line analysis of the elemental composition of Ni-20%Cr coating at different temperatures.....	94
Table 4. 19. Rietveld refinement analysis of Ni-20%Cr coatings.....	96
Table 4. 20. EDS elemental mapping analysis of the elemental composition of Ni- 20%Cr coating at 850 °C.....	98
Table 4. 21. Surface roughness (S_a) and roughness ($HV_{0.2}$) of DSC sprayed coating.	101
Table 4. 22. Wear data with standard deviations of coatings at 25 °C and 850 °C....	104
Table 4. 23. Primary wear and Sub-wear mechanisms of Ni-based coatings at different temperatures.....	106
Table 4. 24. EDS line analysis of the elemental composition of coatings at different temperatures.....	108
Table 4. 25. Crystallite size of coatings at different temperatures.....	111
Table 4. 26. Elemental mapping analysis of counter material at different temperatures.	114

ABBREVIATION

APS	-	Atmospheric plasma spraying
ASTM	-	American Society for Testing and Materials
BCC	-	Body centered cube
BSE	-	Backscattered electrons
COD	-	Crystallographic Open Database
CoF	-	Coefficient of friction
CTE	-	Coefficient of thermal expansion
DSC	-	Detonation spray coating
EDS	-	Energy dispersive spectroscopy
FCC	-	Face centered cube
FESEM	-	Field emission scanning electron microscopy
GD-OES	-	Glow Discharge Optical Emission Spectrometry
GoF	-	Goodness of fit
HT-XRD	-	High-temperature X-ray diffraction
HTT	-	High-temperature tribometer
ICDD	-	International Center for Diffraction Data
SLPM	-	Standard liter per minute
TET	-	Turbine entry temperature
TGO	-	Thermally grown oxide layer

UDM	-	Uniform deformation model
W-H	-	Williamson-Hall
XPPA	-	X-ray peak profile analysis

NOMENCLATURE

Actual lattice parameter	l_o
Ambient temperature	T_o
Coating thickness	μm
Coefficient of friction	μ
Coefficient of thermal expansion	α
Crystallite size	D
Diffraction angle	2θ
Elevated Temperature	T
Lattice strain	ε
Length of a lattice parameter	l
Load	N
Micro-hardness	HV
Sliding velocity	V
Sliding distance	m
Speed	rpm
Volume	V
Wave length	λ
Wear rate	ω

CHAPTER 1

INTRODUCTION

The necessity of employing protective coatings on superalloys using thermal spray technology is emphasized throughout the chapter. Furthermore, the strength of the materials chosen for investigation, Inconel718, was demonstrated. A problem based on an ongoing issue in the aero-engine sector related to failures of gas turbine material at severe temperatures was given in the problem identification section. The following chapter defines the study of the research objectives. This section depicts the material chosen, coating deposition techniques, test parameters, conditions, and the work schedule. Finally, the chapter concludes with the thesis organization.

Tribology, the science, and technology of interacting bodies in relative motion, including friction, wear, and lubrication, is an interesting but highly complex and broad subject that involves many research areas, including mechanical engineering, materials science, physics, chemistry, and mathematics. Despite its enormous significance to industry and daily life, tribology is still largely unknown. The industrial world includes many types of machinery with moving parts that come into contact with one another. Tribology is essential to know what happens during these interactions and is required for machine design and reliability. For example, there is now a high demand for machines that use less energy to produce the same performance and have longer-term parts. Tribology may play an essential role in their design and online monitoring to increase component lifespan. Controlling friction and wear at the interfaces of contacting surfaces is critical for smooth, dependable, efficient, and long-lasting functioning. Wear is more important than friction because it produces catastrophic and functional failures that reduce efficiency and incur substantial financial losses.

According to Holmberg and Erdemir, tribological interactions generate 23% (119 EJ) of global energy consumption (Holmberg and Erdemir 2017). Nearly 20% of this is utilized to counteract friction, and 3% is used to restore damaged components caused by wear. The amount of energy loss caused by friction and wear is expected to be reduced by 40% (46 EJ) in fifteen years and 18% (21.5 EJ) in eight years, saving up to 1.4% of GDP yearly through the use of new materials, lubricants, and surface

modification technologies. Because a large amount of a developed country's GDP is squandered in overcoming the adverse effects of friction and wear (in the form of direct loss of useable energy and replacement costs for machine elements impacted by wear), one of the primary goals of tribology research is to develop methods and materials to reduce friction and wear. As a result, significant effort is being directed towards (i) studying the characteristics and increasing the importance of present lubricants and (ii) finding innovative techniques for more effectively lubricating surfaces (for example, by reducing the friction and wear rate, and increasing component lifespan).

As technology advances, there is a growing need to build mechanical components operating under extreme circumstances, such as speeds, temperatures, and high loads. Because of changes in thermo-physical properties, surface reactivity, mechanical properties, and tribo-chemical reactions at high temperatures, the friction and wear behavior of industrial components is of significant relevance. Because few viable solid or liquid lubricants work effectively at high temperatures for contacting metals, the ability of the contacting surfaces to self-lubricate is based on interactions with their surroundings, as suggested by Blau (Blau 2010). Attempts are being made to employ substitute materials or coatings with improved oxidation resistance, increased lubricating capabilities at higher temperatures, and enhanced performance of materials.

Self-lubricating materials are a broad group of compositions that include one or more solid lubricants that reduce CoF and wear rate with high sliding contacts without external lubricant. In recent years, their employment in high-temperature (HT) environments has increased in prominence in applications from metal forming to aerospace and power production. Solid lubrication technology has grown quickly in the last five decades, owing principally to the requirements of the aerospace and automobile sectors. Because of the temperatures, a liquid lubricant is ineffective in such extreme environments. The mechanical components required lubrication and durability can be given by incorporating a high-temperature solid lubricant into the metallic components and generating a metallic composite layer with a solid lubricating composition. The reliability of aero engines is directly related to the wear resistance of turbines and blades (Zhen et al. 2014).

Solid lubricants are employed when liquid lubricants fail to withstand the demands of intricate technologies such as cryogenic temperatures, high vacuum, radiation, high temperatures, dust, corrosive conditions, and clean surroundings. Materials used for solid lubricants have low CoF and wear rates and are durable in various states. As a result, knowing the material and tribological characteristics of solid lubricant-containing materials and coatings is required for successful application. Concrete lubricant coatings are primarily used in harsh applications to reduce the CoF and wear rate (such as aerospace, very low or high temperatures, high loads, high speeds, and high vacuum) where conventional materials and lubricants are incapable of providing the desired levels of efficiency or longevity. Over the last few decades, significant progress has been made in designing and developing solid lubricant coatings.

The current trend in tribology is to reduce the use of liquid lubricants (primarily for environmental concerns) and to extend the use of self-lubricating solid materials and coatings. The lubricant coatings have advanced significantly in recent years, and they may now provide exceptionally low CoF and wear rates under different test conditions. Solid lubrication in various ambient atmospheres is a difficult challenge that tribologists have faced for decades and have yet to conquer since most lubricants function efficiently only in a restricted range of ambient circumstances.

Besides, the influence of other important temperature-dependent properties, such as thermal expansion, recrystallization, and stress relaxation, on the dry sliding wear behavior at elevated temperatures has not been explored. As a result, the present research attempts to correlate the temperature-dependent properties and lubricants to expand the regime of suitable lubrication over a wide temperature range of Ni-based DSC coatings on their high-temperature dry sliding wear behaviour.

1.1 Turbine materials

The most critical issue is the operating temperature of the turbine components. As a result, suitable materials retain their desirable characteristics exceptionally well at high temperatures. These are the materials that can tolerate high temperatures. Some examples are turbines, rockets, and heat exchangers. Higher turbine entry temperature

(TET) is usually sought from a thermodynamic perspective when designing a gas turbine engine since it enhances engine efficiency and performance. A higher TET, on the other hand, inevitably places a significant demand on the thermal capability of materials used in gas turbine hot-section components (e.g., combustor liners, turbine blades, and nozzle guide vanes).

Components in relative motion frequently suffer thermal fatigue, high-temperature creep, fatigue fracture, unexpected friction, and wear, decreasing the operational efficiency in harsh conditions (high temperature) and necessitating the development of new technological solutions to address the ongoing challenges (Shi et al. 2020) (Gautam et al. 2019) (Pham et al. 2020) (Wang et al. 2018) (Li et al. 2017) (Torres et al. 2016). The operating conditions tolerable by the material characteristics limit the performance parameters for various applications. Early contemporary aviation engines, for example, relied heavily on and were limited by the high-temperature durability of nickel-based superalloys in their hot section components.

1.2 Superalloys

Many gas turbine components must tolerate severe loads and temperatures while in service. Superalloys are high-temperature materials developed for applications such as compressors and combustion chambers leading to turbine sections. These materials include nickel, iron-nickel, and cobalt-nickel base alloys with an operating temperature of around 1000 °F (540 °C). Superalloys are mostly used in turbine engines, jet engines, chemical plants, and nuclear power plants. Superalloys are used in the defence and aerospace industries due to their extensive material characteristics at elevated temperatures, depending on the applications of wrought or cast (Cemal Kushan et al.). Ni-based superalloys have strong mechanical and chemical characteristics at temperatures exceeding 0.6 times their melting point, including high strength, creep, and moderate oxidation resistance at high temperatures. Superior wettability and adhesion energy properties are also displayed at elevated temperatures (Pollock and Tin 2006) (Tang and Xu 2018) (Baicheng et al. 2017). Ni is stable because there is no phase change of its face-centered cubic (FCC) structure from room temperature to melting point at 1455 °C, and it is very soluble in alloying elements. The FCC matrix of a Ni-

based superalloy can be reinforced by dissolving alloying elements to generate strengthening precipitates, carbides, or dispersive oxide-particles.

1.2.1 Inconel718

Since 1965, Inconel718, with other modifications, has been used in manufacturing. It is a Ni-Cr-based superalloy with a wide material composition and mechanical strength range. Ni and Cr protect the materials against corrosion, oxidation, and other surface damage at high operating temperatures. Alloy 718, a precipitation-hardenable nickel-chromium grade, is a high-strength superalloy used at temperatures up to 648 °C. Inconel alloys are composed of Ti, Al, Co, Nb, Cu, and W to increase strength and corrosion resistance. Fe is also contained in the substance, varying from 1 to 20%. These combinations also contain Ti and Al traces, increasing mechanical properties and weldability. They are employed in the oil and gas, aerospace, gas turbine, and military sectors due to their commensurate wear resistance, high corrosion resistance, and outstanding mechanical characteristics at high temperatures (Grzesik et al. 2018) (Trosch et al. 2016) (Rong and Gu 2016).

1.3 Different coating techniques

Three types of coatings are commonly used as protective coatings in high-temperature applications: Diffusion, Overlay, and Thermal barrier coatings.

Diffusion coatings are aluminide-type (NiAl) coatings formed on the surface of nickel-base superalloys by the diffusion and chemical interaction of an externally supplied Al with the Ni in the superalloys. The higher the aluminum content in the aluminide coatings, the easier it is to form and maintain a protective alumina layer, improving the superalloy performance.

Overlay coatings are intended to solve the problems encountered with diffusion coatings. Overlay coatings are deposited on the surface of the substrates. Because the overlay coatings eliminate superalloy substrate modification, the appropriate composition, microstructure, and mechanical characteristics may be preserved.

A thermal barrier coating (TBC) prevents the oxidation of superalloy components (Vaßen et al. 2008). TBC is a coating system comprising two distinct layers on the substrate. The outer layer includes a low thermal conductivity ceramic topcoat that thermally insulates the underlying metallic elements from the hot gases, allowing for a primary temperature reduction between the hot and metallic components. The bond coat improves adhesion between the top coat and the substrates while also protecting the substrates from corrosion and oxidation. There are several surface modification techniques accessible and employed in the industry. Still, only a handful are most successful and relevant, such as Chemical vapour deposition (CVD), Physical vapour deposition (PVD), and Thermal spray (Fotovvati et al. 2019). An overview of such technologies is depicted in Fig. 1.1.

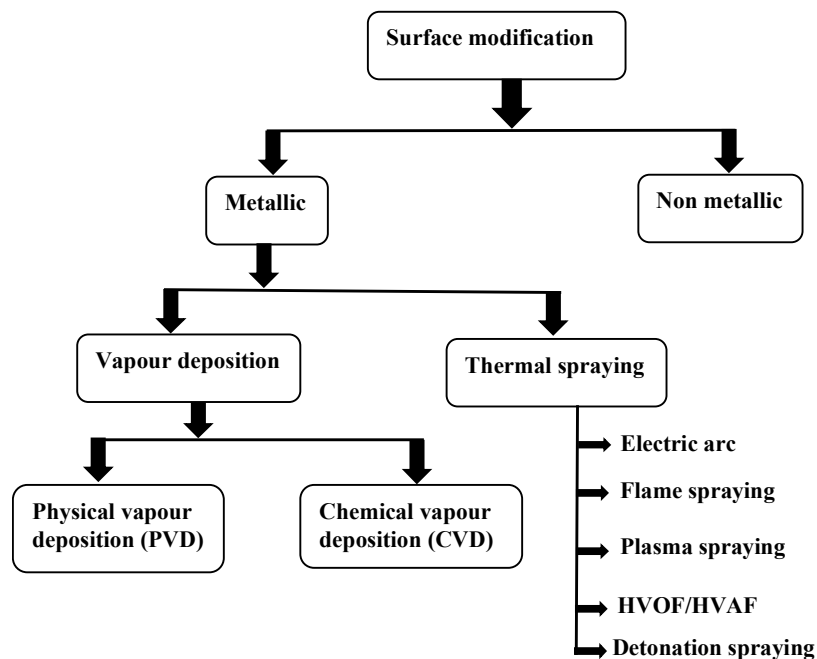


Fig. 1.1. Surface modification techniques.

1.3.1 Physical Vapor Deposition (PVD)

The method includes the condensation of vapours at ultra-high vacuum conditions. It is incredibly adaptable and flexible in material deposition, intermetallic, ceramic, or other compounds. Nearly any metal that does not undergo dissociation may be readily deposited on a substrate, such as ceramics, metals, or plastics. PVD coating may be utilized in various applications, including aerospace, automotive, biomedical

instruments, optical, guns, ornamental, and microelectronics. Typically, the coating deposition rate is low. PVD coatings provide high impact strength, temperature, abrasion resistance, and excellent durability (Selvakumar and Barshilia 2012).

1.3.2 Chemical Vapor Deposition (CVD)

The vapour of the coating material, which is generated by volatilization from either a liquid or a solid substance, moves towards the substrate surface due to a pressure differential or the action of the carrier gas. A vapour phase reactant gas or other chemicals generates a metallic composite coating. At atmospheric pressure, the coating is formed by thermal breakdown or a chemical interaction (with gas or vapour). Chemical reactions often occur at temperatures ranging from 150 to 2200 °C and pressures ranging from 50 Pa to atmospheric pressure. Electric resistance, inductance, and infrared heating are all substrate heating techniques. A coating is deposited atom by atom to the heated substrate. Although CVD coatings typically exhibit excellent adherence, the constraints of high-temperature substrates limit their use on surfaces that can withstand these temperatures.

1.3.3 Thermal spray

The thermal spray is an industrially accepted method to deposit dense overlay coatings without impairing the original properties of substrates. In the thermal spray technique, heat energy is employed to deposit layers. The spray coatings are separated into three sections: the appropriate coating material (Powders and wire or rods). Second, thermal energy is used to melt the feedstock material. Third, the molten/unmolten material is propelled with high velocity to deposit the coating on the substrate.

The thermal spraying approach provides the following significant benefits.

- (a) Metals, alloys, ceramics, cermets, and carbides may all be effectively deposited on any substrate.
- (b) Thin coatings may be effectively deposited due to the rapid deposition rate.
- (c) Coatings are mechanically attached and metallurgically bonded to the substrate.

(d) Parts may be rebuilt rapidly and affordably.

(e) By using a high-quality coating substance in thermal spray, the components can outlast the initial ones.

1.3.3.1 Plasma spraying

A plasma jet acts as a heat source and a particle accelerator in the plasma spray process. The jet is generated by a high-frequency direct current passing through a gas stream containing a mixture of gases (argon, nitrogen, hydrogen, and helium). An electrical arc is produced by connecting an anode and a cathode. The gun's nozzle emits this plasma. Coating feedstock powder is injected into the plasma jet and deposited on the substrate.

Plasma spraying is the most common deposition technique in TBCs. Depending on the process parameters and gases used, plasma temperatures range from 6000 °C-15000 °C, and powder particle velocity can exceed 1500 m/s (Liu et al. 2022). The feedstock material is melted in the plasma, and a plasma jet propels droplets toward the substrate. This technology can also be used in an atmosphere known as Atmospheric Plasma Spray (APS). The spray procedure may also be done in a controlled atmosphere known as Vacuum Plasma Spray (VPS) or Low-Pressure Plasma Spray (LPPS). Removing oxygen from the spraying process may improve coating quality. However, environmental handling equipment and lengthy process durations add to the expense of these procedures.

1.3.3.2 Detonation spraying

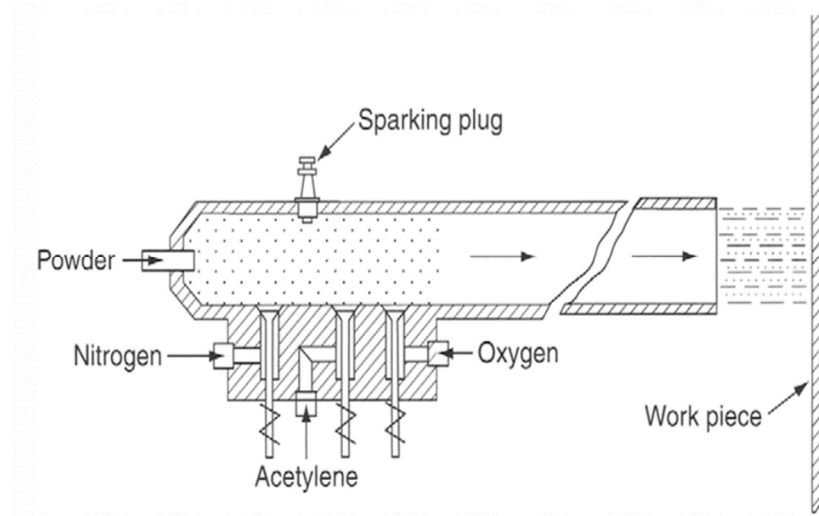


Fig. 1.2. Detonation spray coating process (Singh et al. 2012).

Detonation spray coating (DSC) is a thermal spray coating method that provides little porosity, excellent adhesive strength, and uniform microstructures with compressive residual stresses (Purushotham et al. 2022). In principle, the DSC technique produces high-pressure supersonic waves in a chamber filled with a combustible gaseous combination of fuels such as butane, acetylene, oxygen, and propane (Sundararajan et al. 1998). The expanding gas releases molten/unmolten particles toward the substrate surface to produce the coating. The coating equipment is housed in a barrel. As seen in Fig. 1.2, it has poppet valves that enable nitrogen, oxygen, and fuel gas into the system. A carrier gas enters the feedstock coating material as powders into the barrel through a fixed port. The combustible combination of oxygen and fuel is produced into the barrel via the poppet valve. Nitrogen is pumped into the barrel to protect the poppet valves from hot gases.

After injecting the gases into the barrel, a spark plug ignites the fuel gas combination. The explosion generates temperatures of 4500 °C (8132 °F), melting the feedstock materials. It also produces high-pressure waves at speeds of 3000 to 4000 m/s. After the explosion, the expanding gases propel the semi-molten/molten material at speeds of up to 800 m/s toward the substrate and coating material discharge (Kamal et al. 2009). The gun is purged with nitrogen gas, completing one cycle. Each cycle

applies a few millimeters of coating onto a substrate. DSC cycles are regularly repeated at one to fifteen pulses per second. The typical coating thickness is between 70-350 μm .

1.3.3.2.1 structure and working cycle of detonation spray coating (DSC)

The process of DSC is cyclical. The structure and step sequence of the DSC working cycle is illustrated in Fig.1.3. Eight important stages will be explored to determine the basic physicochemical phenomena in the operating process:

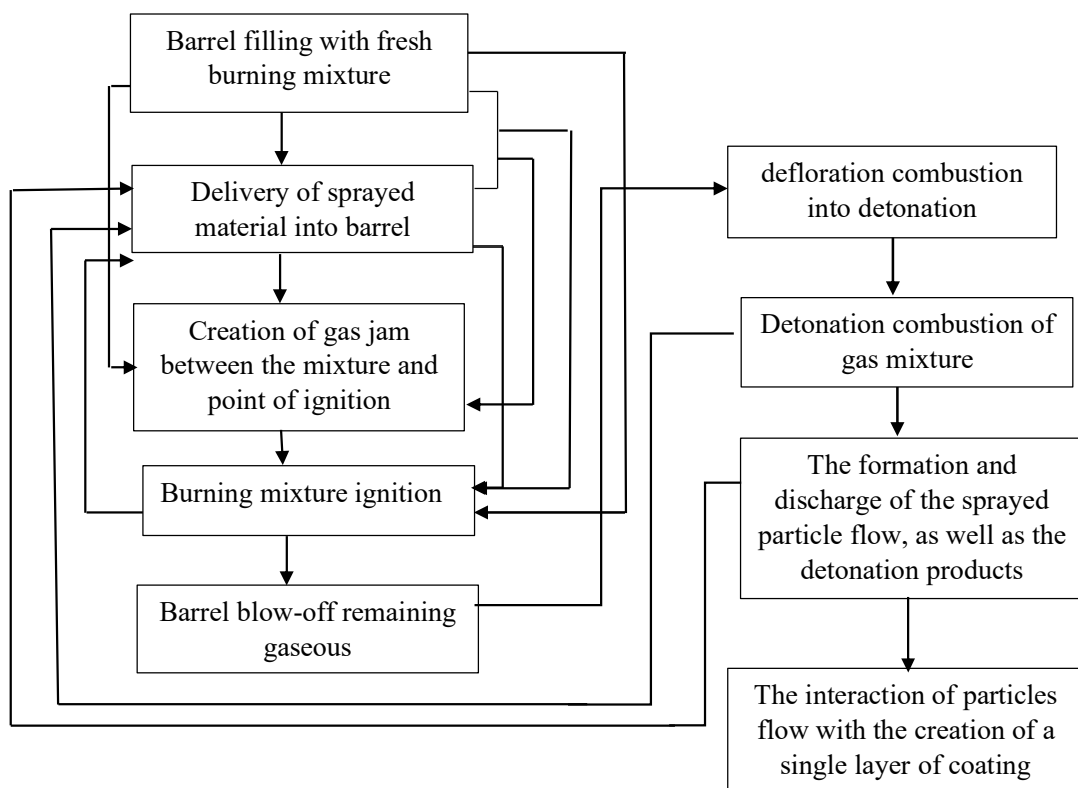


Fig. 1.3. DSC working cycle.

1.3.3.2.2 Process Parameters in Detonation Spray Coating

When using detonation spraying, various process factors affect adhesion strength, powder melting, coating characteristics, and the final deposition efficiency. The parameters of the coating method and their impacts have been explored.

D-gun spray coating gas mixture: The Feedstock material is heated and combined with acetylene, butane, propane, and oxygen.

Carrier gas: The powder is transferred from the hopper using a carrier gas. The primary gas is generally used as the carrier gas.

Powder flow rate: It affects the coating thickness and other mechanical characteristics. The appropriate mass flow rate is determined by feedstock material chemistry, particle size, and other powder parameters. Spraying at a low mass flow rate may cause coating buildup to be delayed. An extremely high mass flow rate, on the other hand, may result in partial melting and significant coating porosity.

Stand-off distance: This is the distance between the tip of the gun and the surface of the substrate. A lower stand-off distance might not give sufficient flight time to melt, resulting in melting and high unmolten particles entrapped in the coating. If the stand-off distance is too high, molten particles may freeze before reaching the target. In the case of alumina, it has been discovered that increasing the stand-off distance beyond an excellent value increases porosity and lowers coating thickness (therefore, deposition efficiency).

Powder-related variables: Powder-related parameters include feedstock powder size, distribution, phase composition, powder shape, processing history, etc. These variables have a significant influence on coating. Too fine a feedstock powder, for example, may vaporize during heating, reducing deposition efficiency. Large powder particles may not completely melt and are thus inappropriate for coating. Spherical particles should not be sprayed with the same conditions as angular powders since they do not have the same flow characteristics.

Surface preheating: As previously stated, the grit-blasted substrate obtains water and other condensates from the environment. Before spraying, the substrate should be heated to eliminate impurities from the surface.

In summary, the literature review reveals little study has been done into the Ni-based composite coatings of tribological behaviour at elevated temperatures. The current research mainly focused on the dry sliding friction and wear behaviour of DSC sprayed Ni-based coatings at different conditions. That correlates with temperature-dependent properties such as thermal expansion, recrystallization, stress relaxation, and oxidation. The wear mechanisms behind friction and wear have been explored at

different elevated temperatures. The study's knowledge base is intended to improve understanding of the tribological behavior of these Ni-based coatings and increase component lifespan in technical applications in high-temperature sectors.

CHAPTER 2

LITERATURE REVIEW

This chapter introduces the phenomena of wear, types of wear mechanisms, and the factors influencing wear and lubrication (liquid and solid or both). It is followed by an observation of the significance of solid lubrication, which includes a summary of how it affects tribological properties. The chapter also includes a detailed examination of various procedures used for the deposition of wear-resistant coatings, explicitly focusing on the relevance of the thermal spraying process and critical process factors that impact the microstructure and quality of coatings. The chapter also includes a brief explanation of the high-temperature wear of materials. The chapter also extensively literature survey on the high-temperature tribological behaviour of composites and coatings. The problem formulation can be found at the end of the chapter.

2.1 Tribology

Most machine components work in different environments involving relative motion between two surfaces. It is crucial to the operation and robust performance of essential machine components. Tribology is "the science and technology of interacting surfaces in relative motion," which includes friction, lubrication, and wear (Bhushan B, Author and Ko Pak Lim, Reviewer 2003). It is derived from the Greek term *tribo*, which means "to rub," and the suffix *logy*, which means "the study of."

A standard tribological system consists of four components. The first two components are the sliding surfaces of two bodies (Counterpart and disk material). The third component is an interfacial medium, a lubricant (liquid, solid, gas, or a combination), or another intermediate layer (glaze layer). The final component is the surrounding environment.

Friction is a prevalent occurrence that is observed in people's daily lives as well as in the majority of industrial applications. Controlling friction reduces energy waste and improves machine efficiency (Medabalimi et al. 2021). Material wear from a surface can cause severe damage and failure of the component or the machine (KC

1996). Friction is the primary source of wear and energy dissipation, and according to (Liu et al. 2019), various kinds of friction use around 1/2 to 1/3 of the world's energy. A huge percentage of the world's resources are squandered in overcoming friction in one form or another. Lubrication (solid or fluid) helps minimize friction and wear. As a result, for a machine to survive, wear and friction must be decreased or managed (Bhushan B , Author and Ko Pak Lim , Reviewer 2003). A good selection of materials, lubricants, and surface modification techniques is the most common strategy for reducing CoF and minimizing wear rate and catastrophic failure of machine parts or the machine itself.

2.1.1 Wear and its classification

Wear is associated with surface interactions, particularly the surface material's loss and deformation caused by the opposite surface's mechanical action. Wear is the gradual material loss from the surface of the substrate caused by the interfacial rubbing process (Ramesh et al. 1991). Wear can be categorized based on the appearance of the worn portions or the mechanisms and circumstances that exist during material removal. The wear mechanisms and cases are characterized as follows: (i) abrasive wear, (ii) adhesive wear, (iii) fatigue wear, (iv) erosive wear, (v) impact wear, and (vi) Chemical wear.

Abrasive wear occurs when two surfaces come into contact, one tougher and one rougher. Abrasive wear occurs when material from one surface is removed or displaced by the sharper edges of another surface or by sharper, errant particles. This kind of wear is risky because it can happen quickly after introducing a contaminant, resulting in rapid wear rates and causing significant surface damage.

Adhesive wear is related to low sliding velocity, minimal load, and smooth surfaces. This is a general sort of wear that can occur in any equipment and is difficult to eradicate but can only be decreased. Adhesion processes involve the interaction of two opposing surfaces in relative motion. When the asperities come into close contact, they may weld together, leading to a bond at the junction with a rupture strength higher than the yield strength of the contacting solids. In such a case, a fracture in one

of the defects might develop, resulting in material transfer from one contacting body to the other.

Fatigue wear is the continually repeated cycles of a stress state on a component's surface, resulting in small mechanical damage in the surface and subsurface portions with each stress state. Finally, damage accumulation causes surface failure due to distortion and fracture.

Erosive wear is the result of frequent deformation and cutting. Erosion occurs when the action of fluids and particles progressively wears away a solid surface. Material erosion can occur in four ways: (1) impingement of solid particles on a solid surface, (2) impingement of liquid droplets against a solid surface, (3) movement of hot gases over a solid surface, and (4) cavitation at a solid surface in liquid media. Erosion generated by solid particle impingement is the most common type of erosion.

Impact wear is caused by the repeated impact of two surfaces, as opposed to erosive wear caused by the effects of solid particles on a surface.

Chemical wear results from a chemical reaction at a surface interacting with one or more mechanical wear processes. Sliding surfaces suffer corrosive wear in corrosive environments. However, the reaction layer can sometimes protect the surface or function as a lubricant.

2.1.2 Factors that can influence the wear mechanisms

2.1.2.1 Hardness

Hardness is a fundamental material property that describes its resistance to deformation or scratching and significantly influences wear mechanisms in materials. In some cases, extremely hard materials may still experience wear if they are brittle or if other factors, such as friction or contact stresses, are unfavorable. However, it can improve wear performance comparatively. This is because the hardness of the particles present at the contact must be considered. Archard's equation (2.1) (Niu and Tian 2018) might explain the hardness-wear resistance relationship:

$$V_w = K \times \frac{SN}{H} \quad (2.1)$$

V_w represents the wear scar volume, K is the frictional coefficient, S is the sliding distance, N is the load, and H is the hardness. According to equation (2.1), increased coating hardness helps to superior wear characteristics. The wear rate of the coating is related to the applied load (N) and sliding distance (m) (Kumar et al. 2016).

2.1.2.2 Loads (N)

The effect of normal load and sliding speed on the formation of protective glaze layers is complicated and depends upon the interaction of other components. In general, the presence of relatively high stresses promotes wear debris aggregation and sintering. However, if this threshold is exceeded, such layers begin to fracture and shatter, increasing wear. It was demonstrated that self-healing cracked oxides are possible under specific conditions, notably at high temperatures and low strain rates. He studied that if the velocity at which the fracture faces separate is slower than the rate at which the oxide develops inside the scale, the latter will tend to seal the crack (Cheng et al. 2019).

2.1.2.3 Speed and sliding distance

Variations in sliding speed can have a significant impact on wear rate changes. (Medabalimi et al. 2021), For example, Medabalimi attempts were made to solve this issue by combining wear data from the literature for partly oxidized NiCr coatings using the combined flame spray and plasma spray technique into a wear-mechanism map.

A longer sliding distance may also increase the heat generated by frictional forces. This increased temperature can cause protective oxide layers to develop on the interacting surfaces, allowing them to withstand wear. It is one of the causes for such surfaces' varying wear performance (Medabalimi et al. 2021).

According to Archard's equation, a sliding distance should have an equal relationship with volume loss (Niu and Tian 2018). The sliding distance in a wear test can affect the severity of wear by exposing the material to prolonged contact with the counter-body,

potentially leading to increased material loss or wear due to repetitive sliding or rubbing action.

2.1.2.4 Surface roughness (S_a or R_a)

Surface roughness significantly impacts surface wear performance, incredibly abrasive and adhesive wear. Even though certain surfaces are quite smooth at the start of their activities, they might get roughened over time. They can gradually achieve a surface roughness equilibrium known as run-in roughness. Actual contact between rough surfaces occurs only at specific points (asperities). The wear behavior of such characters should be explored on a tiny scale. In this case, the load effects should be considered concurrently since increasing load might lead to the merging of neighboring asperities and the formation of a micro-contact (Purushotham et al. 2023).

2.1.2.5 Temperature

Coating wear rate and coefficient of friction values are significantly influenced by partly oxidized coating. High shear Stress between oxidized and partially oxidized splats generates microcracks, which increase the wear rate at ambient temperature (Parthasarathi et al. 2012).

High-temperature conditions cause tribo-oxidation, resulting in lower hardness, yield strength, and higher ductility. It leads to enhanced plastic deformation, preventing wear and preventing wear (Huang et al. 2016).

2.1.2.6 The influence of surface films on a wear process

At high temperatures, Ni-based coatings, deposited by thermal spray techniques, can form stable, protective oxides (NiO , Cr_2O_3 , and $NiCr_2O_4$). These oxides can directly impact the wear behavior and contribute to reducing the friction coefficient and wear rate (Karaoglanli et al. 2017) (Medabalimi et al. 2021), (Kiryc et al. 2023), (Bolelli et al. 2020). The coefficient of friction (CoF) and wear rate in coatings and substrates decreased gradually as the temperature increased. While considering the wear rate of the DSC Ni-20%Cr coatings in the present study, the performance is on par with the high-velocity oxy-fuel (HVOF) sprayed MCrAlY coatings and atmospheric plasma sprayed Ni-20%Cr (Medabalimi et al. 2021)(Kiryc et al. 2023).

Varga (Varga et al. 2013) investigated the wear reduction effects of oxide layer (Tribo-layer) development at increased temperatures. They observed that the growth of tribolayers at elevated temperatures, as well as thickness and appearance, were reliant on the microstructure and, more importantly, the dispersion, size, and structure of the coarse, hard phases of the materials investigated. Similarly, other authors found that the presence of tribolayer (or mechanically mixed layer-MML) increases the friction and wear resistance of the materials, particularly at high temperatures (Antonov et al. 2012)(Badisch et al. 2010)(Winkelmann et al. 2010).

When the wear debris (oxide particles) was compacted into a homogenous oxide film, the development of these protective glaze oxide layers and other intermetallic compounds enters the friction pair, reducing adhesion and ploughing on the coating, resulting in a lower CoF and wear rate (Munagala et al. 2019)(Novak and Polcar 2014)(Jiang et al. 1998)(Stott 2002).

The formation of protective layers is prevalent in unidirectional and reciprocating sliding systems. This is because the development of wear debris at the contact is facilitated in these configurations (Straffelini et al. 2001). However, Inman (Inman et al. 2005) demonstrated that such layers can form even under prohibited debris retention conditions. The formation of oxide layers can provide excellent friction control and wear prevention, but their use is limited depending on whether they occur under prescribed tribological circumstances. The ability to promote their formation and maintain their stability is so important. The impact of several nanometer-sized oxide particles on sliding steel surfaces was examined. They observed that adding small particles to certain oxides increased the production of protective tribolayers (Kato and Komai 2007).

2.1.2.7 Lubrication

Lubrication is another important aspect of wear control. Wear is heavily dependent on the lubrication process. Lubrication reduces wear in many moving systems (Chien and Cramer 2019).

2.1.2.8 Contact area

The contact area is also significant for calculating the wear rate of contacting bodies. Wear has an inverse relationship with contact area. When abrasive particles make point contact with the surface, the friction coefficient and wear increase. When the contact area is larger, the friction coefficient value decreases, and the wear rate decreases (Purushotham et al. 2023).

2.1.2.9 Counterpart

Counterpart characteristics have a significant impact on material wear. When the hardness of the counter surface material is higher, and the surface finish is lower than the disk material (workpiece), the wear rate of the counter surface is lower, and the substrate material deteriorates faster. The abrasive particles of the counterpart are harder since abrasive particles quickly enter the material during operation, and the wear rate of the substrate material is higher.

2.1.2.10 Microstructure

The microstructure is also a significant factor in influencing material wear. The relationship between microstructure and wear resistance is complex and influenced by specific wear mechanisms and tribological systems. Coarse microstructures, primarily composed of solidified hard phases, can have high hardness and resistance to abrasive wear. In contrast, fine-grained microstructures, produced through techniques like Hot Isostatic Pressing, may minimize sliding wear.

2.1.3 Techniques to Deposit Wear-resistant Coatings

Overlay coatings, specifically thermal sprayed coatings, have been seen as a reliable solution to protect the parts from wear damage and high-temperature oxidation and corrosion resistance with thermal efficiency (Habib et al. 2022), (Yamazaki et al. 2022), (Chavana et al. 2022). Several investigations have been done on the performance of their protective coatings to enhance the tribological characteristics of superalloys. Multiple studies have demonstrated that Ni-based coatings deposited over the mechanical components as a dense coating or protective bond layer to increase wear

and erosion resistance (Sampath et al. 2004)(Mahesh et al. 2008)(Purushotham et al. 2022).

The thermal spray is an industrially accepted method to deposit dense overlay coatings without impairing the original properties of substrates. Among the currently available thermal spray methods, high-velocity oxy-fuel (HVOF), Atmospheric plasma spraying (APS), and Detonation spray coating (DSC) are mostly chosen for efficient protective coatings for high-temperature applications (Sundaresan et al. 2021). One of the most significant issues of APS is that the plasma torch generates high energy and temperature, causing oxide inter-lamellar and crack-like defect formations (Xian et al. 2021). The DSC is one of the promising techniques for depositing a wide range of materials and propelling with high velocities (above 800 m/s) during the detonation spraying process, resulting in a negligible decomposition of feedstocks. Thus, dense coatings with excellent adhesion strength, low porosity, and compressive residual stresses can be achieved (Purushotham et al. 2022)(Kaushal et al. 2012).

2.1.4 High-temperature wear of materials

As technology advances, there is a huge demand for mechanical systems operating under harsh conditions such as temperatures, speeds, and environments. Elevated temperature phenomena can be seen in combustion engines, aircraft systems, mining, and metalworking operations. Most alloys and metals have a diminishing trend in hardness and yield strength at increasing temperatures. One may expect reduced wear resistance at higher temperatures based on the decline in inherent mechanical properties. However, this effect should be used with caution because other factors such as heat conduction, microstructural changes, thermal fatigue, material transfer, element segregation forming brittle phases on the substrate, or oxidation can alter the tribo-contact region, affecting the wear response of the material.

Components (gas turbine processes) in relative motion frequently suffer thermal fatigue, high-temperature creep, fatigue fracture, unexpected friction, and wear, decreasing the operational efficiency in harsh conditions (high temperature) (Shi et al. 2020)(Gautam et al. 2019)(Pham et al. 2020)(Wang et al. 2018)(Li et al. 2017)(Torres et al. 2016). Because of the temperatures, a liquid lubricant is ineffective in such

extreme environments. By incorporating a solid lubricant with high-temperature resistance into the metallic bulk components and forming a metallic composite layer with a solid lubricating composition, the mechanical components' required lubrication and improved endurance may be accomplished at increased temperatures. The reliability of aero engines is directly related to the wear resistance of turbines and blades (Zhen et al. 2014).

At normal/typical temperatures, the frictional surface exhibits dominating abrasion. No continuous protective layer is generated because the operating temperature is inadequate to grind the wear particles. The interaction of abrasion and subsequent oxidation results in extreme wear and untoward abrading of the three bodies (Purushotham et al. 2022). The most important aspects of the wear process are the loads (N) and total sliding distance (m). Apart from temperature, the sliding surface's oxidation kinetics significantly lead to material removal during wear.

Research investigations on the dry sliding friction and wear behaviors of Ni-based coatings at normal temperatures revealed the formation of mechanically mixed layers (MML) at the sliding interface, resulting in reduced friction and wear (Jiang et al. 1998)(Stott and Wood 1978).

The tribological wear study on microstructural and wear behavior of the MCrAlY (M=Ni, Co or both) coatings on a Ni-based and stainless steel AISI 304 substrates was carried out using an alumina (Al_2O_3) ball on a disc configuration tribometer at room and high temperatures. The observations at room temperature demonstrated that abrasion wear is the most dominating wear mechanism, with some adhesion and the material being plastically deformed around the track's edges (Shi et al. 2021)(Hao et al. 2019)(Pereira et al. 2015).

Many research articles have studied wear studies on Ni-based superalloys and the effect of various protective coatings on tribological properties. The primary wear mechanism of Ni-based superalloy closely corresponds to plastic deformation, and abrasive wear with high hardness and fine grain size microstructure contributes to better wear resistance (Li et al. 2015)(Günen 2020). The tribological performance of Ni-Al

was improved by adding the solid lubricant h-BN and highly hard WC–Co (Hsiao et al. 2013).

Several investigations on the increased temperature wear of metallic materials have been published (Radu and Li 2007)(Inman and Datta 2008)(Roy et al. 2004)(Wang and Li 2003). All experiments have determined that a glazing layer forms on the substrate under specified weight, temperature, and sliding speed conditions. According to Blau, the tribo-layer (glaze layer) is generated at the interface of two mating components due to continuous mechanical activity at extreme temperatures (Blau 2010).

Rynio (Rynio et al. 2014) also emphasized the function of tribo-layers, dubbed 'glazes' that form due to frictional contact at high temperatures, claiming that glazes (tribo-layers) have the potential to divide the two mating surfaces in motion and therefore prevent direct contact. Oxide layers may wear off due to repeated sliding, but new glazes develop and protect the surfaces from more damage.

Stott (Stott 2002), kato and Komai (Kato and Komai 2007) demonstrated that oxidized debris affects wear behavior at increased temperatures in several ways. It has been found that while sliding, some wear debris comes out of the interface and has no effect on wear behavior, while others become caught between the mating surfaces. The entrapped worn debris particles undergo recurrent deformation and crushing, resulting in tiny particles that are oxidized. These oxidized particles gather in some locations and stick to the mating surfaces, creating a compacted layer that acts as a load-carrying film and lowers metal-to-metal contact. If the oxide solidifies before breaking, a glazing layer is formed, and wear is generally reduced to extremely low levels. However, it has been claimed that oxides at the interface of tribo-systems are not necessarily advantageous for reducing friction and wear. Detachment of a hard and brittle oxide may have more severe wear through abrasive particles, whereas a ductile and lubricious oxide may minimise both friction and wear. The characteristics of oxides, such as strength, adherence to the substrate, and ability to be sintered, therefore generating glazing layers, are highly impacted by the materials in contact, as well as the environment and surroundings.

According to the literature, several researchers used thermal spray methods to explore the tribological behavior of NiCr coatings produced on various substrate materials. The Cr₃C₂-NiCr coating was shown to have good wear, erosion, and corrosion resistance characteristics in these tests (Karaoglanli et al. 2017), (Zhang et al. 2007).

Another study on the wear of Ni-5%Al Bi₂O₃ composite coatings improved lubricating performance at 800 °C. The improvement in wear resistance was realized by the regeneration of a protective layer on the worn surface composed mainly of Bi₂O₃ and NiO (Sun et al. 2021).

The addition of TiO₂/ZnO to Ni-5%Al coating and increases wear resistance under thermomechanical stress (Shi et al. 2020). Sliding wear performance and microstructural characterization of CoNiCrAlY bond coatings generated by Atmospheric plasma spraying (APS), High-velocity oxy-fuel (HVOF), and Cold gas dynamic spraying (CGDS) were studied. CGDS coatings exhibited higher roughness and lower volume loss than HVOF and APS coatings (Karaoglanli et al. 2014).

HVOF coatings such as MCrAlY (CoNiCrAlY and NiCoCrAlY) and NiCrMo were deposited on AISI 310 stainless steel substrates. The sliding wear resistance improved as the nickel content of the coating materials increased. The friction coefficient rises with the cobalt content (Szala et al. 2020).

Sliding wear is the most common tribological hassle, which may be attributed to various environmental and technological factors (Roy 2018)(Zakeri et al. 2022). Friction and wear reduction decisively reduces global energy saving (Medabalimi et al. 2021). Thermal spray coatings such as Cr₂O₃ hard phase reinforced NiMoAl/NiCr have shown promising results for such (Radil and DellaCorte 2016)(Lubell et al. 2008).

The transferred material is the causative factor for the formation of tribo-layers, which addresses the wear reduction in an abrasive environment at higher temperatures. The study concluded that the development, thickness, and appearance of tribo-layers at high temperatures depend on the microstructure and challenging phases of the materials studied (Varga et al. 2013). Similarly, several other researchers found that the presence of tribo-layers increases the tribological properties of the tested materials, particularly

at high temperatures (Antonov et al. 2012)(Badisch et al. 2010)(Jones and Llewellyn 2009)(Winkelmann et al. 2010).

2.2 Insitu high-temperature X-ray diffraction (HT-XRD)

XRD may be used to determine the phase of a crystalline substance. XRD may also offer information on unit cell dimensions. Because of its non-contact, non-destructive nature, X-ray is perfect for analyzing certain materials. If the wavelength and diffraction angle are known, Bragg's law may be used to determine the crystallite state of a material. X-ray examination reveals the intensity of the diffracted waves from the crystal set. This might result in the lattice parameter and elastic strain derived from peak position, crystallite size, lattice strain being calculated from peak breadth, and phase proportions from peak intensity (Choudhury et al. 2018).

A well-developed crystal has an isotropic extension to infinity. The small size of a crystal prevents this perfect growth, which increases observable diffraction peaks. Peak width analysis can yield two essential properties: crystallite size and lattice strain (Mote et al. 2012). Polycrystalline aggregates produce non-uniformity of D of particles with particle size. Crystal imperfections, such as lattice dislocation, influence the distribution of lattice constants. This distributional metric is called lattice strain (Thandavan et al. 2015).

The X-ray diffraction (XRD) method may be used to investigate lattice strain, one of the essential structural characteristics that might impact physical properties. X-ray line broadening can be used to study dislocation distribution. It also changes the peak position of the diffraction angle, which is affected by D (Khorsand Zak et al. 2011)(Rajesh Kumar and Hymavathi 2017). Other methods for measuring D and lattice strain (ϵ), but W-H is a simple method for determining D where the peak width is considered a function of 2θ (Abhijith Vijay et al. 2023).

X-ray peak profile analysis (XPPA) is a simple and effective method for measuring lattice strain (ϵ) and crystallite size (D) (Bindu and Thomas 2014). The influence of lattice strain and crystallite size can directly be correlated to the width and shift of the X-ray Bragg peaks. Several analytical routes are proposed for measuring

the crystallite size (D) and lattice strain (ϵ), which leads to the diffraction peak broadening. The Williamson-Hall (W-H), Rietveld refinement, Warren-Averbach, pseudo-Voigt function, and Fourier methods are more widely used (Mote et al. 2012)(Das Bakshi et al. 2018). The w-H method is a simplified integral peak broadening approach assuming a uniform deformation model (UDM), and the technique is relatively simple to adopt (Maniammal et al. 2017). Besides, the W-H method can also consider the crystalline anisotropic (elastic constants) (Rosenberg et al. 2000)(Biju et al. 2008).

2.2.1 Coefficient of thermal expansion

Thermal barrier coatings (TBCs) design comprised of superalloy substrate, bond coat, and ceramic top are deposited using thermal spray methods. The strain tolerance due to the high in-plane compliance can be achieved by the high porosity and an array of segmented cracks or columnar structures (Jackson et al. 2016). TBC systems usually fail due to residual stress caused by the thermal expansion mismatch at the coating and substrate interface. Whatever the location of the failure, the cracks initiate due to the significant thermal expansion mismatch between the substrate, bond coat, and ceramic top coat (Shen et al. 2022). Therefore, examining the coefficient of thermal expansion (CTE) of new materials is essential. Furthermore, the CTE mismatch at the interface might cause rumpling, which leads to coating spallation (Evans et al. 2001)(Balint and Hutchinson 2003).

Internal stresses are generated during processing and service, and if not appropriately handled, they can lead to premature yielding or cracking (Bano and Nganbe 2013)(Biermann et al. 1996). Due to the difficulties of obtaining real-time information at various temperatures, the contribution of changes in the thermal expansion (CTE) coefficients among different phases to thermal stress is frequently underestimated. The availability of superalloy CTEs at increased temperatures, particularly those of distinct phases, is crucial for determining the optimal thermal and machining technique. Mechanical dilatometry, optical imaging, and interference approaches can only be employed to calculate the mean CTE of bulk materials. The

CTE measurement of single-phase alloys usually be precise; however, the CTE of two-phase alloys is determined by considering the volume fraction of secondary phases.

Haynes et al. calculated the CTE of different types of alloys based on the composition, where the CTE values ranged from $15\text{-}20 \times 10^{-6}/\text{K}$ at $1100\text{ }^{\circ}\text{C}$. More published data were available for wrought IN718, though this was limited to a maximum of $900\text{ }^{\circ}\text{C}$. The CTE values of wrought IN718, IN620, and IN625 are limited to a temperature of $900\text{ }^{\circ}\text{C}$ (O'Flynn et al. 2020). The CTE of IN600 was $18.1 \times 10^{-6}/\text{K}$ at 1200 K , measured by HT-XRD (Raju et al. 2004).

However, little information about such high-temperature overlay coatings' thermal expansion and recrystallization is available. As stated above, material properties will drastically influence intra-splat cohesion (the integrity of coating), interfacial adhesion (adhesion between the substrate and coating), and the coated components' lifetime. HT-XRD technique is a complemented method to evaluate coatings lattice and phases. Information about crystallite size, lattice strain, and lattice parameters with temperature can be obtained to comprehend the properties of the materials. Indeed, the in-situ HT-XRD can help measure the lattice strain and lattice parameter coefficient of thermal expansion without detaching the overlay coating from the substrate. Hence, the methodology is faster and more precise (Kala et al. 2022)(Liu et al. 2022).

Conventionally, thermal expansion has been determined using the dilatometry method, as seen from the literature, where the coatings must be detached from the substrates. However, the measurement is complicated and complex as the free-standing coatings tend to bend/roll during the expansion/contraction due to the large magnitude of residual stress developed during the coating process. The idea of the present study was to evaluate the thermal expansion and understand the recrystallization of the as-deposited overlay coatings. So, the experiments were carried out in a controlled atmosphere to avoid the influence of atmospheric oxygen or other elements. Unwanted pick up of oxygen will change the chemistry of the outer surface layer and the property (thermal expansion).

The dilatometry technique has been generally used to measure thermal expansion, as demonstrated in the literature, where the coatings must be separated from the substrates. In-situ HT-XRD is considered a useful method for evaluating the thermal expansion of NiCoCrAlY deposited by DSC in a controlled environment (Kala et al. 2022). However, it has not been discussed how the coating process conditions impact the thermal expansion, recrystallization, and stress relaxation accomplished by in-situ HT-XRD.

In recent years, the influence of other critical temperature-dependent properties, such as thermal expansion, recrystallization, stress relaxation, and oxidation on the dry sliding wear behaviour of Ni-based composite coatings (Ni-5%Al and Ni-20%Cr) at elevated temperatures (25 °C and 850 °C) has not been explored. The dilatometry technique has been generally used to measure thermal expansion, as demonstrated in the literature, where the coatings must be separated from the substrates. Conversely, in-situ HT-XRD has been considered an effective tool for evaluating thermal expansion, recrystallization, and stress relaxation (Kala et al. 2022) (Abhijith Vijay et al. 2023). The data generated from the HT-XRD, together with the proven analysis method such as the Williamson-Hall (W-H) method (Maniammal et al. 2017), would be highly beneficial to evaluate and correlate the temperature-dependent materials properties (Abhijith Vijay et al. 2023).

2.3 Phase diagrams

2.3.1. Ni-Al Phase diagram

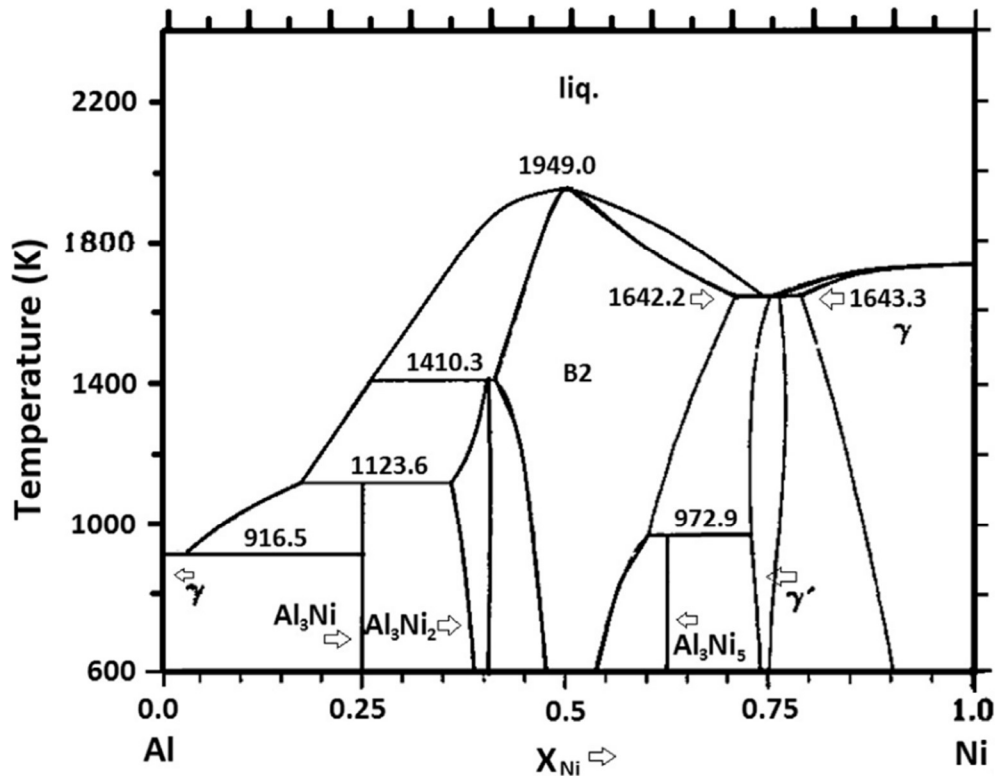


Fig. 2. 1. Binary Al–Ni phase diagram (Bochenek and Basista 2015).

The Al-Ni system is a significant topic due to its high melting intermetallic phases, such as the $AlNi_3$ compound. It is crucial for strengthening nickel-base superalloys and providing a protective layer against oxidation and sulfidation at high temperatures. Research has primarily focused on the solid-solid relationship between Ni and Al, as diffusion in the solid state is crucial for creating and degrading aluminide coatings on heat-resistant alloys. However, the interaction between liquid Al and solid Ni has received little attention. Recent studies have explored the interaction between liquid Al and solid Ni, discovering only the Al_3Ni and Al_3Ni_2 phases following isothermal reactions at 600, 700, and 800 °C and ensuring good thermal stability (Bochenek and Basista 2015) (Schilke 2004).

2.3.2. Ni-Cr Phase diagram

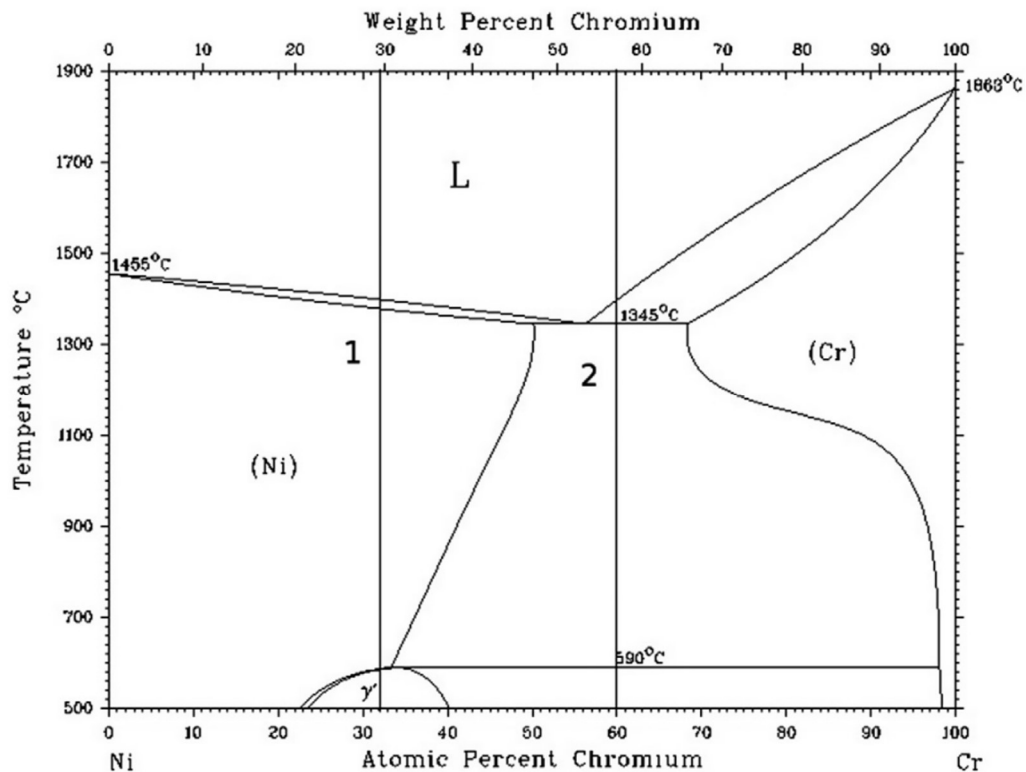


Fig .2. 2 Phase diagram of Ni–Cr system (Ustinovshikov 2012).

Researchers at the United States Department of Energy (DOE) have utilized the CALPHAD method and Thermo-Calc to construct binary phase diagrams for Ni-Cr, Ni-Mo, Ni-W, and, among others, Cr-Mo, with varied degrees of success (Andersson et al. 2002). The Ni-Cr binary phase diagram was one of the areas where improvement was achieved. The phase diagram for this system, reveals the ordering and synthesis of Ni₂Cr at low temperatures (below 590 °C), which is not anticipated by Thermo-Calc using an existing thermodynamic database for Ni (Chan et al. 2006).

According to (Chan et al. 2006), the ordering process that occurs around Ni₂Cr is a first-order reaction best characterised by the 590 °C peritectoid the decomposition of (Ni)+(Cr) to γ' (ordered Ni₂Cr). However, that component of the phase diagram must be regarded provisional (Chan et al. 2006). The Ni-Cr phase diagram at higher temperatures (>900 K) was estimated using a mix of first-principles computational techniques and the CALPHAD methodology. The ordering reaction near 590 °C was not expected. (Miller et al. 2018) brought out and analyzed in depth the failure of the

first-generation CALPHAD algorithms to predict phase diagrams for certain ordered phases (Ustinovshikov 2012). As a result, there appears to be a need to update the thermodynamic model or the database for the Ni₂Cr phase.

2.4 Objectives and Scope of Work

2.4.1 Scope of proposed research work

The study of high-temperature tribology has significantly evolved in recent years, and it is evident that there is a need to get a more in-depth understanding of this challenging and demanding area of research. As a result, the primary objective of this research is to develop and enrich the knowledge of the wear-related information of different materials at higher temperatures. The high-temperature X-ray diffraction (HT-XRD) explored high-temperature properties such as stress relief, recrystallization, and thermal expansion.

2.4.2 Research gaps

In recent years, there has been an increase in the number of applications and technical processes that operate in severe conditions such as high temperatures. There is a need for innovative information related to tribological phenomena occurring at elevated temperatures and technical solutions to enable the development of new technologies and methods.

The friction and wear behaviour of DSC sprayed Ni-based (Ni-5wt%Al, Ni-20%Cr) coatings on IN718 superalloys are particularly interesting because they are commonly used in hot section components and can also be used in a wide range of other technological applications, particularly at high temperatures. Several studies on Ni-based composite coatings have been conducted to bridge knowledge gaps, but high-temperature tribology has been given insufficient attention.

According to the literature survey, the tribological behavior of Ni-based (Ni-5%Al and Ni-20%Cr) coatings with Al₂O₃(alumina) counterparts at high temperatures and high-temperature characteristics such as stress relieving, recrystallization, and thermal expansion effects on improving the tribological properties at elevated temperatures have yet to be investigated. Although adhesion and oxidative wear have been the most

important wear mechanisms in high-temperature tribological systems, a thorough understanding of the mechanisms is still inadequate.

Considering the wide range and lack of information, it is acceptable to conclude that broader and more multidisciplinary tribological studies at increased temperatures are needed.

2.4.3 Objectives of the proposed research Work

1. To examine the microstructure of the detonation sprayed Ni-5%Al and Ni-20%Cr coatings
2. To evaluate surface morphology and microhardness of coatings
3. To determine the crystallite size, lattice strain, and thermal expansion characteristics of DSC coated samples
4. To investigate dry sliding friction and wear behaviour of Ni-based coatings on IN718 substrate at ambient conditions (25 °C) and elevated temperature (850 °C)
5. To analyze the ambient condition (25 °C) and high-temperature (850 °C) wear tracks and identify the wear mechanisms

2.4.4 Limitations

The tribological experiments performed in this work aren't intended to replicate real-world applications. Even though some coating materials and circumstances are related to high-temperature activities, this research aims to understand better temperature-dependent material characteristics such as stress relieving, recrystallization, thermal expansion, and oxidation. At increased temperatures, a significant effect on the dry sliding wear resistance of the detonation-sprayed coating has been explored with an appropriate mechanism.

2.4.5 Flow chart of a proposed work

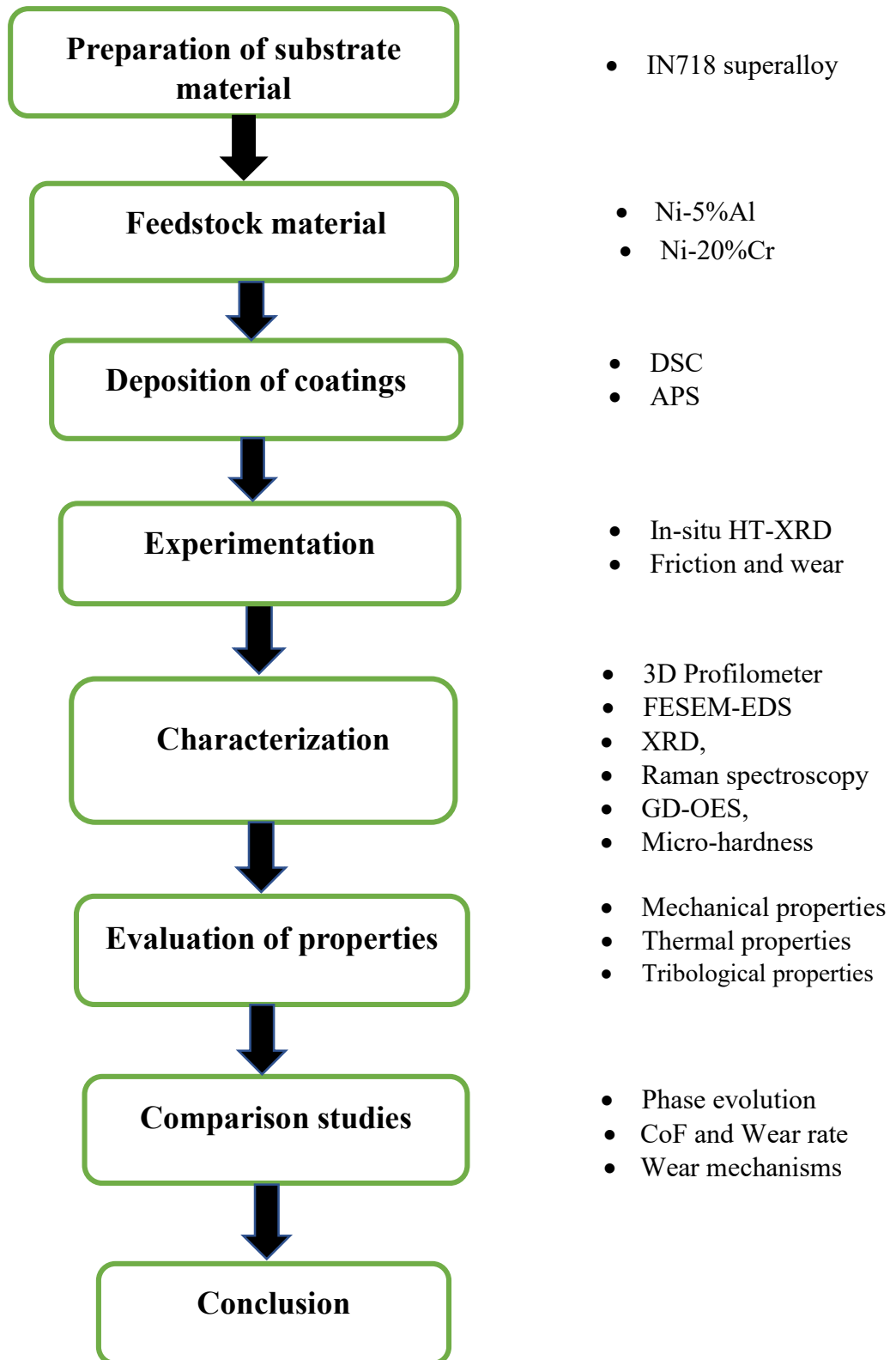


Fig. 2. 3 Flow chart of a proposed activity

2.5 Outline of Thesis

The current thesis presents a systematic study of the proposed objectives. A brief skeletal structure of the thesis is given below,

Chapter 1:

This chapter discusses the components of a gas turbine engine and emphasizes the significance of using thermal spray coating on superalloys. The strength of the substrate materials chosen for investigation, Inconel718, and high-temperature friction and wear behaviour of the coating during operating conditions are also discussed.

Chapter 2:

This chapter includes a detailed literature survey on high-temperature friction and wear, a clear representation of the material chosen, its working environment, and the research objectives with the work plan. Thermal spray coating materials for high-temperature coating methods and the test conditions with the work plan are presented. Finally, the chapter ends with the organization of the thesis.

Chapter 3:

Substrate and feedstock materials, coating methodology, experimental setup, testing evaluation procedure, and characterization tools are discussed in this chapter.

Chapter 4:

This chapter discusses the dry sliding friction and wear behaviour of Ni-based coatings material at elevated temperatures. To compare coated INI718 are compared to the bare alloy. The result from metallurgical characterization techniques is discussed in detail. From the results, the effect of stress relieving, recrystallization, thermal expansion, and coating oxidation have been discussed with a suitable mechanism.

Chapter 5:

Based on the results and discussion, the Summary and conclusion of the research work and the scope for future work are reported in this chapter.

CHAPTER 3

EXPERIMENTAL PROCEDURE AND MATERIALS

3.1 Experimental procedures

3.1.1 Substrate

In this work, nickel-based superalloy (IN718) was employed as the substrate material, and the coefficient of thermal expansion value ranges from $15\text{-}15.5 \times 10^{-6}/^\circ\text{C}$ at 1200°C (Haynes et al. 2014). The usual chemical composition and average microhardness of the substrate material are listed in Table 3.1. Samples with diameters of around $20\text{cm} \times 20\text{cm} \times 5\text{cm}$ are cut from the sheets and polished using emery papers of 200, 400, and 600 grit sizes, followed by 1/0, 2/0, 3/0, and 4/0 grade abrasive sheets. Finally, before coating deposition, the samples are degreased with acetone and grit blasted with alumina powders (Grit 45) (36 mesh size) to create a surface roughness, which ensures better metallurgical bonding between the coating and substrates interface and achieves good adhesion.

Table 3.1. Chemical composition of nickel-based superalloy (IN718).

Substrate	Chemical composition (wt%)											Microhardness (HV _{0.2})
	Ni	Fe	Cr	Ti	Al	Mo	Mn	Si	Cu	C	Nb	
IN718	53.88	17.68	17.87	1.2	0.55	2.92	0.14	0.24	0.11	0.03	4.97	195±11

3.1.2 Feedstock material

Two commercially available thermal spray-grade feedstock powders of NiAl (Amperit 281, H.C. Starck GmbH, Germany) and NiCr (Amperit-251, H.C. Starck GmbH, Germany) with a particle size of 4-45 μm were used for the present study. The nominal chemical composition of these powders is presented in Table 3.2. These feedstock powders are heated and dried to remove the moisture before coating deposition.

Table 3.2. Nominal chemical composition of feedstock powder used.

Powders	Chemical composition (wt%)		
	Ni	Cr	Al
NiAl	95	--	5
NiCr	80	20	--

3.1.3. Coating deposition techniques

The coating was deposited on the IN718 substrate by atmospheric plasma spraying (APS) and Detonation spray (DSC) techniques. APS coatings were performed by a plasma-sprayed torch (Sulzer Metco 9 MB gun). Hydrogen and argon were used for plasma generation. Multiple pass coating deposition was performed using a 6-axis (ABB) robot manipulator to produce a coating of the desired thickness. For DSC, a horizontal DSC system (ARCI, Hyderabad) with a long barrel was used to deposit coatings. The APS requires high temperatures that may degrade the substrates. They were cooled using air jets from behind while spraying. Because detonation spraying involves considerably lower temperatures, no such substrate cooling was used. Compatibility and thorough process parameter optimization were completed before coating generation. The coating thickness of about $250 \pm 25 \mu\text{m}$ was deposited on IN718 substrates using both deposition methods. The optimal spraying process parameters are given in Table 3.3.

Table 3.3. Spraying parameters for APS and DSC coatings.

Coating parameters	APS	DSC
Primary gas flow rate (SLPM)	42 (Argon)	31 (Acetylene)
Secondary gas flow rate (SLPM)	5 (Hydrogen)	38 (Oxygen)
The voltage generated (V)	62	--
Plasma arc current (A)	500	--
Powder feed rate (g/min)	50	--
Standoff distance (mm)	100	165
Frequency (Shots per second)	--	3

* SLPM-Standard liter per minute

3.2. Testing methods

3.2.1 Microhardness examination

Microhardness attributes change the material mechanical characteristics associated with material wear behavior. Hardness tests were carried out on cross-section specimens with a coating thickness of $250 \pm 25 \mu\text{m}$, and the surface of the samples was finely polished using SiC grit sheets. Hardness measurements were performed after the wear test at various temperatures ($25 \text{ }^\circ\text{C}$ and $850 \text{ }^\circ\text{C}$) using a Vicker micro-hardness tester (Shimadzu, Hmv-G20st) to investigate the effect of temperature on the hardness and a pyramid-shaped diamond indenter pressed on a specimen with a 136° angle between opposing sides. At least 10 microhardness values were taken from each sample under 200g loads and a dwell duration of 15 seconds. Four samples from each state were statistically analyzed, obtaining accurate average micro-hardness values with standard deviation errors.

3.2.2. Tribological evaluation

Tribological wear studies for dry sliding friction coefficient (CoF) and wear resistance evolution were performed on coated substrates ($20\text{mm} \times 20\text{mm} \times 5\text{mm}$) using a 3 mm diameter spherical alumina (Al_2O_3) counterpart with a hardness of $700 \pm 20 \text{ HV}$. Al_2O_3 retains high hot hardness and excellent heat stability. Its use approaches a service situation, including contact with a hard counterpart (for example, a ceramic) or a hard phase-containing counterpart (Bolelli et al. 2015). As the introduction mentions, this applies to both blade tips sliding against abradable seals and foil bearings. Although specialized test rigs are available to replicate the precise working conditions in applications (Radil et al. 2016)(Watson and Marshall 2018), Al_2O_3 is also chemically inert. As a result, it does not produce extra tribo-chemical interactions, which would complicate interpretation and limit the generalizability of the findings. It was determined that a transfer coating generated on the counterpart while sliding had an essential role in the composites' capacity to self-lubricate.

Coated sample surfaces were polished to a roughness of $\text{Sa} \leq 1.9 \pm 0.4 \mu\text{m}$ using SiC sheets before the experiments to preserve the same surface conditions. These

friction and wear tests were performed at 25 °C and 850 °C in stagnant air using a high-temperature tribometer (HTT) with a ball-on-disk tribometer (Anton Paar, Austria) seen in Fig. 3.1. The tribo-system was calibrated, and the test parameters were established following the ASTM G99 standard (Standard 2000) in Table 3.4. It was heated to 850 °C at 10 °C/min and then stabilized for one hour. The difference between the actual and set temperatures was ± 2 °C. At least three test repetitions were performed for each condition to determine statistics and test repeatability.

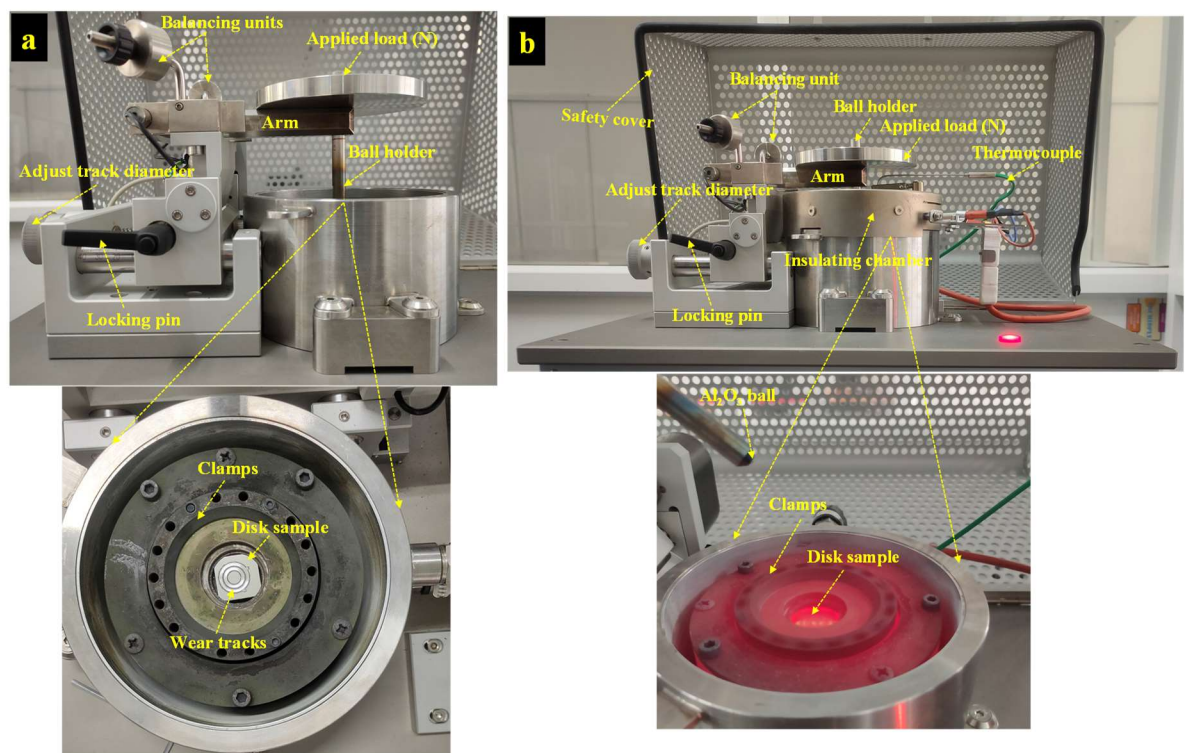


Fig. 3.1. Experimental setup of a ball-on-disk tribometer at two elevated temperatures. (a) Room temperature (25 °C), (b) High temperature (850 °C).

Table 3.4. Test parameters for dry sliding friction and wear experiments.

Test parameters	Conditions
Counter material (ϕ)	Alumina (3mm)
Applied load (N)	6 and 10
Temperature ($^{\circ}\text{C}$)	25 and 850
Sliding speed (m/s)	0.1
Sliding distance (m)	138
Track diameter (radius)	4 and 6
Time (min)	23
Motor speeds (rpm)	238.73 and 159.15

3.2.3. In-situ high temperature X-ray diffraction (HT-XRD)

Before the in-situ HT-XRD experiments, the coated samples were reduced to a dimension of 10mm x 10mm x 1mm. The heat is transmitted from the platinum heating foil to the coated substrate. The samples must be thin down to 1 mm or less to ensure uniform heating during the measurement during the in-situ HT-XRD experiments. The coated substrates were polished using SiC grits to preserve the same surface condition. The in-situ HT-XRD experiments were carried out using a Malvern Panalytical 3rd generation Empyrean XRD equipped with an ANTON PAAR heating stage. The coated samples were placed on the platinum heating foil in the heat stage, as shown in Fig. 3.2(d). An Rh-Pt thermocouple welded with platinum foil measures the temperature. The temperature is precisely adjusted to within $\pm 1^{\circ}\text{C}$.

Before the experiment, the chamber was flushed with high-purity argon, and a vacuum pressure of around 10^{-4} millibar was sustained. The Cu-K α ($\lambda=0.154$ nm) source was used for diffraction at a temperature interval of 100 $^{\circ}\text{C}$ at each stage, as seen in Fig. 3.2(a). The computerized system controlled a mean scan step size, a heating rate, and a holding period at each measurement temperature. The Panalytical X'pert high plus software was used for primary collecting data and preliminary analysis. The 2θ

calibrations for the room temperature (25 °C) run are performed using silicon standards.

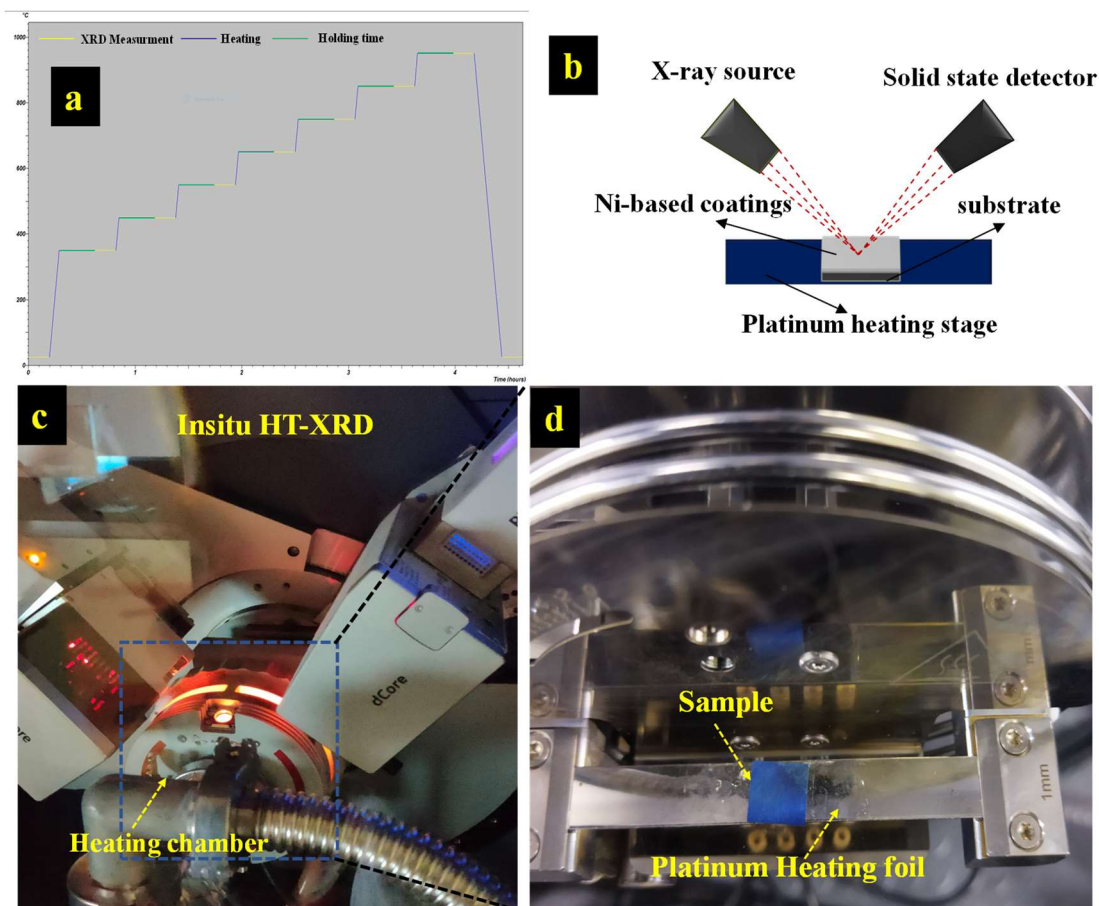


Fig. 3.2. HT-XRD setup. (a) Heating program of the experiment (b) Schematic diagram of HT-XRD (c) Heating setup (d) Sample stage (Platinum heating foil).

Table 3.5. Test parameters for in-situ HT-XRD.

Test parameters	Conditions
Vacuum pressure (millibar)	10^{-4}
Scan step (°)	0.026
Heating rate (°C/min)	10
Temperature (°C)	25 and 1150
Diffraction angles	30-80
Holding period (min)	20

3.3 Surface characterization

An XRD analysis was used to characterize the phase and crystal orientation at the surface layers using X'Pert High Score Plus software (Panalytical). The phases and crystal orientation were analyzed using the International Center for Diffraction Data (ICDD) and Crystallographic Open Database (COD, 2021). The Rietveld refinement was used to quantify the phases. The crystallite size (D) and lattice strain (ϵ) were measured using the W-H technique. The Pseudo Voigt analytical function is a linear Gaussian+Lorentzian function. The experimental data were fitted using the Pseudo Voigt and asymmetry functions. The weighted R profile (Rwp) and goodness of fit (GOF) parameters assessed the fit quality between experimental and computed diffraction data.

A confocal optical scanning 3D profilometer (NANOVEA, ST-400, USA, resolution 100 μm) was used to quantify surface roughness and surface profilometry (2D and 3D topography). A 3D surface profiler (Fig. 3.3) was used to scan and analyze the disc wear scar to calculate wear loss using the breadth and depth profiles and wear rate. Metallurgical identification (morphology, tribolayer formation, wear mechanism) of samples was performed on a cross-section and surface morphology using secondary electron (S.E) and backscattered electron (BSE) detectors at different magnifications in a JEOL (JSM6300, Japan) Field emission scanning electron microscope (FESEM) with the 20 mm working distance and voltage of 20 Kv. FESEM-EDS (EDAX, JSM6300, Japan) performed a microanalysis to quantify the chemical composition and elemental mapping in the region of interest. Porosity was measured on cross-sectional microstructure images using Image-J software.

A Raman spectrometer (Renishaw centrus 2R4P63, Wire 5.4 - software, U.K.) was used to analyze the typical composition of oxide layers on worn surfaces. The Raman data were continuously collected with a 10s exposure time and two accumulations. Glow discharge-optical emission spectroscopy (GD-OES) was used to examine the quantitative depth profiles and the chemical composition of the coatings in a DC discharge in argon using a GDA750 RF Generator (GD profiler-2, Horiba, France) in a DC discharge in argon, with Flushing time: 70 s, Preintegration time: 30 s,

Background: 5 s, Depth: 52.35 μm , Pressure: 700 Pa, Power: 35 W, Module: 6 V, Phase: 5 V.

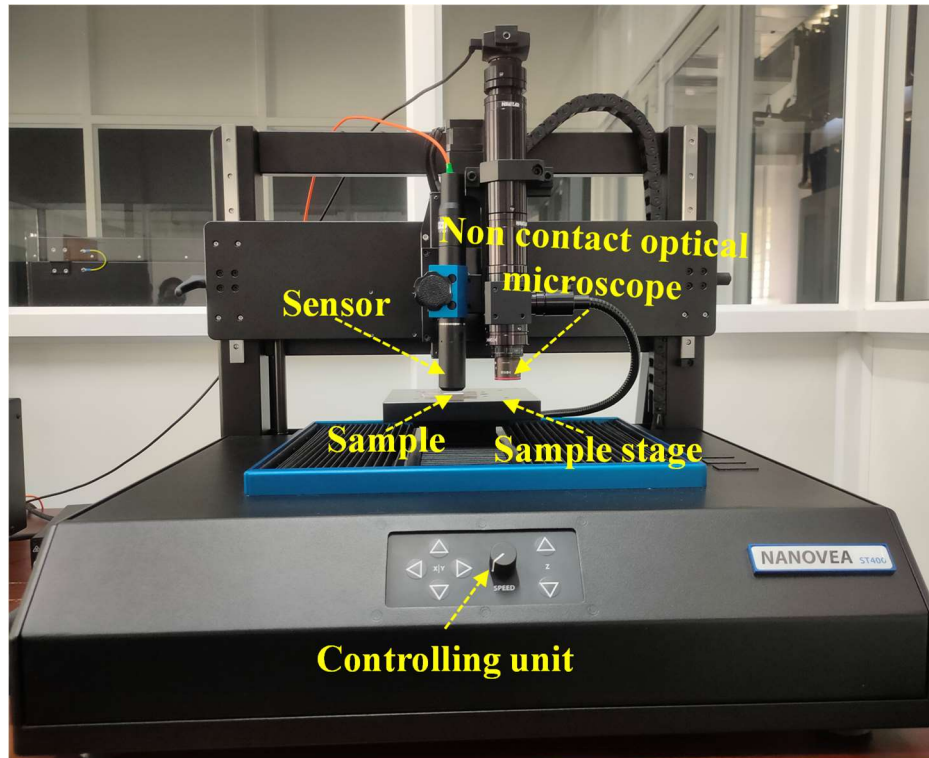


Fig. 3.3. Non-contact optical scanning 3D profilometer.

3.4 Calculation procedure

3.4.1. Coefficients of thermal expansion (CTE)

Thermal expansion coefficient values were calculated using calibrated lattice parameters vs. temperature. The CTE values in the heating case are computed using the room temperature lattice parameters. The mean CTE, α , is from 25 °C (Kala et al. 2022).

$$\alpha = \frac{l-l_0}{l_0(T-T_0)} \quad (3.1)$$

Where α indicates the CTE, l is the expansion length of a lattice parameter at temperature T , and l_0 represents the original length of the lattice parameter at temperature T_0 , which is usually taken from room temperature at 25°C.

3.4.2. Scherrer method

The XPPA measured the peak broadening attributable to dislocation with lattice strain and crystal size. Both instrumental and sample effects have been considered to determine the breadth of the Bragg peaks. Instrumental broadening must be considered to examine the crystallite size (D) effect and lattice strain (ϵ). A diffraction pattern should be collected from the silicon (Si) standard material, which helps evaluate instrumental broadening. The average crystallite size (D) was obtained from the Scherrer formula shown below.

$$D = K\lambda / \beta_{hkl} \cos\theta_{hkl} \quad (3.2)$$

Where D denotes average crystallite size, K is the Debye - Scherer constant (0.94-1.15), λ is the wavelength of Cu-K $_{\alpha}$ radiation ($\lambda=0.154$ nm), β_{hkl} is the peak widening of the hkl diffraction peak measured at FWHM intensity, and θ_{hkl} is the diffraction angle ($^{\circ}$) samples. It gives a very approximate estimation of the crystallite size.

3.4.3. Williamson–Hall (W–H) plot

Unlike the Scherer method, the W-H process considers line broadening for calculating precise lattice strain. UDM assumes that the lattice strain is constant in all crystallographic orientations and ignores crystal anisotropy. W-H plotting $\beta_{hkl}\cos\theta$ versus $4\epsilon\sin\theta$ and fitting the data with a linear equation is written as (Kala et al. 2022).

$$\beta_{hkl}\cos\theta = \epsilon(4\sin\theta) + \frac{K\lambda}{D} \quad (3.3)$$

From the above equation, the y-axis is $\beta_{hkl}\cos\theta$ and $4\sin\theta$ is the x-axis. The y-intercept ($K\lambda/D$) and liner slope fit will directly give the values of crystallite size (D) and micro-strain (ϵ), values respectively.

3.4.4. Specific wear rate

After the wear test, the topography of the entire wear tracks was measured using the non-contact optical 3D profilometer. It was employed to scan and analyze the wear scar to evaluate the wear rate and wear volume with the help of width and depth profiles. According to the ASTM G99 standard, the specific wear rate was calculated using the following Eq. (3.4) (Kiryc et al. 2023):

$$\omega = \frac{V}{D \times L} [\text{mm}^3/(\text{N.m})] \quad (3.4)$$

ω was the wear rate in $\text{mm}^3 \text{N}^{-1}\text{m}^{-1}$, V was the wear volume loss in mm^3 , measured by a 3D profilometer, D indicated the total sliding distance (m), and L represented the applied load (N). Errors in calculated ω values and μ are comparable to the corresponding standard deviation.

CHAPTER 4

RESULTS AND DISCUSSIONS

4.1. Sliding Wear Behaviour of Ni-5%Al Coating Deposited by Detonation Spray on IN718

4.1.1. Characterization of IN718 and Ni-5%Al coated samples

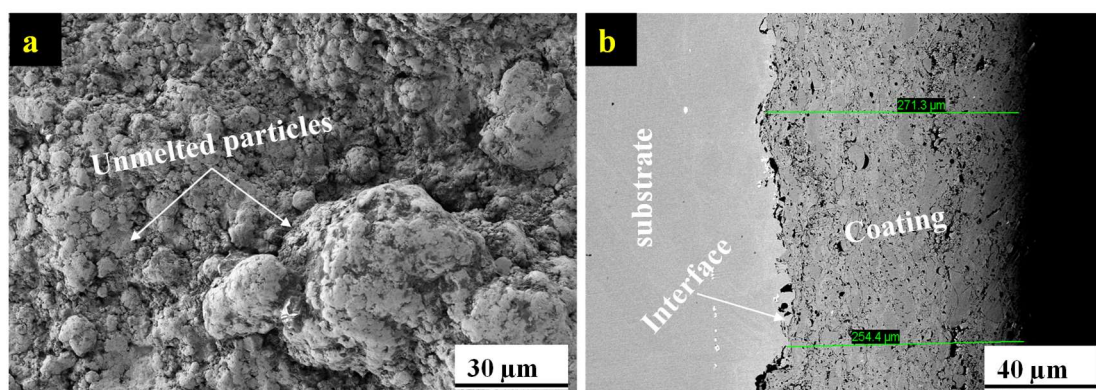


Fig. 4.1. SEM micrographs of as-deposited Ni-5%Al coating; (a) Surface morphology of as-sprayed condition (b) Cross-section of coating.

As shown in Fig.4.1(a), the coating surface morphology was moderately homogeneous, partially melted, and unmelted powder particles entrapped on the coating surface in the detonation spraying coating (DSC). The as-deposited layer was dense and uniform, with sparse surface porosity, and had a typical lamellar structure. Fig. 4.1(b) illustrates the cross-section image of the Ni-5%Al coated substrate. The qualitative examination shows that the coating had shown excellent adhesion between the interface of the coating and substrate material. Further, there was no detachable delamination or evidence of micro and macro cracks. Few fine pores at the interface may be attributed to the molten or semi-melted or unmelted particles during thermal spraying. Adhesion is purely mechanical interlocking between the asperities of the substrate and rapidly solidified molten or semi-melted or unmelted particles. The coating thickness was around $250 \pm 28 \mu\text{m}$ measured at different locations in the SEM micrographs.

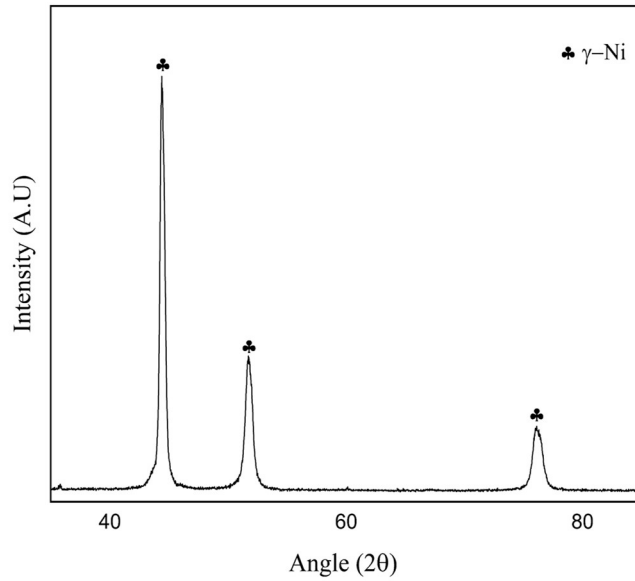


Fig. 4.2. XRD patterns of as-deposited Ni-5%Al coating.

Fig. 4.2 shows the XRD analysis of the as-deposited Ni-5%Al coating, revealing the presence of a crystalline γ -Ni phase with a crystallite size of 15.4 nm using the Scherrer formula. In this instance of Ni-5%Al coated superalloys, the primary phase is γ -Ni, an FCC solid solution.

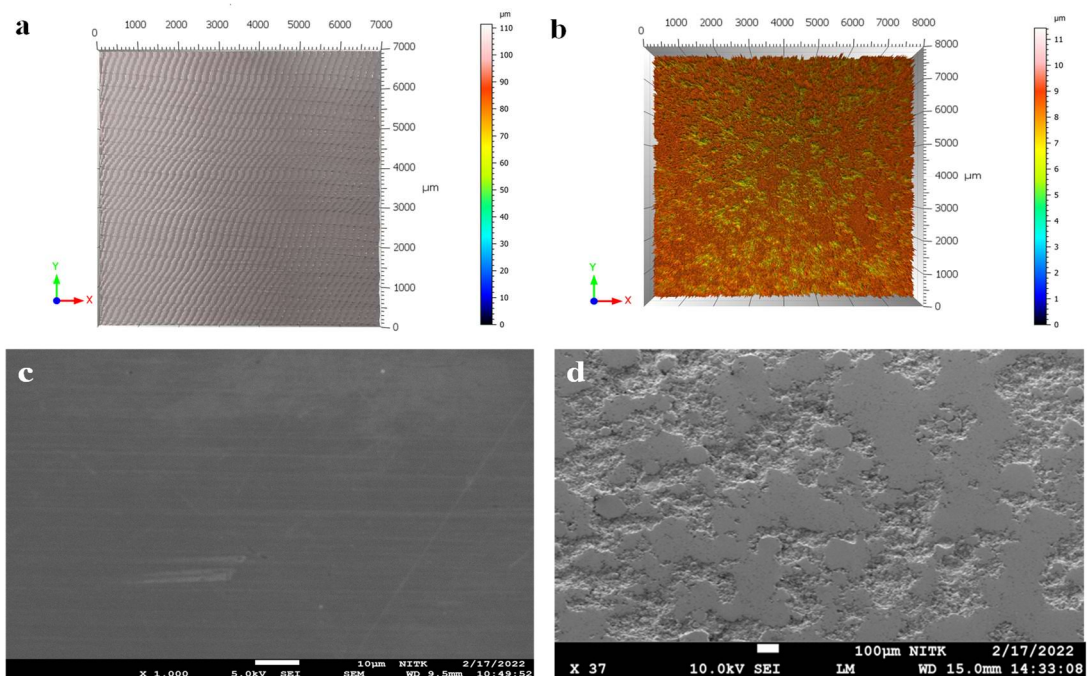


Fig. 4.3. Non-contacting optical microscope 3D-profile and FE-SEM micrographs of the polished samples: (a and c) IN718 and (b and d) Ni-5%Al coating.

The partially melted and unmelted particles on the surface of the Ni-5%Al coating samples were removed using metallography polishing. As seen in Fig. 4.3, the polished surface of the coating and uncoated IN718 appeared to be relatively smooth and uniform. The surface roughness values (S_a) of IN718 superalloy and Ni-5%Al coated samples have been smoothed to 1.102 μm and 0.392 μm , respectively, as given in Table 4.1.

The microhardness of IN718 superalloy and Ni-5%Al coating are given in Table 4.1. The micro-hardness of DSC Ni-5%Al coating was superior to that of bare IN718 substrate. The high microhardness of the coating can be correlated to the high residual stress due to the high cooling rate and excessive plastic deformation during coating formation (Bai et al. 2011).

Table 4.1. Mechanical properties of substrate and coating.

Samples	Hardness ($HV_{0.2}$)	Roughness (S_a , μm)
IN718	195 \pm 11	1.102
Ni-5%Al	305 \pm 21	0.392

4.1.2 Sliding Wear

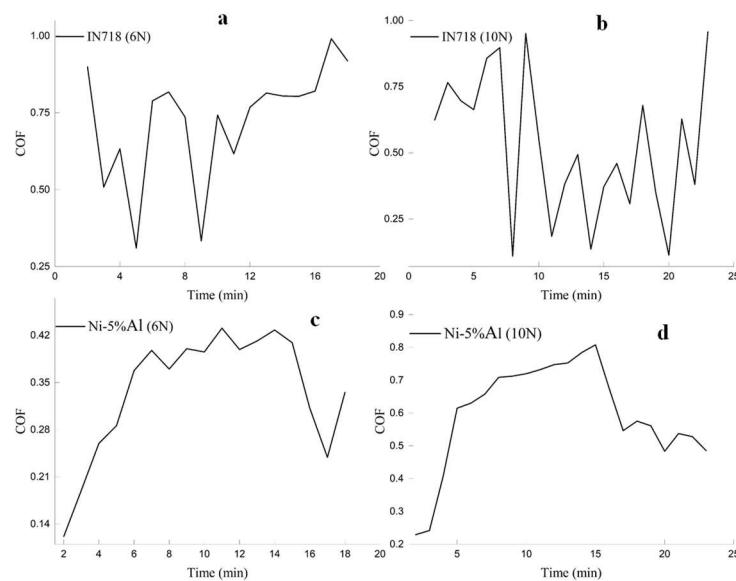


Fig. 4.4. Coefficient of friction curves of the IN718 and coating at 25 °C under 6N and 10N loads: (a and b) IN718 substrate (c and d) Ni-5%Al coating.

The friction coefficient (CoF) during the dry sliding wear test carried out at different loads is given in Table 4.2, and the CoF vs. Time graph is shown in Fig. 4.4. The results demonstrated that the uncoated IN718 suffered the highest friction compared to the Ni-5%Al coating under the sliding wear conditions. The trend in variation of CoF as a function of loads (6N and 10N) for IN718 and coated IN718 appeared to be the same. The partial oxide layer on the sample's surface was ruptured at the start of the experiment, significantly raising the CoF due to dry friction and maintaining stability beyond the run-in time.

The volume loss increases as the average load increases from 6N to 10N, while the resistance toward dry sliding wear appears high for Ni-5%Al coated IN718. Coated IN718 exhibited superior wear resistance in both loading conditions than bare IN718. While varying the load from 6N to 10N, no significant changes in CoF were noticed in the IN718 substrate, as the wear mechanism (abrasion wear) appeared to be the same.

The average CoF of coatings at varying loads was low compared to the IN178 substrate. The average CoF increased from 0.29 to 0.47 as the load increased from 6N to 10N, a common trend expected in dry sliding wear. The ramping up of CoF may be attributed to the partial oxide film of the Ni-5%Al coating being ruptured at the beginning of the experiment. Then, oxide debris accumulated on the wear track between the specimen and the ball contact interface. The presence of worn debris first causes variation in the CoF. When three-body friction develops, CoF decreases. The continuous variation in the CoF was noticed due to repeated generation and removal of oxide debris at the interface during the sliding wear test (Szala et al. 2020).

Table 4.2. Coefficient of friction of IN718 and Ni-5%Al coating at 25 °C temperatures under 6N and 10N loads.

Samples	Loads (N)	Diameter of the wear track (mm)	Friction coefficient (μ)
IN718	6	6	0.71±0.2
	10	10	0.70± 0.4
Ni-5%Al	6	6	0.29±0.1
	10	10	0.47±0.9

4.1.3 Worn out Surface Morphology analysis by 3D profilometer

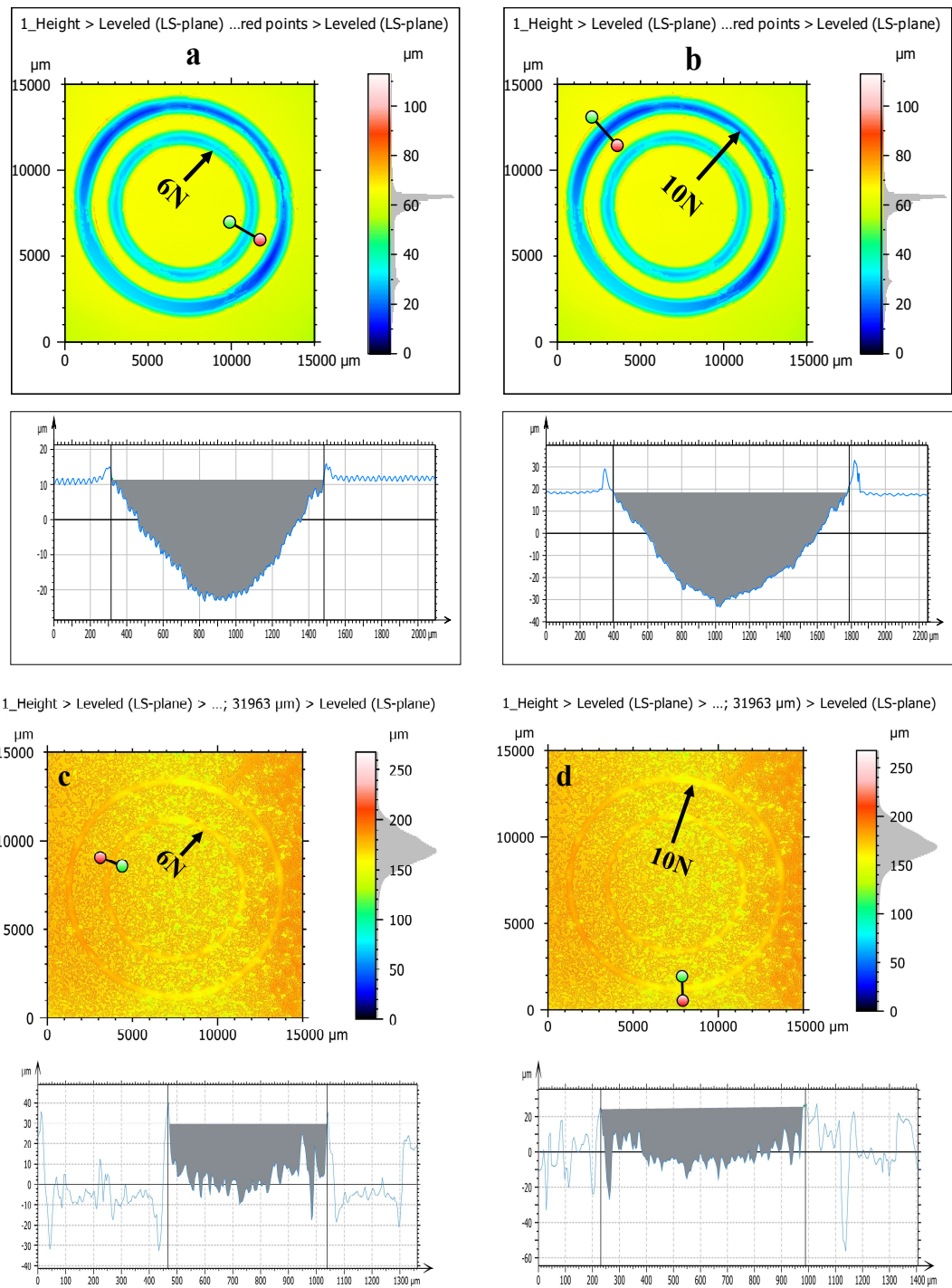


Fig. 4.5. Non-contacting optical microscope 3D profile of wear tracks with depth profiles under 6N and 10N loads: (a and b) IN718 substrate (c and d) Ni-5%Al coating.

Fig. 4.5 displays the 2D profiles of wear tracks of IN718 substrate and Ni-5%Al coating at 25°C. The amount of material lost was determined from 2D confocal profiles (Fig 4.5(a-d)) by evaluating the width and depth of the wear tracks for typical loads of 6N and 10N of inner and outerwear tracks with diameters of 4mm and 6mm, respectively, with a total of 5500 cycles. It is to be noted that the effective area of contact between the alumina ball and IN718 substrate is considerably higher than the effective area of contact between the alumina ball and coating. The same has been reflected in the wear characteristics also.

The volume loss of materials was calculated from these profiles by considering the width and depth of the wear tracks. Due to the higher hardness, the wear rate of Ni-5%Al coating was lower than the IN718 substrate, as shown in Fig. 4.6. The superior coating performance can be attributed to the dense microstructure with a crystallite size of about 15 nm and high microhardness.

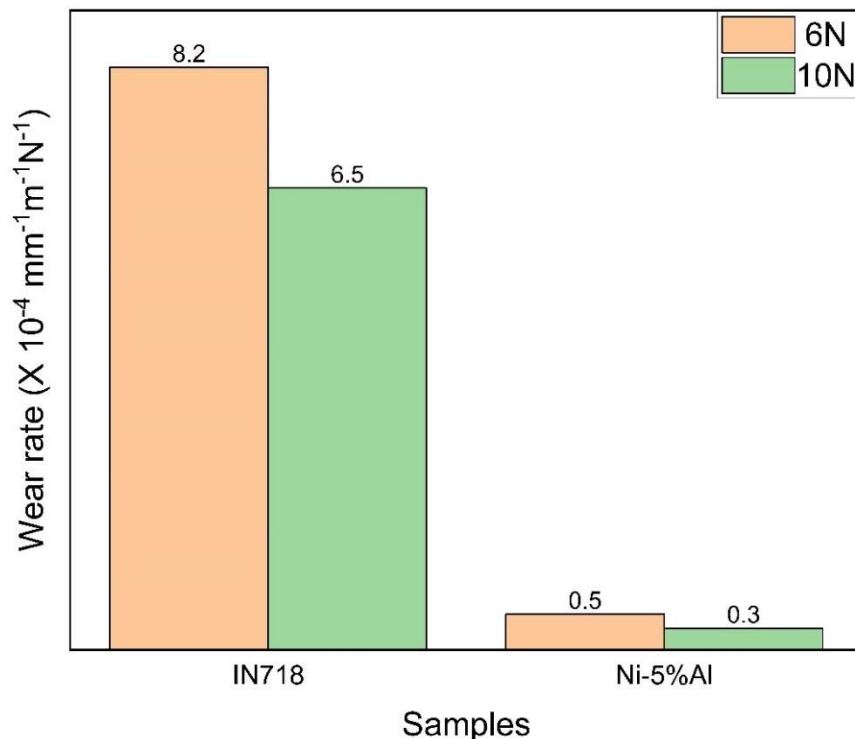


Fig. 4.6. Wear rate of IN718 and Ni-5%Al coating at 25 °C under 6N and 10N loads.

Table 4.3. Depth, width, and volume loss of the IN718 and Ni-5%Al coating at different loads.

Samples	Loads (N)	depth of tracks (μm)	Width of tracks (μm)	volume loss (mm^3)
IN718	6	35.08	1174	0.69
	10	52.36	1443	1.40
Ni-5%Al	6	47.61	573	0.049
	10	51.92	759	0.072

4.1.4. Worn surface of wear tracks

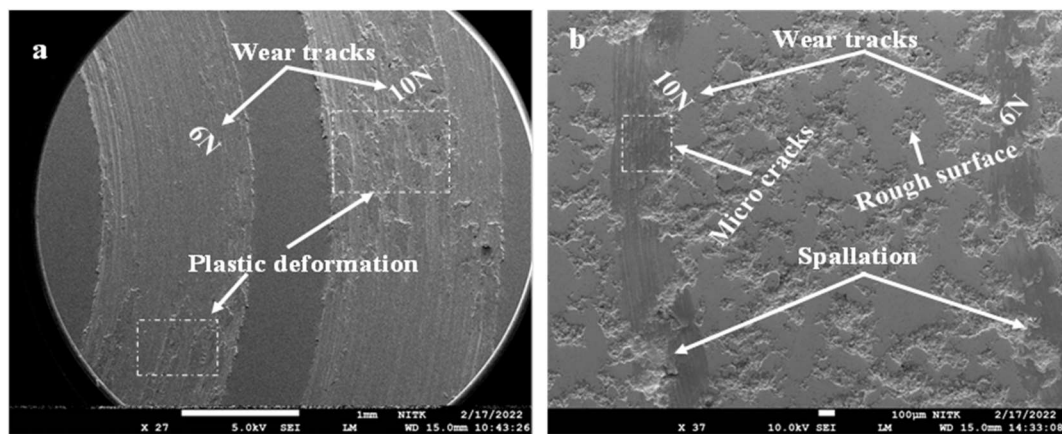


Fig. 4.7. SEM micrographs of the worn surface of the IN718 and Ni-5%Al coating at 6N and 10N loads: (a) IN718 substrate (b) Ni-5%Al coating.

Fig. 4.7 shows the SEM morphology of wear tracks of IN718 substrate and Ni-5%Al coating at different loads. The wear scars on the surface of the IN718 substrate were apparent and visible, but the wear tracks on coated specimens were not prominent. SEM images revealed that abrasion was the primary damage mode for the IN718 and Ni-5%Al coatings. The IN718 substrate shows evidence of ductile (plastically deformed) abrasive grooving marks, but no adhesive kind of tearing was noticed even in a magnified image Fig 4.7(a). The Ni-5%Al coated surface has fewer microcracks, spallation, and scratches. Both materials exhibit plastic deformation at the track's edges, typical of most metallic materials at ambient temperatures (Zhou et al. 2014). Due to the coating's high hardness, the same did not occur on the coated surface. The microhardness found in the coating morphology reduces the effective area of contact, as seen

in the depth profile shown in Fig. 4.5. As a result, minimal volume loss (Table 4.3) and wear rate of Ni-5%Al coated substrates can now be linked to a smaller effective area of contact between the frictional pair and hence showed excellent wear resistance in Fig. 4.6.

4.2. High temperature sliding wear behaviour of detonation sprayed Ni-5wt%Al coating

4.2.1. Microstructural characterization of Ni-5wt%Al coating

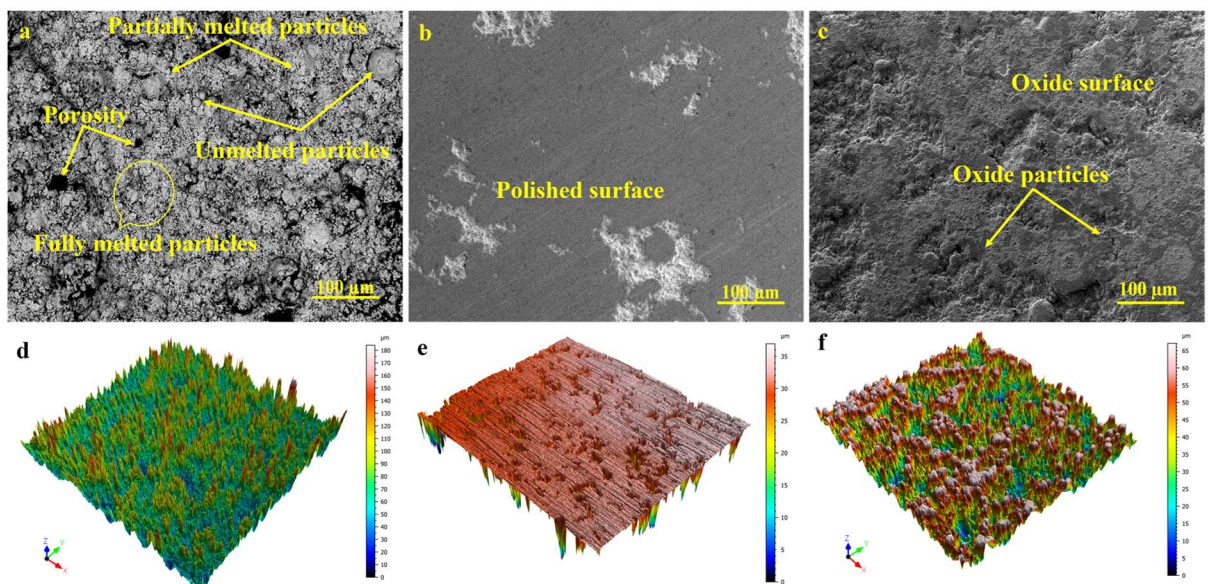


Fig. 4.8. FESEM and 3D profilometry micrographs of Ni-5wt%Al coating by DSC spraying technique (a,d) As-deposited; (b,e) Polished specimens tested at 25 °C; (c,f) Polished samples tested an 850 °C".

Fig. 4.8 depicts FESEM images, 3D morphological pictures, and their corresponding surface roughness characteristics of Ni-5wt%Al coating. Partially melted and unmelted particles are seen sparsely on the as-deposited coated surface, as shown in Fig. 4.8(a). Porosity is also present in small proportions. The 3D micrographs revealed that the Ni-5wt%Al coating had various micro and nano-sized roughness features. Because of the unmelted and semi-melted particles distributed throughout the surface, the as-sprayed coating had a maximum roughness value of $13.83 \pm 0.9 \mu\text{m}$. Fig. 4.8(d) is characterized by a high peak and less densely packed roughness features. Due to the high velocity of impinging molten powder particles during the DSC process, the coating had sparse porosity and a relatively homogenous microstructure. The resulting coating was dense and well adhered to the substrate, with a thickness of $250 \pm 25 \mu\text{m}$.

The polished samples were relatively smooth and homogeneous, as in Fig. 4.8(b&e). The roughness values were smoothed to $2.79\pm 0.06 \mu\text{m}$ by polishing. The Ni-5wt%Al coating was oxidized during dry sliding frictional conditions at 850 °C. Simultaneously, finely protruding uneven ridges in the nanoscale were predominantly seen on the coating surface, increasing the surface roughness to $11.83\pm 0.02 \mu\text{m}$ in Fig. 4.8(c&f).

FESEM-EDS was used to estimate the elemental distribution of Ni-5wt%Al coating precisely, and the findings are presented in Table 4.4. The chemistry of the feedstock is around 93.5wt% Ni and 5.5wt%Al, almost equivalent to the theoretical value of Ni-5wt%Al. Furthermore, the as-deposited coating's elemental composition is identical to Ni-5wt%Al powders. It also implies that all elements are homogeneously deposited throughout the spraying process without visible segregation. However, the percentage of aluminum (Al) and oxygen (O) have marginally increased to 6.2% and 4.6%, respectively, and Ni has fractionally decreased due to the losses incurred during the coating process.

Table 4. 4. Surface roughness and Elemental distribution of feedstock powder and as-deposited Ni-5wt%Al coating.

Coating	Sample conditions	Surface roughness (S_a , μm)	Chemical composition (wt%)		
			Ni	Al	O
Ni-5wt%Al	As-sprayed	13.83 ± 0.9	89.2 ± 0.6	6.2 ± 0.1	4.6 ± 0.3
	After polishing	2.79 ± 0.06	87.9 ± 1.2	7 ± 0.3	5 ± 0.1
	850 °C	11.83 ± 0.02	70 ± 0.9	3.1 ± 0.3	26.9 ± 1.5

4.2.2. Microhardness

Table 4.5 presents the Vickers microhardness values at the cross-section under the loading (200 g) conditions after the wear test at 25 °C and 850 °C. The microhardness of the Ni-5wt%Al coating is not only influenced by the coating process but also by its chemical composition and microstructure. As a result, the microhardness of coatings at 25°C and 850°C differ significantly. After the wear test at 25 °C, the

average microhardness of the coating was 330 ± 35 HV_{0.2}, comparable to previously published values (Wang et al. 2014). The As-deposited Ni-5wt%Al coating has relatively higher micro-hardness values. The high-strain hardening, rapid solidification, presence of partial oxides, and metallic phases in the coating deposition may all be attributed to the enhanced microhardness of the coating (Bai et al. 2011). After the wear test at 850 °C test, the reduction in microhardness (270 ± 30 HV_{0.2}) of the coatings was reduced significantly due to the softening and annealing effect, resulting in coarser grains that reduce shear strength, which may encourage plastic deformation (Hou et al. 2015). The residual stress induced during thermal spraying and relieving is visible during thermal softening (Hager et al. 2009). There is no evidence of plastic or shear transformation zones forming from the corners of the indentations developed for the samples at 25 °C and 850 °C. This indicates the high toughness and significant ductility in both temperatures.

Table 4. 5. Vickers microhardness of Ni-5wt%Al coating and counterpart at 25 °C and 850 °C.

Materials	Hardness (HV _{0.2})	
	25 °C	850 °C
Ni-5wt%Al	330 ± 35	270 ± 30
Alumina Ball	700 ± 20 HV	700 ± 20 HV

4.2.3. Dry sliding friction and wear behaviour

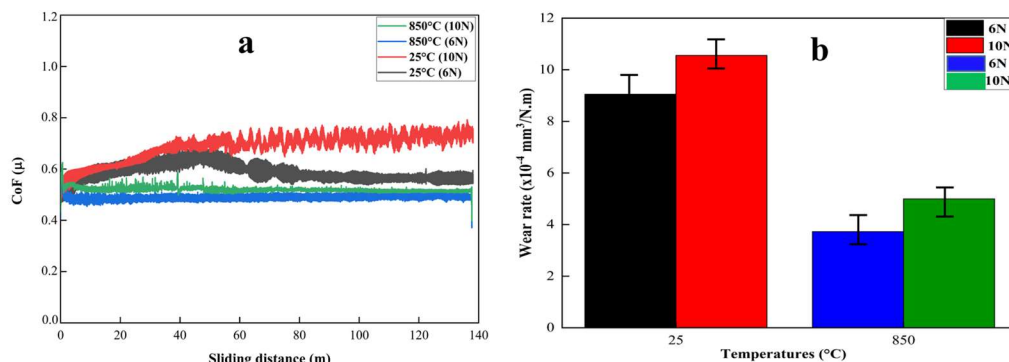


Fig. 4. 9. Dry sliding friction and wear behavior of a Ni-5wt%Al coating sliding against an alumina ball in stagnant air at 25 °C and 850 °C. (a) CoF vs. sliding distance, (b) Wear rate vs. temperature.

Fig. 4.9 demonstrates the dry sliding friction and wear behavior of a Ni-5wt%Al coating sliding against an Al₂O₃ counterpart in stagnant air at RT (25 °C) and HT (850 °C). At 25 °C, the CoF values of Ni-5wt%Al coatings decreased (6N) or stabilized (10N) after the first 20 to 30 meters (run-in period), and later on, it reached steady-state friction behavior. The initial high in CoF during the run-in period can be understood from the initial fragmentation, cracking, and detachment of the outer layer. When the worn debris entered the friction pair, it instantly reduced to low steady-states due to increased frictional and sliding contact zones.

Furthermore, when the worn-out particles are accumulated and compacted into a homogenous NiO oxide film at 850 °C, CoF is immediately reduced to a low steady state (Jiang et al. 1998). Forming an oxide lubrication layer of NiO at high temperatures benefits achieving a low friction coefficient at high temperatures (Ye et al. 2022). This result has already been found in comparative research on Ni-based tribo-systems (Hager et al. 2010)(Li et al. 2014). The formation of these oxide films and other intermetallic compounds enters the contact interface between the friction pair, reducing the adhesion phenomenon and thereby resisting the ploughing action on the coating. Low friction values obtained for Ni-5wt%Al coatings at high temperatures are shown in Table 4.6.

To further evaluate the coatings' tribological performance, Fig. 4.9(b) shows the wear rates of the Ni-5wt%Al coatings along with varied loading (6N and 10N) conditions at 25 °C and 850 °C. The relatively high wear rates of nickel-based coatings can also be attributed to material transfer from coating to counterpart (Medabalimi et al. 2021)(Kiryc et al. 2023)(Bolelli et al. 2020)(Hao et al. 2019). Sliding wear generates many third bodies (tribo-material), but only a fractional portion gets selectively delaminated and is evacuated from the system. Few particles get cold-welded with the wear track and retained in the tribo-couple. The retained layer is transformed into a glazed self-lubricative layer. It acts as a solid or solid/liquid lubricant, allowing for reduced rates by minimizing the frictional coefficients.

Wear scar geometry is analyzed to quantify the material loss in wear volume (Fillot et al. 2007). Non-contact optical profilometer devices easily demarcate the wear scar from the unworn region to acquire quantitative data. Wear volumes (V) were

measured directly by the software about a zero-point and compared to estimated values (V) obtained according to ASTM G99 standards inferred lesser values in 850 °C due to their lower steady-state CoF values with unexpected tribo-oxidation (NiO) under friction, heat, and stressed-shearing conditions. Decreased hardness, lower yield strengths, and increased ductility explain this. As a result, wear damage is scantier, although plastic deformation occurs at about 850 °C (Huang et al. 2016). On the other hand, the coating's wear rate, a compacted oxidation layer (NiO), usually forms while sliding and is protective and resistant to friction and wear (Medabalimi et al. 2021). A detailed discussion of tribo-chemical layer formation (NiO) is included in the following sections.

Table 4. 6. Sliding wear behaviour of Ni-5wt%Al coatings at 25 °C and 850 °C.

Coating	Load (N)	Coefficient of Friction		Wear rate ($\times 10^{-4}$ mm^3/Nm)	
		25 °C	850 °C	25 °C	850 °C
Ni-5wt%Al	6	0.523 \pm 0.09	0.486 \pm 0.107	9.05 \pm 0.05	3.73 \pm 0.87
	10	0.623 \pm 0.19	0.490 \pm 0.05	10.65 \pm 0.1	5.0 \pm 0.16

4.2.4. Topographical evolution of the worn surface of Ni-5wt%Al coatings

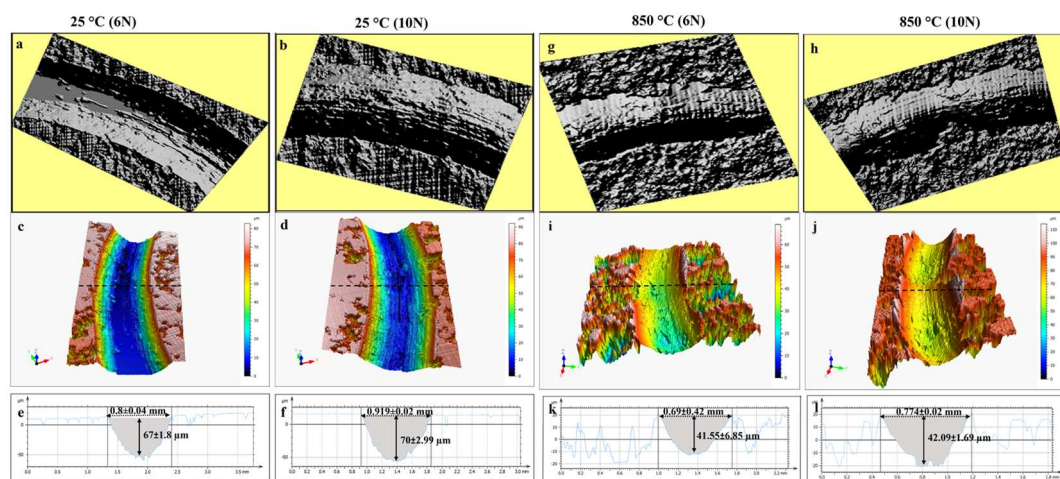


Fig. 4. 10. Non-contacting optical 3D topographies of wear scars of Ni-5wt%Al coating after dry sliding wear test at 6N and 10N loads. (a-f) RT (25 °C) and (g-l) HT (850 °C).

Table 4. 7. Dimensions and roughness parameters of the wear tracks with standard deviations of Ni-5wt%Al coating at 25 °C and 850 °C.

Coating	Loads (N)	Width (mm)		Depth (μm)	
		25 °C	850 °C	25 °C	850 °C
Ni-5wt%Al	6	0.8 \pm 0.4	0.69 \pm 0.4	67 \pm 1.8	41.5 \pm 6.8
	10	0.9 \pm 0.1	0.74 \pm 0.2	70 \pm 2.9	42.1 \pm 1.6

Fig. 4.10 depicts the 3D profiles of the wear tracks after the dry sliding wear test at 25 °C and 850 °C under varied loading conditions of 6N and 10N for a constant sliding distance of 138 m. Table 4.7 shows dimensions and roughness parameters on the wear tracks, viz. width, depth, and R_a . The depth and width of the wear tracks in these 2D profiles were used to compute the wear volume of the material removed for each sample. When worn track dimensional results of the Ni-5wt%Al coating were analyzed based on the applied loads of the sliding wear tests, it is evident that the 10N results possess marginally higher wear track dimensions, namely width and depth with increased roughness values compared to the 6N worn track results. For instance, if we have a wear transition between the interval of employed loads, the wear rate could increase or reduce the Ni-5wt%Al coating wear test results. The highly pronounced wear track dimension also substantiates the marginal rise in the roughness values in the 10N worn tracks. When the worn track results were analyzed from a temperature perspective, the test results at 850 °C showed that worn tracks possess relatively narrow width and minimal depth compared to the room temperature results. At room temperature, the Ni-5wt%Al coating showed significant worn track width and depth caused by friction when slid under 6N and 10N loads, as seen in Fig. 4.10(a-d). Upon the severe shearing action of friction, the spreading adhesive layer of the coating peels off the worn surface more quickly in room temperature conditions. As shown in Fig. 4.10(g-j), it is evident that the Ni-5wt%Al coatings' worn scars are smaller at high temperatures than those at ambient temperatures. The as-deposited coatings' plough depth has significantly decreased due to the superior wear properties at 850 °C. The noticeably decreased plastic deformation has narrowed the worn track width on the lateral sides, attributed to the plough depth reduction.

4.2.5. Analysis of worn surface morphologies of Ni-5wt%Al

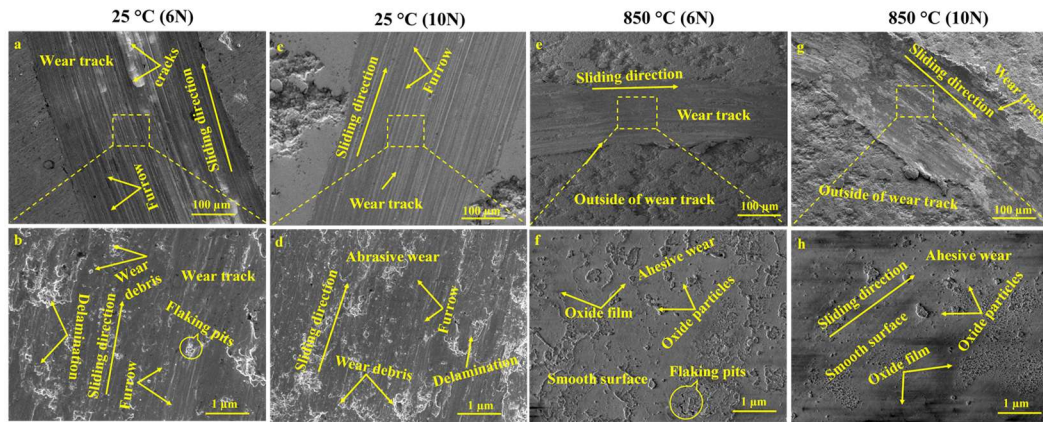


Fig. 4. 11. Worn surface morphologies of Ni-5wt%Al coating (a-b) 6N (c-d) 10N loads at RT (25 °C) and (e-f) 6N (g-h) 10N loads at HT (850 °C).

The FESEM technique was used to observe the worn surfaces of Ni-5wt%Al coating to analyze the predominant wear mechanism associated with the coating in temperatures (25°C and 850°C) under varied loading (6N and 10N) conditions. The worn surfaces exhibit parallel furrows, micro-cracks, and delamination characteristics of debris and grooves on the coatings at room temperature. It indicates that the wear process is abrasive and surface fatigue. The parallel furrows with micro ploughing were indexed in Fig. 4.11(a&c), and surface fatigue was visible by the delamination shown in Fig. 4.11(b&d) (Fischer et al. 2018)(Zum Gahr 1987). The loose, fragmented, hard-abrasive particles on delamination generate many parallel grooves that can be seen along the wear track. Abrasive debris was produced due to the prolonged delamination developed during the repetitive sliding wear process. Depending upon the geometry of the debris and the entrapment due to the applied load, it can be embedded in coatings by cold welding. It may stick to the counterpart balls or act as loose particles between the two contacts, generating a three-body abrasive configuration. Micro-cracks on coatings (Fig. 4.11(a)) are induced mainly by residual stress during sliding contact (Wang et al. 2018). Furthermore, cracks and delamination develop when the contact pressure exceeds the yield strength of the material (Mussa et al. 2020). Spalling debris was entrapped and lodged in the cracks, decreasing CoF and wear rates throughout the sliding process.

When the surrounding temperature rises to 850 °C, the furrows alleviate due to the glazed oxide layers, which are present superficially. At 850 °C, the dimensions of the wear scars decrease with increasing temperature (Fig. 4.11(e&g)). This is related to the self-lubricating characteristic of the progressively developing tribo-layer on coating and wear resistance. The coating's dominant wear mechanism includes agglomeration of oxide layers (oxidative wear) and fissures of the oxidized surfaces (Fig. 4.11(f&h)), as noticed from the severe peeling of the oxide layer. The wear mechanism of Ni-5wt%Al coating seems to be predominantly sticky with severe score marks. At 850 °C, smooth tribo-layers develop over the worn surfaces, and adhesive grooves are evident, suggesting adhesive wear (material transfer). The hardness of the gentler friction pairs has an inverse relation with adhesive wear. As a result of the softening of the Ni-5wt%Al coating spread out along the sliding direction, resulting in plastic deformation of the coating (Hao et al. 2019). Because the coatings are significantly softer when rubbing at 850 °C, the oxidative tribo-layer formed at the coating surface leads to improved wear resistance. Therefore, the tribolayer reduces the friction coefficient, reducing the wear rate at 850 °C.

4.2.6. FE-SEM and Elemental mapping analysis on the worn surface of Al₂O₃ ball

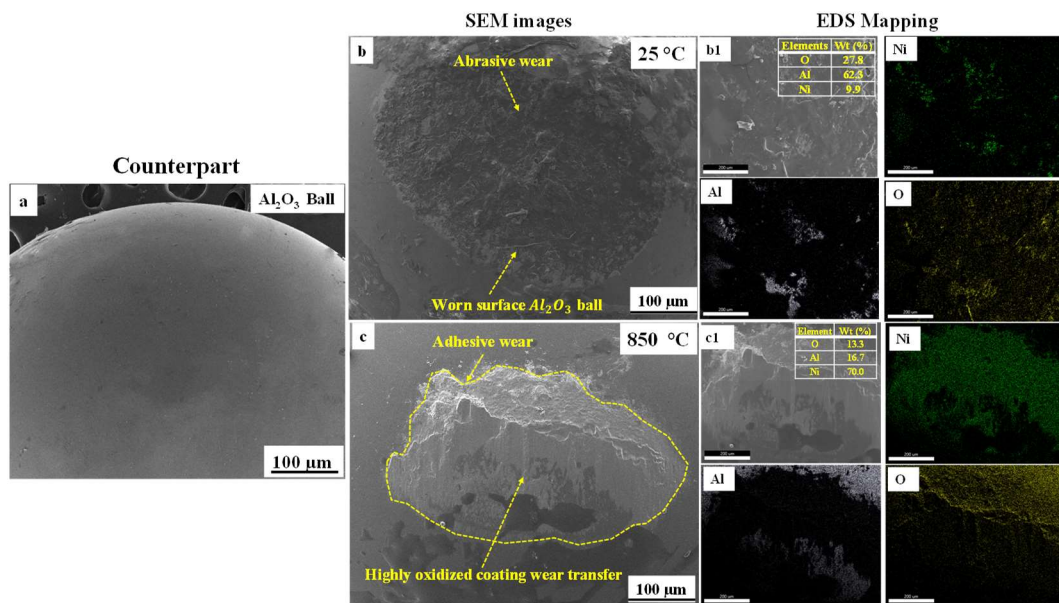


Fig. 4. 12. FESEM micrographs and Elemental mapping on the worn surface of Al₂O₃ ball at different temperatures. (a) Unworn surface of the counterpart (b and b1) 25 °C (c and c1) 850 °C.

For the comparative analysis, FE-SEM micrographs and elemental mapping were performed on the worn surfaces of the Al_2O_3 counterpart sliding against Ni-5wt%Al coating at both room and high temperatures. Because of the self-lubricating behavior of the progressively growing tribo-layer on the paired counterpart surface, the diameters of the wear scars reduce with rising temperature and, therefore, wear resistance increases gradually. As seen in Fig. 4.12, the worn surface counterpart is rough at room temperature. Wear debris, delamination, and grooves appear with a sliding direction, indicating abrasive and surface fatigue mechanisms. Although some wear debris is clumped, single particles are scattered throughout the worn surface.

On the other hand, the worn topographies at 850 °C differ substantially from those at lower temperatures (Fig. 4.12(b)). The highly oxidized coating material is transferred to the counterpart, and small wear debris particles adhere to the Al_2O_3 surface (a grey colour region in "b"), which would account for mechanical mixing (a sub mechanism of tribo-chemical reactions) tribo oxide layer lubricating ability (Fischer et al. 2018)(Zum Gahr 1987). Smooth tribo-layers form over the worn surface when wear is minimal (Fig. 4.12(b)). This thin glazed layer reduces frictional coefficient and wear by acting as a barrier between the rubbing surfaces.

EDS mapping of an Al_2O_3 ball coupled with a Ni-5wt%Al coating at 850 °C demonstrates that a significant amount of Ni is transferred onto the Al_2O_3 surface with severe oxidation (Fig. 4.12(b1)). When sliding against the coating, the Ni and O are discernible on the worn Al_2O_3 surface. This suggests that nickel oxide contributes considerably to the frictional decrement at high temperatures, as seen in Figs. 4.12(b1). It is obvious that material transfer happens, and a compact oxide layer covers the worn Al_2O_3 surface when it matches the coating at 850 °C. This layer comprises Ni, Al, and O. It enables the restoration of the contacting surface by producing a self-lubricant layer predominantly composed of numerous oxides, hence lowering friction and enhancing wear resistance.

4.2.7 EDS analysis of the wear surface of the coating at 25 °C and 850 °C

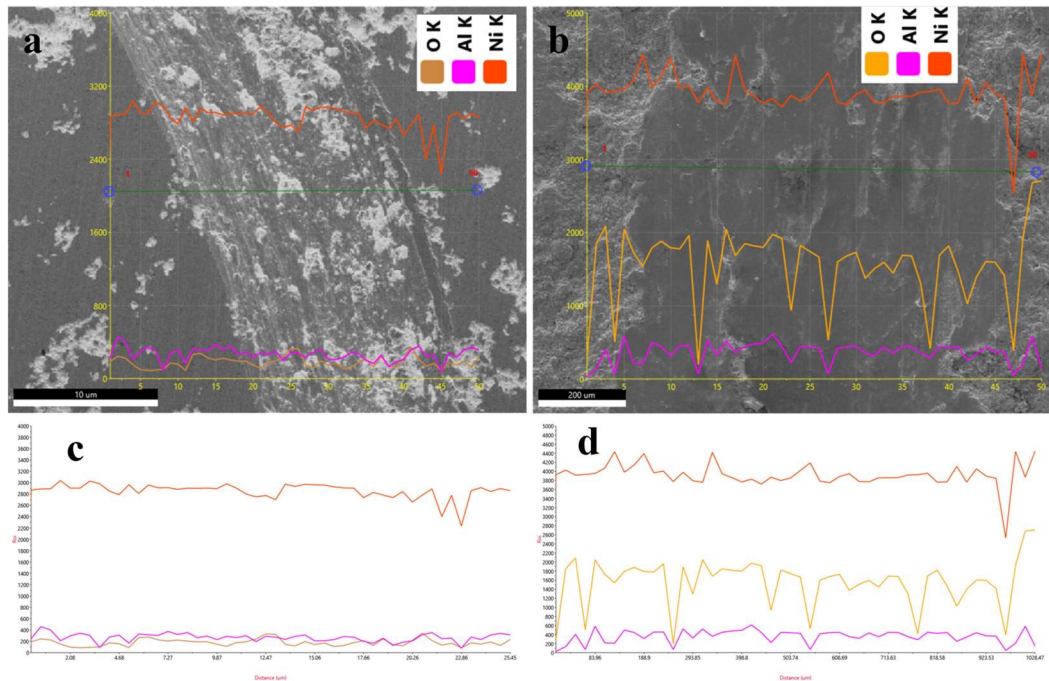


Fig. 4.13. EDS line analysis of element content on the worn surface of the coating cross-sections at (a and b) 25 °C and (c and d) 850 °C.

Fig. 4.13 shows an EDS line scan of the worn surface of room temperature and high-temperature (850 °C) Ni-5wt%Al coating samples. Fig. 4.13(c&d) shows the element line distribution spanning the green line on the wear track seen in Fig. 4.13(a&b). Fig. 4.13(a) presents SEM micrographs of the Ni-5wt%Al coating surface tested at 25 °C against its Al₂O₃ counterpart. An abrasive layer may be detected on the worn surface. The oxidation of the wear scar (Fig. 4.13(c)) is lower because the wear track has a significantly higher nickel and aluminum content than the others. Fig. 4.13(d) shows the oxidized wear track. The oxidative layer mainly comprises Ni and O components (Table 4.8). During the experiment, the Ni-based matrix would be oxidized and encouraged to form a complete protective layer. It demonstrates that the adhesion layer is formed due to a chemical reaction produced by in-situ friction. Many distinct grain boundaries formed during recrystallization may relieve local tensile stress, improving tribological superiority (Hao et al. 2019).

Table 4. 8. EDS line analysis of the elemental composition of Ni-5wt%Al coating at different temperatures.

Coating	Elements	Elemental composition (wt%)	
		25 °C	850 °C
Ni-5wt%Al	Ni	90.7±0.8	69±1.2
	Al	5.0±0.2	3.1±0.4
	O	4.3±0.3	26.9±0.7

4.2.8 Raman spectroscopy

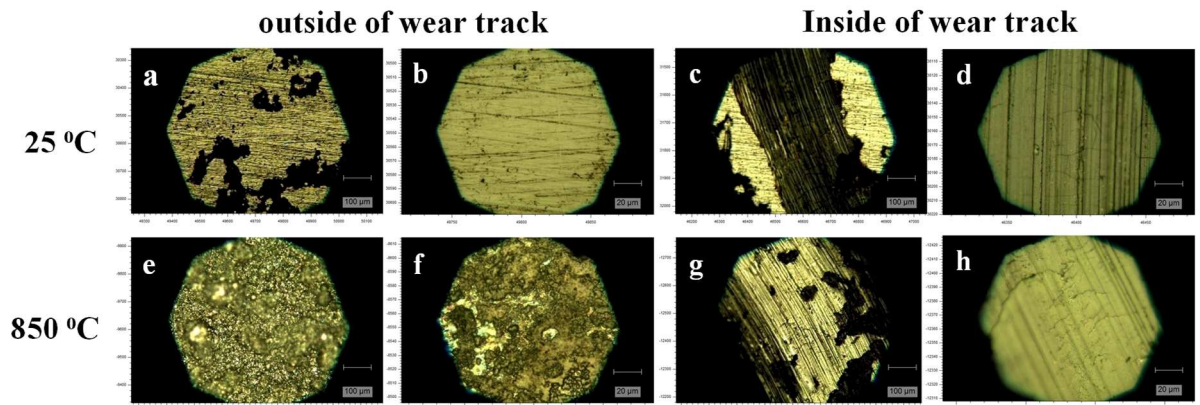


Fig. 4. 14. Raman topography of outside and inside the worn scar of Ni-5wt%Al coatings at 25 °C and 850 °C. (a-d) 25 °C (e-f) 850 °C and (a,b and e,f) outside of the worn scar (c,d, and g,h) inside of the worn scars.

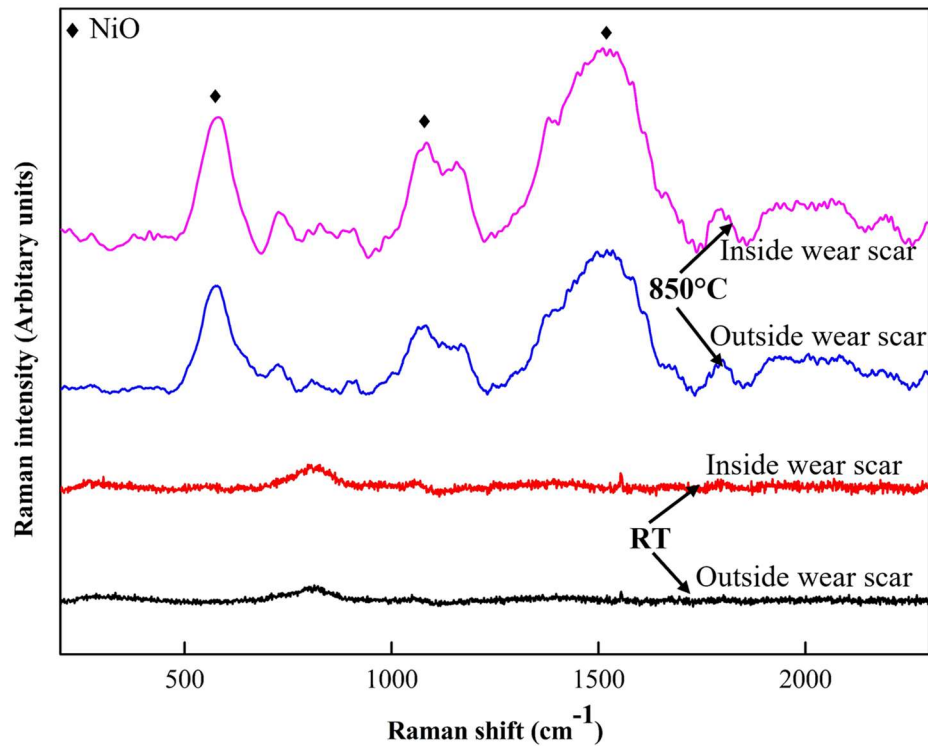


Fig. 4.15. Raman spectra of outside and inside the worn scar of Ni-5wt%Al coatings at 25 °C and 850 °C.

Raman spectra were also acquired to determine the chemical phase compositional alterations by analyzing the surfaces of the coatings. The Raman spectra obtained inside and outside the worn grooves (presented in Fig. 4.14) of the Ni-5wt%Al coating tested at 25 °C and 850 °C are shown in Fig. 4.15. According to the Raman spectra, no metal oxides were found in the specimens tested in 25 °C sliding wear. Under strained shearing and temperature circumstances (850 °C), peaks of NiO can be found within the worn track with the Ni-5wt%Al coating, and the glazed layer growth results in friction reduction and enhanced wear resistance. NiO is responsible for the 570, 1070, 1170, and 1511 cm^{-1} peaks. The NiO peak intensity at 1511 cm^{-1} increases as the fraction of NiO on the worn surface increases. The formation of a dominating NiO phase on the worn surface supports the friction reduction at 850 °C, owing to an increase in NiO-rich tribo-layer (Torgerson et al. 2018). According to the Raman spectroscopy observations, the decrease in CoF and wear at higher temperatures is caused by oxidation of the coating and an increase in the amount of retained NiO oxide layer during the sliding wear test.

4.2.9 Cross-sectional analysis of a Ni-5wt%Al coating

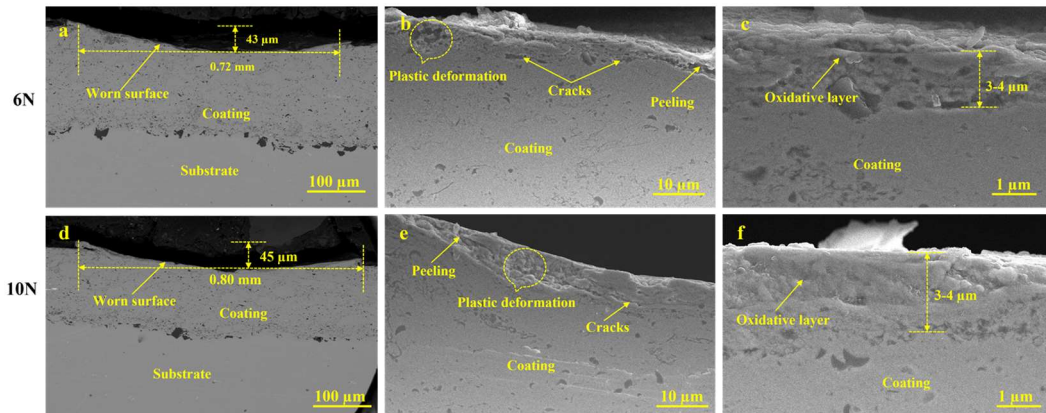


Fig. 4. 16. Cross-sectional (sub-surface) FESEM images of the worn surface of a Ni-5wt%Al coating at 850°C under typical loads. (a-c) 6N and (d-f) 10N.

The cross-section analysis of the wear scar was conducted further to understand the coating's wear process at the interface. Fig. 4.16 illustrates an SEM cross-section micrograph of the coating after the wear test at 850 °C. A subsurface fissure in the coating is broken through beneath the surface. Because of the stress distribution and continuous rubbing, the shear stress generated by friction peeled the surface tribo-layer of the coating when the crack caused the component to break through. The material is quickly worn out during the initial sliding because of the smaller contact area of the counter alumina ball. Some smooth surfaces are evident on the cross-section, as illustrated in Fig. 4.16, which predominantly incorporate oxide agglomeration and fissure surfaces, as well as severe exfoliation (peeling) of the oxide layer, indicating that oxide is transferred to the opposite side.

In contrast, the wear mechanism of the Ni-5wt%Al coating appears to be primarily sticky, with severe score marks and adhesive grooves confirming adhesive wear. On the other hand, the oxidative layer provides superior lubrication at higher temperatures. The significantly thin oxide film is a barrier between the rubbing surfaces (friction pair) and improves the tribological characteristics.

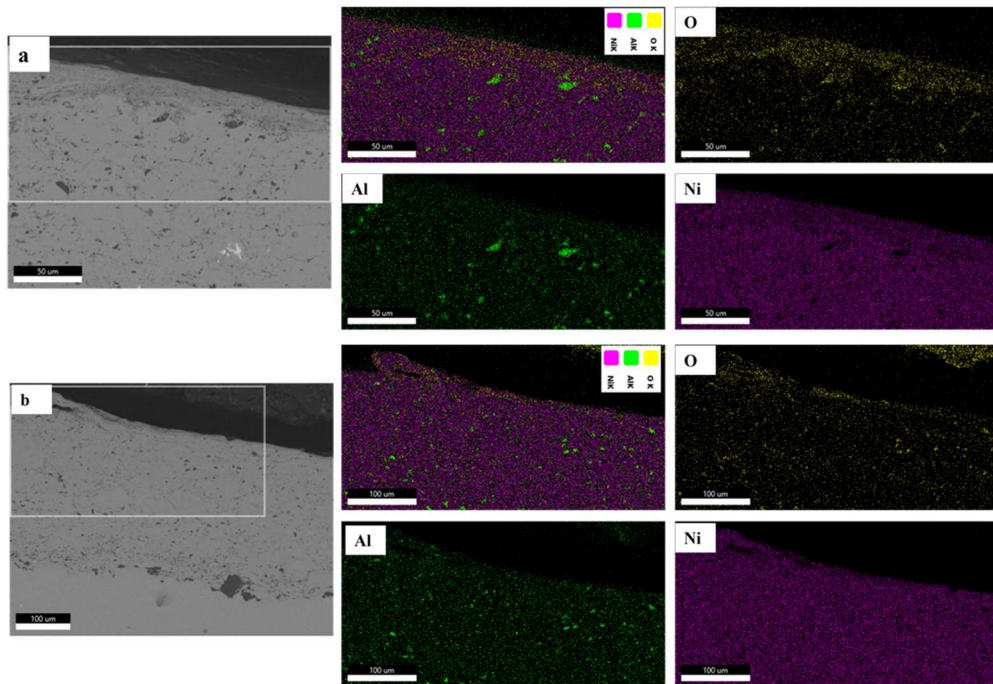


Fig. 4. 17. BSE micrographs and corresponding EDS element mappings of the cross-sections of the worn surface of Ni-5wt%Al coating at 850 °C. (a) 6N (b) 10N.

Fig. 4.17 depicts the cross-section FE-SEM morphology of the post-wear (850 °C) coating. At 850 °C, the homogeneously reorganized hierarchy within the Ni-5wt%Al coating revealed a lubricating layer mainly composed of NiO. It indicates that the oxidative layer, which is homogeneous and dense with a thickness of roughly 3-4µm, is successfully attached and uniformly dispersed throughout the coating. Fig. 4.17 illustrates that after friction and wear testing at 850 °C, Ni and O elements developed on the worn surface. Temperature also enhanced the chemical affinity of Ni-5wt%Al and NiO, resulting in a relatively continuous and compact lubricating layer. These boundary oxides may refine the coating's grain size, which is advantageous for reducing internal stress (Hao et al. 2019). At 850 °C, it may be beneficial in improving adhesion to avoid oxidative layer exfoliation from the coating, resulting in increased wear and friction.

Table 4. 9. Shows an elemental mapping analysis of a Ni-5wt%Al coating at 850 °C using FESEM-EDS.

Coating	Loads (N)	Elemental composition (wt%)		
		Ni	Al	O
Ni-5wt%Al	6	75.4±0.7	5.1±0.5	19.4±0.2
	10	72.5±0.6	5.8±0.3	21.6±0.1

4.2.10. Peak shift and lattice parameters behaviour of Ni-5wt%Al during the high temperature

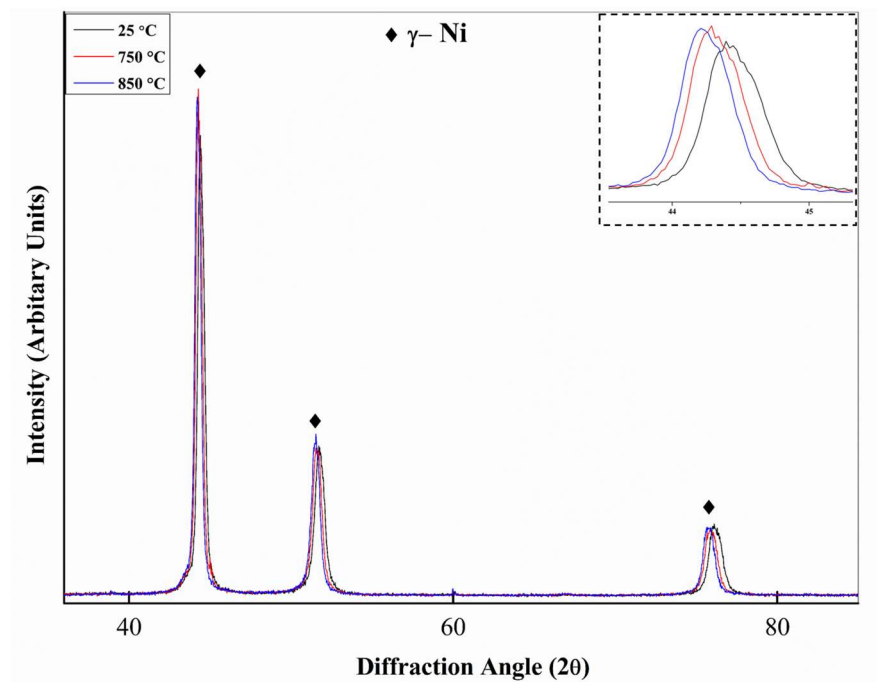


Fig. 4. 18. Shifting of the highest intensity peak of Ni in Ni-5wt%Al coating from RT (25 °C) to HT (850 °C) at in-situ HT-XRD.

The XRD pattern of in-situ HT-XRD characterization of Ni-5wt%Al coating at 25 °C (as-deposited), 750 °C₂ and 850 °C, as shown in Fig. 4.18. According to the HT-XRD investigation, significant phases revealed in the Ni-5wt%Al coatings have an FCC structure. While in this study, it can be seen that only pure γ -Ni (solid solution crystal structure) is the dominant crystalline phase. The intensity of the peaks observed at high temperatures (750-850 °C) is much narrower than that of as-deposited coatings, indicating crystallinity and coarser crystallite size.

No significant difference was observed between the room temperature XRD data in a typical atmosphere and a vacuum. It is observed that the diffraction peaks shift to the left side from the original 2θ position as the temperature rises. The peaks shift indicates the residual stress relaxation and lattice expansion (Kala et al. 2022). As a result, the strain relieving in the coating is apparent due to the high-temperature exposure. Peak broadening (widening) indicates the crystallite size and lattice strain. During coating deposition, molten particles will impact the substrate or already deposited particles and cool rapidly at a rate of 10^6 - 10^8 K/s, resulting in an amorphous structure. The crystalline phase in the coating may result in narrow peaks compared to broad peaks. Phase shifts, the formation of new planes, lattice strain effects, and other factors might significantly influence the change in peak position in XRD patterns.

4.2.11. Thermal expansion behaviour of Ni-5wt%Al coating

Thermal expansion measurements were taken on a DSC sprayed Ni-5wt%Al coating from ambient temperature to 850 °C. Thermal expansion is one of the most significant factors in forecasting the lifetime expectancy of TBCs. Table 4.10 shows the average linear coefficients of thermal expansion (CTEs) determined from lattice constants. A superalloy substrate has a thermal expansion of 15 - $15.5 \times 10^{-6}/^{\circ}\text{C}$ (Texier et al. 2016)(Jackson et al. 2016)(Haynes et al. 2004), which is equivalent to ultrathin Ni-5wt%Al coated specimens.

The thermal expansion of the coating interface and the superalloy base material expands with temperature due to the intensification of the crystal lattice vibration at high temperatures. The CTEs increase linearly across the whole temperature range, significantly greater than the IN718 substrate. The higher thermal expansion of the coating than the substrate lowers the possibility of cracks and spallation at the interface in high-temperature conditions (Saladi et al. 2014).

Table 4. 10. Thermal expansion coefficient and lattice parameters of Ni-5wt%Al coating at different temperatures.

S. No	Temperature (°C)	Lattice parameters (Å) (a=b=c)	CTE (x 10 ⁻⁶ /°C)
1	25	3.524	--
2	750	3.563	14.47
3	850	3.571	16.16

4.2.12. Crystallite size and Lattice strain

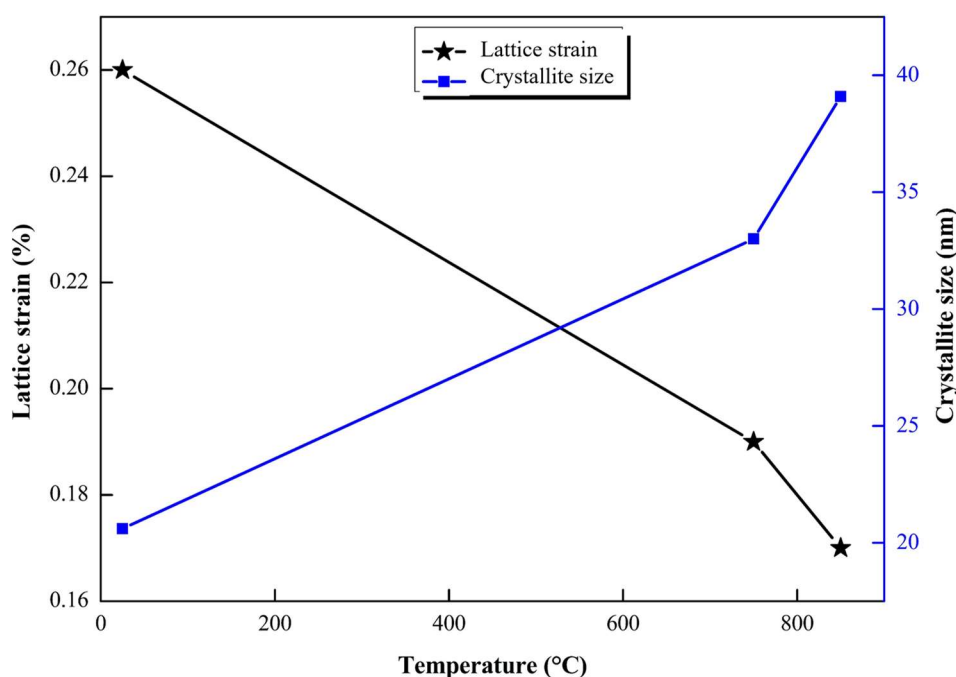


Fig. 4. 19. Crystallite size (D) and lattice strain (ϵ) with the elevated temperature of Ni-5wt%Al coatings.

The crystallite size and lattice strain of Ni-5wt%Al coatings on elevated temperatures were calculated using the Williamson-Hall (W-H) plots. The plots are compared in Fig. 4.19 with positive slopes and Y-intercepts. The crystallite size and lattice strain values at each stage are calculated from diffraction peaks (Fig. 4.18). At ambient temperature, the sample's average crystallite size and lattice strain are 20.6 nm and 0.26, respectively. A gradual decrease in lattice strain and increase in crystallite size with temperature (25 °C –850 °C) is evident in Fig. 4.19. As stated earlier, the lattice strain contribution to the XRD line broadening effect could not be ignored for

finer crystallites. There might be variations in the crystallinity of the coatings. The temperature eventually affected the formation of more fine crystals. At high temperatures (750-850 °C), the release of the lattice strain can be attributed to the driving force for the recrystallization. The temperature eventually affected the formation of finer crystals.

The physical interpretation of the friction and wear behavior of the Ni-5wt%Al coated surface at 25 °C and 850 °C can be explained further. The stress concentration in this contact area favors the nucleation of microcracks, which promotes crack growth and interaction with one another under ambient temperature. The worn surfaces have parallel furrows, micro ploughs, and delamination features of debris and grooves, suggesting that abrasive and surface fatigue mechanisms cause the wear process.

At 850 °C, Ni oxidizes, resulting in the formation of the glazing tribo-layer (NiO). This is attributed to the self-lubricating property of the progressively increasing tribolayer on coating and wear resistance. The coating's substantial wear mechanism includes agglomeration of oxide layers (oxidative wear) and fissures of the oxidized surfaces, as evidenced by severe peeling of the oxide layer. The wear mechanism of Ni-5wt%Al coating appears to be significantly sticky, with severe score marks and smooth tribo-layers appearing over the worn surfaces and adhesive grooves, indicating adhesive wear. This decreased tolerance is caused by an inner attack of oxygen and a lesser outward diffusion rate of Ni ions. The results of this experiment were consistent with continuous friction as the grains refine and recrystallize in the oxide layer. Thermal expansion at 850 °C and recrystallization reduce local tensile residual stress and contribute significantly to anti-wear and tribological superiority.

4.2.13. Limitations of the study and scope for improvement

It should be noted that the wear rates reported in the current experiments are more prominent when compared with the wear rate of tooling. The present study involves an alumina ball as a counter body, and its thermal coefficient of expansion at room temperature ($8.4 \times 10^{-6}/^{\circ}\text{C}$) is lesser than that of the IN718 substrate discs ($15-15.5 \times 10^{-6}/^{\circ}\text{C}$), the higher wear rates caused due to the thermally triggered degradation was evident and reported. Usually, the ceramic counter body (alumina ball) is preferred

to avoid unwanted oxidation and for better thermal stability. Although the thermal conductivity of IN718 increases with the operating temperature, the thermo physical property does not contribute to its wear resistance at 850 °C. The present study intends to improve the wear characteristics of the Ni-5wt%Al coating above 800 °C. Still, in contrast, the sliding wear results revealed a higher order of wear rate with the coating's limitation. However, the current study also provides the scope for improvement for further studies. The longevity of the coating under the sliding wear resistance can be improved by the proposed steps: Optimization of the coating parameters further so that the (DSC) Ni-5wt%Al coating can withstand higher temperatures, use the coating pins or ball like geometry made up of similar materials, employing suitable post-processing treatments.

4.2.1. In-situ high temperature X-ray diffraction study on atmospheric plasma and detonation sprayed Ni-5wt%Al coatings

4.2.1.1. In situ high-temperature XRD

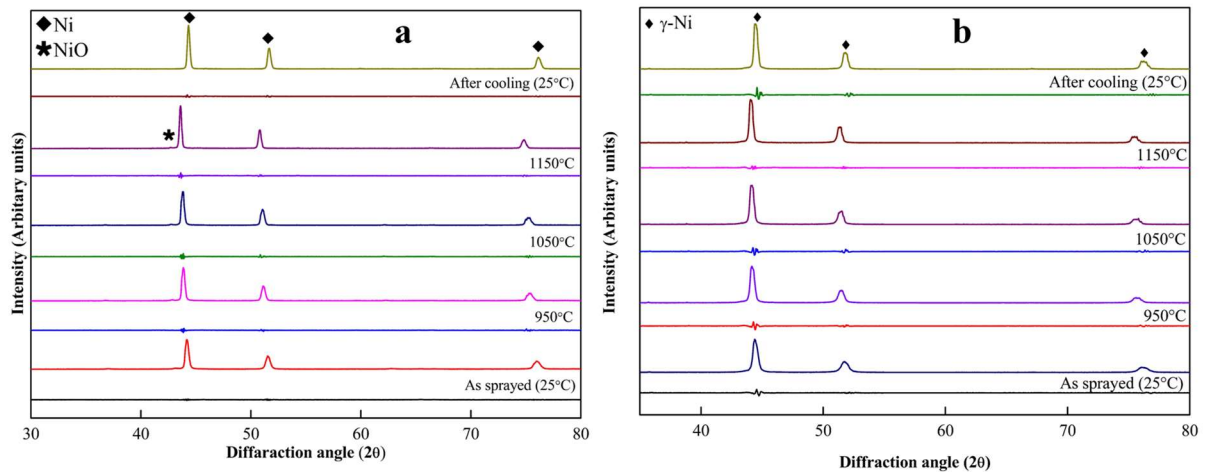


Fig. 4. 20. Stacking and Difference plots for the fit patterns of in-situ HT-XRD of Ni-5wt%Al coating after Rietveld refinement; (a) APS, and (b) DSC.

The Ni-5wt%Al coating temperature was raised to a high temperature (1150 °C) from room temperature as per the program shown in Fig. 3.2. The diffraction patterns were recorded at different stacked temperatures indexed as shown in Fig. 4.20. According to the HT-XRD investigation, the intensity of the peaks recorded at the high

temperature is highly narrow compared to the peaks of as-deposited coatings, indicating crystallinity and coarser crystallite size. The broader peaks correspond to as-deposited coatings, indicating the presence of residual stress and strain hardening during deposition. The residual thermal stresses are usually dominated in APS as the process involves high flame enthalpy. At the same time, the strain hardening effect is highly pronounced in DSC, which involves higher kinetic energy (spray particle velocity is high) than thermal energy. The comparative analysis revealed that both coating techniques had retained major phases observed in the coating. Significant phases in the Ni-5wt%Al coatings have an FCC structure in APS and DSC coating techniques. While in this study, it can be seen that only pure γ -Ni (solid solution crystal structure) is the dominant phase crystalline. No other diffraction peaks are found in DSC, but Ni reacts with atmospheric oxygen in APS due to the high inflight temperature during the deposition process. As a result, the nickel oxide (NiO) has been formed as a minor phase, as shown in Fig. 4.20(b), and no other peaks are seen after cooling down to room temperature from 1150 °C.

Fig. 4.20 shows the Rietveld refinement of APS and DSC coatings performed at ambient and high temperatures (1150 °C) and refined the lattice parameters and peak positions with the help of XRD data. The fitting quality of the experimental data is measured by computing metrics such as the 'goodness of fit' χ^2 and the R factor (R_{wp} = Reference weighted profile). R_{wp} is the simplest straightforward discrepancy index, derived directly from the square root of the quantity decreased, scaled by the weighted intensities. R_{wp} 10% and GOF between 1 and 2% are considered excellent (Toby 2006). The results are shown in Table 4.11, and shifted anchor scan data modeled the background. Experimentally measured lattice parameters using in-situ XRD are more precise and accurate. The Rietveld Refinement was conducted for XRD data for accuracy. The goodness fit has ensured the accuracy, which is well below two.

Table 4. 11. Rietveld analysis for in-situ HT-XRD pattern of Ni-5wt%Al coatings.

Coating	Temperature (°C)	DSC		APS	
		R _{wp}	Goodness of fit	R _{wp}	Goodness of fit
Ni-5wt%Al	As sprayed	8.096	1.04	9.551	1.00
	950	8.96	1.08	9.633	1.033
	1050	9.62	1.12	9.75	1.047
	1150	9.88	1.22	10.25	1.09
	After cooling	10.35	1.28	11.03	1.14

4.2.1.2. Peak shift behaviour of Ni-5wt%Al coating during the HT-XRD

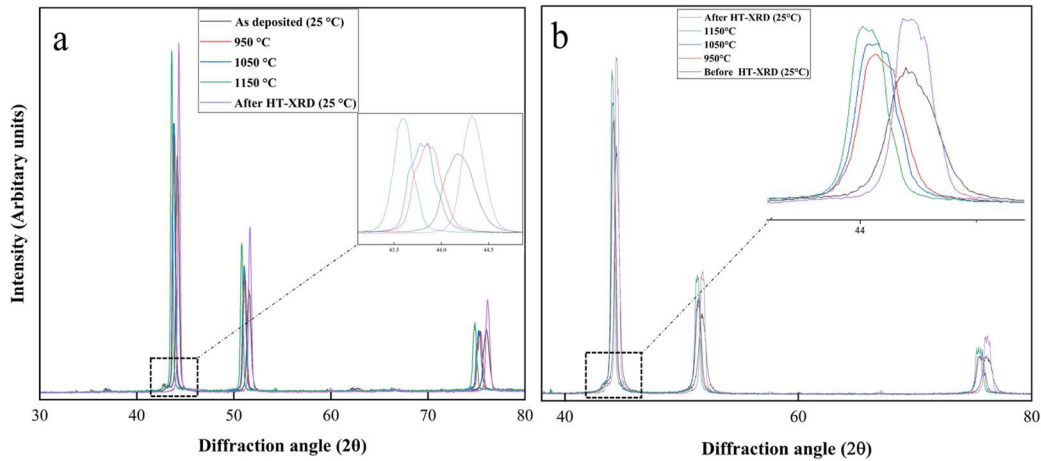


Fig. 4. 21. Peak Shift phenomenon during HT-XRD, (a) APS, and (b) DSC, and the insert indicates the thermal expansion-induced peak shifting phenomena.

The HT-XRD results of APS and DSC sprayed Ni-5wt%Al coating from RT (25 °C), 950 °C, 1050 °C, 1150 °C, and 25 °C (after cooling) are presented in Fig. 4.21. No difference was found between the room temperature XRD data in a typical atmosphere and a vacuum. It is observed that the diffraction peaks shift to the left side from the original 2θ position as the temperature rises. The peak shift indicates the residual stress relaxation and lattice expansion (Kala et al. 2022). As a result, high-temperature peaks are much sharper than room-temperature peaks. At the same time, the strain relieving in the coating is apparent due to the high-temperature exposure. The shape of the peaks will vary according to the competing behavior of a decrease in lattice strain and an increase in lattice parameter. Peak shifting and sharpening with

temperature (Fig. 4.21) indicate stress reduction or lattice expansion in the coating. The peak shift might be influenced by phase changes, the development of new planes, lattice strain effects, and other factors (Abhijith Vijay et al. 2023).

4.2.1.3. Measurement of coefficient of thermal expansion (CTE)

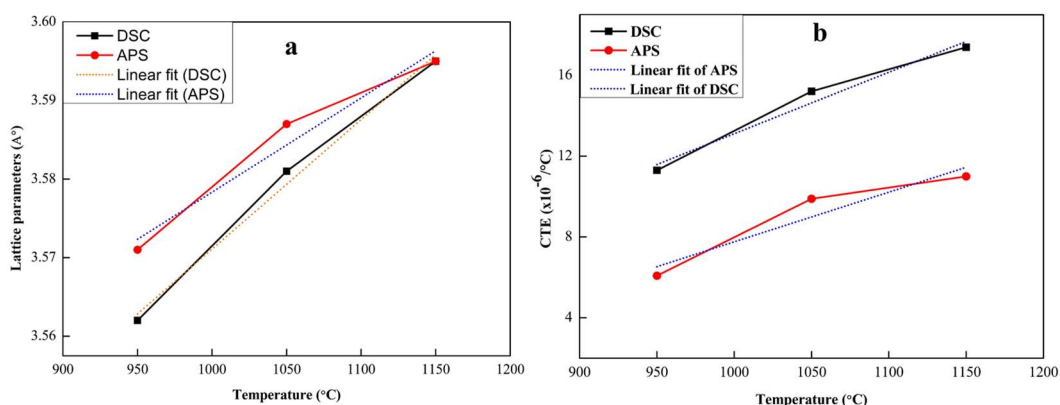


Fig. 4. 22. (a) Lattice parameters and (b) CTE of APS and DSC sprayed Ni-5wt%Al coatings.

Thermal expansion is one of the most important aspects of predicting the lifespan of TBCs. The CTE is closely connected to the crystal structure and any phase transitions that could occur during heating. Thermal expansion measurements were taken on an APS and DSC sprayed Ni-5wt%Al coating from ambient temperature (25 °C) to HT (1150 °C). The lattice parameters corresponding to γ -Ni (FCC) peaks were considered for CTE calculation. The average linear coefficients of thermal expansion (CTEs) values are calculated using the lattice parameter from HT-XRD. The computed value of lattice parameters of γ -Ni phases versus temperature is given in Fig. 4.22(a). It shows the linear trend for both APS and DSC coatings.

Due to the crystal lattice vibration intensifying, the CTEs of γ -Ni phases increase linearly across the whole temperature range. Fig. 4.22(b) shows that the CTE of DSC sprayed Ni-5wt%Al coatings rises to $17.4 \times 10^{-6}/^{\circ}\text{C}$ at 1150 °C, and the CTE is higher and closer to the substrate. Therefore, the thermal expansion mismatch at the coating and the substrate interface is insignificant. It implies that the coating and substrate will have higher crack initiation and spallation resistance due to the low thermal stress generation at the interface. The expansion coefficient of the APS ($11.0 \times 10^{-6}/^{\circ}\text{C}$) is lower than that of DSC ($17.4 \times 10^{-6}/^{\circ}\text{C}$) due to the variation of the Ni

and NiO phases at high temperatures. At high temperatures, there is a variation in the CTE behavior of the two phases (Ni, NiO) (Hazotte et al. 1992). The CTE evolution tendency of γ -Ni phases is similar in both coating processes. It implies that the effect processing method for coating deposition plays a crucial role in thermal expansion. The process-induced CTE mismatch would be expected to influence the interfacial adhesion between the coating and substrate, as discussed in the next section.

It should be noted that the CTE values are obtained with two decimal fractions calculated using eq 3.1. CTE has been measured based on the lattice parameters obtained with four decimals obtained by the COD database. The experimentally measured lattice parameters using in-situ XRD are more precise and accurate. Besides, the present study also considers the Rietveld refinement of XRD data for accuracy. However, there could be sources of errors that may arise from the density (porosity) and inhomogeneous as-deposited microstructure. The in-situ HT-XRD examination of the APS and DSC coatings at different locations may lead to slightly varied CTE values at low and mid-temperature ranges. At high temperatures above 1050 °C, the measured CTE is expected to stabilize as the microstructure tends to homogenize.

4.2.1.4. Crystallite size and Lattice strain

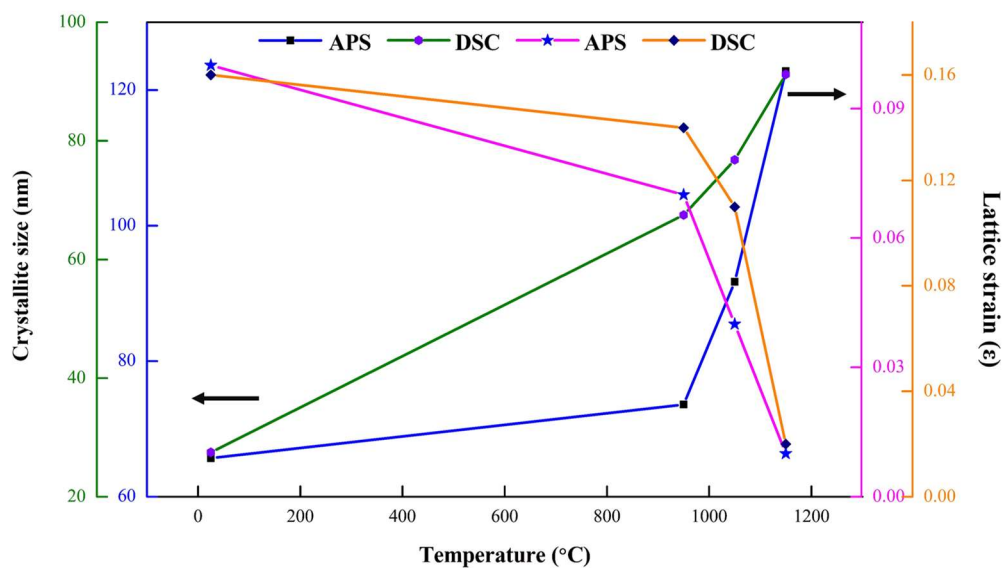


Fig. 4. 23. Crystallite size and Lattice strain of APS and DSC sprayed Ni-5wt%Al coatings using Williamson-Hall analysis through UDM.

The crystallite size and lattice strain of Ni-5wt%Al coatings on 25° C, 950 °C, 1050 °C, and 1150 °C temperatures were calculated using W-H profiles are presented in Fig. 4.48, and the summarized results are shown in Table 4.12. The crystallite size and lattice strain values at each stage are calculated from these diffraction peaks (Fig. 4.21). A decrease in lattice strain and an increase in crystallite size with temperature (25 °C – 1150 °C) is evident in Table 4.12. As stated earlier, the microstrain contribution to the XRD line broadening effect could not be ignored for finer crystallites. There might be variations in the crystallinity of the coatings. The temperature eventually affected the formation of more fine crystals. At high temperatures (950-1150 °C), the release of the microstrain can be attributed to the driving force for the recrystallization. The temperature eventually affected the formation of finer crystals.

It should be noted that the crystallite size of the as-deposited APS and DSC coating is 65.7 nm and 27.5 nm, respectively. The crystallite size of the annealed coating of APS and DSC is 78.0 nm and 53.2 nm, respectively. The results revealed the process-induced effect on the crystallite size variation. DSC process leads to finer crystallite size and helps to retain the feedstock characteristic and, simultaneously, thermally more stable due to the strain hardening effect compared to the APS process. The particle velocity is more incredible during the DSC than in APS, while flame enthalpy is greater in APS than in DSC. Therefore, the nature of DSC helps to retain the feedstock (Ni-5%Al gas atomized powder) characteristic of finer crystallite size. Upon detonation spraying, the powders partially melt and plastically deform heavily (strain hardening).

On the other hand, thermally driven APS tends to increase the crystallite size during spraying, as seen from the result of the APS as-deposited coating being significantly larger than DSC as-deposited coating. It should be the same powder used for both APS and DSC. It is clear from the oxygen content (EDS analysis) increase after in-situ HT-XRD treatment for both DSC and APS coatings. As shown in Table 4, the decrease in the crystallite size from 1150 °C to room temperature can be attributed to the oxidation during HT-XRD. A significant amount of Ni atoms has diffused to form the NiO, which could decrease the average crystallite size. The diffusion of (Ni flux in

the present study) is a significant element from the grain-to-grain boundary during the initial oxidation stage, decreasing the crystallite size (Kim et al. 2015). It should be noted that the crystallite size details are present in the present study based on the XRD data. However, a detailed microscopy study is necessary to confirm further.

Table 4. 12. XRD analysis – Crystallite size (nm) and lattice-strain (%) of Ni-5wt%Al coatings using Williamson-Hall analysis through UDM.

Temperature (°C)	Crystallite size (D, nm)		Lattice Strain (ϵ , %)	
	APS	DSC	APS	DSC
As sprayed (25)	65.7	27.5	0.1	0.16
950	73.6	67.5	0.07	0.14
1050	91.7	76.8	0.04	0.11
1150	122.8	91.2	0.01	0.02
After cooling (25)	78	53.2	0.1	0.1

4.2.1.5. Microstructural evolution of coatings at before and after HT-XRD

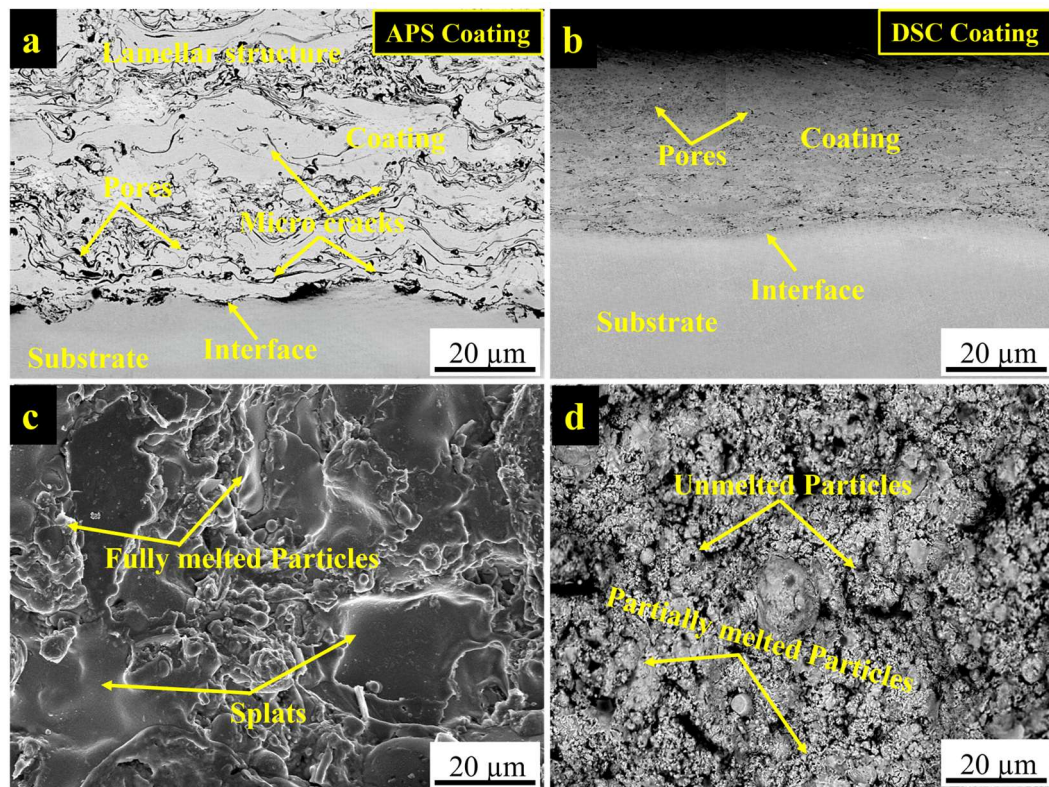


Fig. 4. 24. As-deposited cross-section and Surface morphology of Ni-5wt%Al coatings; (a and c) APS and (b and d) DSC.

Fig. 4.24(a&d) demonstrates the as-deposited cross-sectional and surface morphologies of the APS and DSC coatings on an IN718 substrate. The average thickness of the coatings was around $250 \pm 25 \mu\text{m}$. It can be noticed that the APS sprayed coatings are lamellar with high porosities, voids, and micro cracks. Fig. 4.24(c) shows surface micrographs of an APS Ni-5wt%Al coating. The Ni-5wt%Al powder particles are completely melted and deposited equally over the substrate, with compact cohesive bonding between the molten particles. The pores result from the non-uniform melting of powders when they interact with the high-temperature flame or arc. The kinetic energy of powder particles is usually low in APS processing, which is also responsible for the pores microstructure of the coatings.

On the other hand, DSC coatings exhibit a dense and uniform microstructure with excellent inter-splat bonding and fewer splat boundaries (Fig. 4.24(b&d)). A few pores noticed at the coating/substrate interface might be attributed to semi-melted and unmelted feedstock material entrapped during thermal spraying. The DSC Ni-5wt%Al coating exhibits partly melted and unmolten particles, as illustrated in Fig. 4.24(d). It also has a typical lamellar microstructure with a reasonable amount of porosity in Table 4.13.

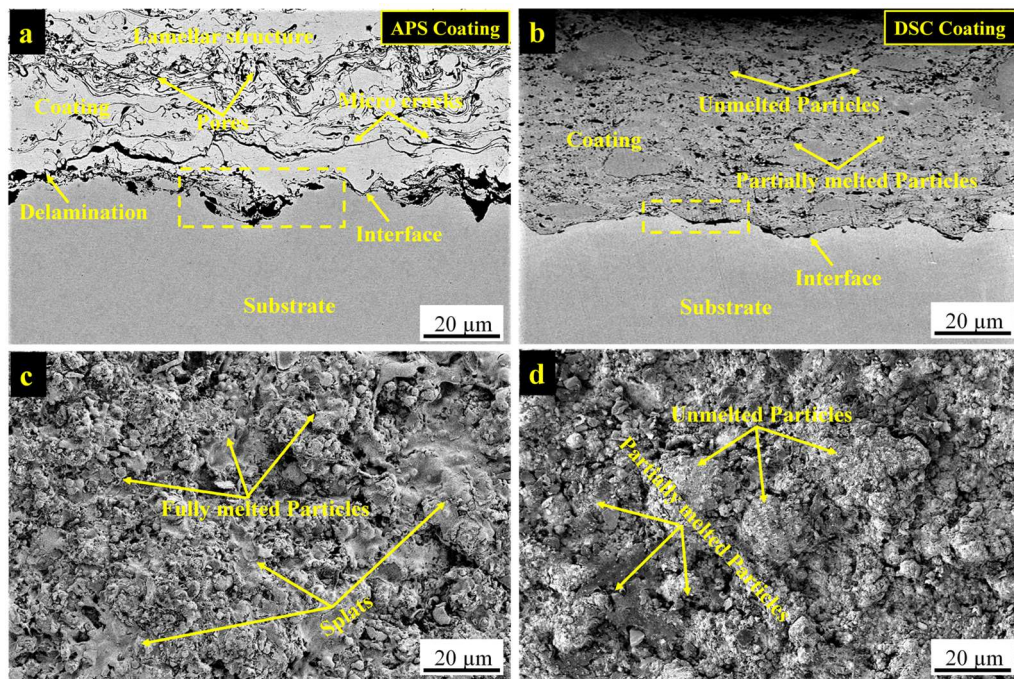


Fig. 4. 25. Surface morphology and cross-section of Ni-5wt%Al coatings after HT-XRD condition at 1150 °C; (a and c) APS and (b and d) DSC.

Fig. 4.50 depicts the morphology and cross-section images of the Ni-5wt%Al coating of APS and DSC samples. The Ni-5wt%Al coating layer can be clearly distinguished from the substrate. The coating was lamellar with high porosities and free of cracks and pore networks. The pores result from the non-uniform melting of powders when they interact with the high-temperature flame or arc. The kinetic energy of powder particles is usually low in APS processing, which is also responsible for the pores microstructure of the coatings (Sadeghimeresht et al. 2016). Powder particles oxidized in a plasma plume during in-flight and high deposition temperature during spraying will also form interlamellar pores. A continuous crack along the Ni-5wt%Al bond coat and substrate was shown in Fig. 4.25(a) of the APS coating. Crack propagation reached a critical level due to increasing residual stress at the bond coat and substrate interface, resulting in bond coat delamination (Xian et al. 2021). However, the coating was not completely peeled off. This behavior can be attributed to the mismatch in CTE of the IN718 substrate and APS coating.

As illustrated in Fig. 4.25(b), the interface adhesion of the DSC Ni-5wt%Al coating with the substrate is excellent. The interface is free of cracks and delamination; however, there are only a few pores and macro cracks (the region shown in the "box"). The pores are formed mainly due to variations in the chemical compositions and thermo-physical characteristics of the as-received powders and the substrate. The molten/semi-molten Ni-5wt%Al particles could not be entirely spread out or trapped to the surface of the substrate during the detonation sprayed process, resulting in a few holes at the boundary. The average thickness of the coatings was around $250 \pm 25 \mu\text{m}$.

The surface micrographs of APS Ni-5wt%Al coating are shown in Fig. 4.25(c). The complete melting of powders can be observed clearly. The Ni-5wt%Al powder particles are melted and deposited equally over the substrate, with compact cohesive bonding between the molten particles. The temperature during APS is high enough to melt Ni-5wt%Al powder. As shown in Fig. 4.25(d), the DSC Ni-5wt%Al coating surface morphology is rough and shows partially melted and unmolten particles, a characteristic of DSC. The moderate heating and high-velocity propulsion of powders result in a dense microstructure. It also has a typical lamellar microstructure with a

reasonable amount of porosity in Table 4.13. However, they are free of cracks and large pores, as seen in the microstructure of APS.

Table 4. 13. Porosity of APS and DSC sprayed Ni-5wt%Al coating.

Coating	Coating process	Porosity (%)	
		As-deposited	HT-XRD
Ni-5%Al	APS	4.46±0.7	3.83±0.3
	DSC	2.14±0.2	2.06±0.1

4.2.1.6. EDS elemental mapping of in-situ HT-XRD Ni-5wt%Al coating

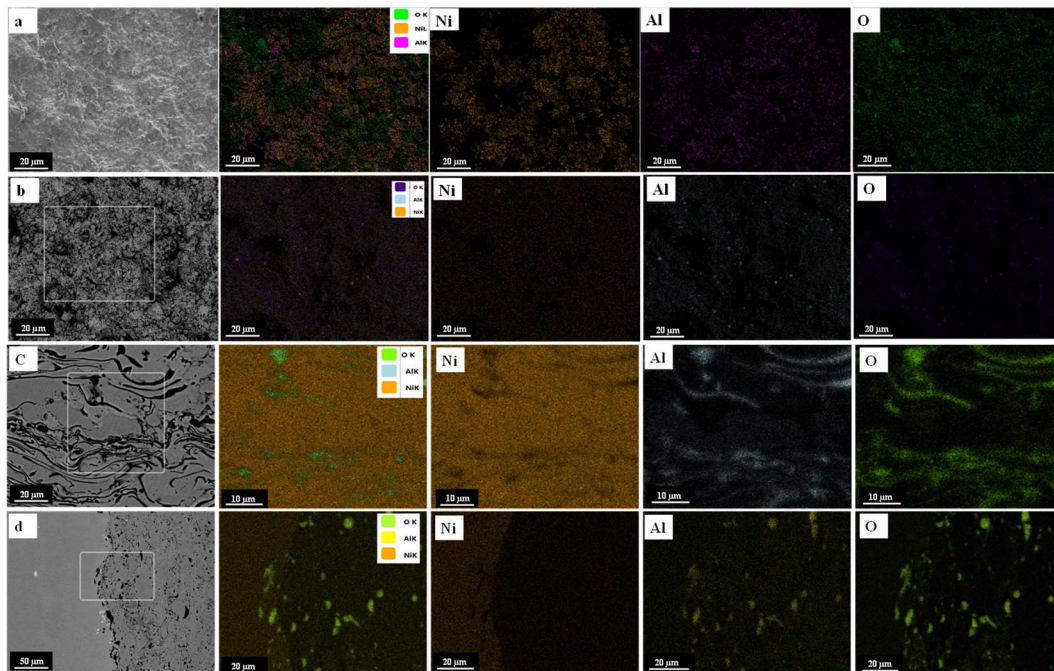


Fig. 4. 26. EDS mapping analyses of element content on the Ni-5wt%Al coating surface and cross-section at as-deposited condition; (a&c) APS and (c&d) DSC.

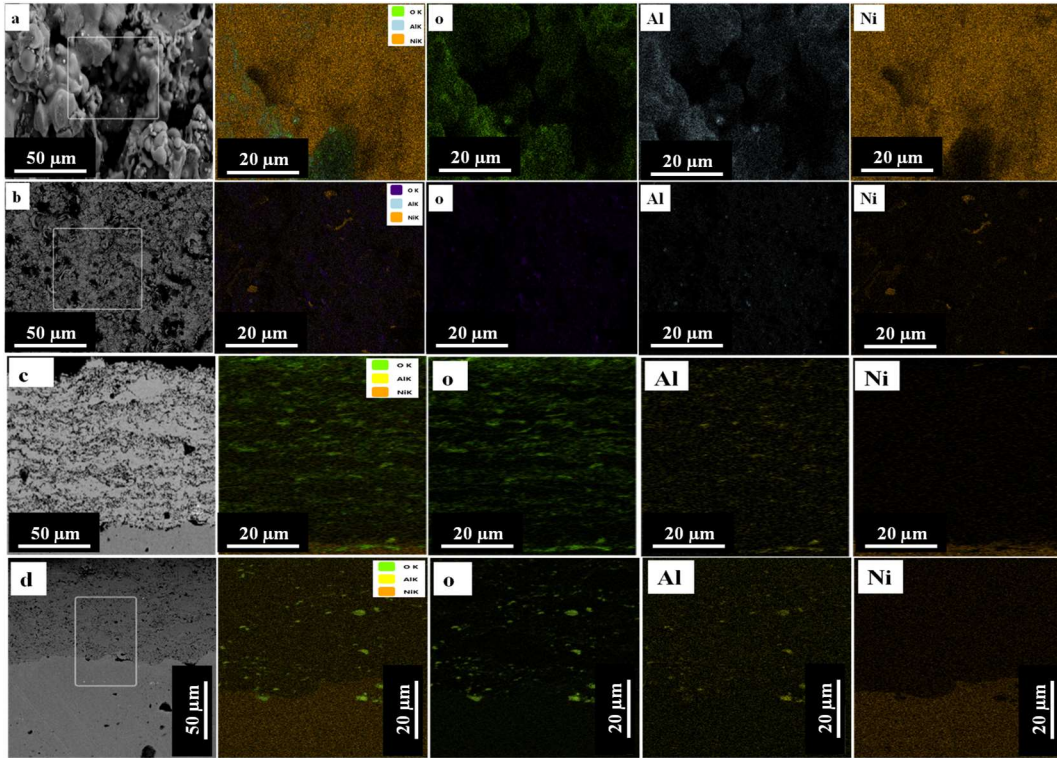


Fig. 4. 27. EDS mapping analyses of element content on the Ni-5wt%Al coating surface and cross-section after the in situ high-temperature XRD at 1150 °C; (a&c) APS and (c&d).

The composition mapping of the Ni-5wt%Al coating surface and cross-section after the in-situ HT- XRD at 1150 °C are given in Fig. 4.26(a-d) and 4.27(a-d). A straightforward comparison can be made between before (as-deposited) and after in-situ treatment of the DSC and APS process. The EDS analysis of the oxidized surfaces shows the distribution of Aluminium (Al), oxygen (O), and Nickel (Ni). The oxygen dispersion can be seen uniformly from the surface to the interface. The formation of high nickel oxides at the surface of the APS Ni-5wt%Al coating indicates the excessive oxidation of coating (Fig. 4.27(a&c)), which XRD has also supported. NiO phase could even cause oxide cracking and oxidize the metal, as shown by the FESEM image (Fig. 4.27(a)). The high porosity and micro-cracks surface in the APS coating can also be the reason for the oxidation (Fig. 4.25(a&c)). An oxidized nature of the APS as-deposited coating microstructure significantly influenced the thermal expansion and the mismatch between the IN718 substrate.

The coating has been substantially oxidized during processing, irrespective of the methods used. However, the residual oxide content of the APS coating is higher than the DSC coating. The atmospheric plasma in APS exposes the powder particles to a more oxygen-rich environment, leading to increased oxidation and a higher residual oxide content in the final coating than DSC. As seen from Table 4.14, the residual oxide content of the coating in the as-deposited condition is relatively lower than that noticed after in-situ HT-XRD. The result can be attributed to the inhomogeneous nature of the as-deposited coatings due to the rapid solidification during the APS and DSC deposition.

In inhomogeneous conditions, the oxides tend to segregate at intersplat boundaries (Molins et al. 2003). After heating in-situ HT-XRD treatment in a controlled atmosphere, oxides redistributed throughout the microstructure more or less uniformly as they became homogenized. The higher amount of oxygen content after the heat treatment is shown in Table 4.14. The size range of particles (5 to 45 μm) determines the melting, partial melting and unmolten (particles), and in-flight oxidation during APS and DSC. As these particles impact the substrate, they solidify rapidly and create inhomogeneous microstructure during APS and DSC depositions (Kala et al. 2022). The pick-up of external oxygen during the controlled atmosphere treatment has not been ruled out here, which might have happened. However, the oxygen content increase is nearly 3-fold after the in-situ HT-XRD treatment of both APS and DSC. There was oxygen pick-up during the HT-XRD. Therefore, the present study considers the quantum of external oxygen pick-up negligible and allows the determination of thermal expansion as-deposited coating in the homogenized state.

On the other hand, the DSC coating (Fig. 4.27(b&d)) shows the characteristic lamellar structure of splats is mostly unoxidized. The intersplat oxidation is visible during DSC. However, the oxygen pick-up is relatively low after in-situ HT-XRD of DSC coating compared to APS coatings. It is clear from the evaluation that the initial as-deposited microstructural constituents, such as oxides, play a substantial role in the resultant CTE of the as-deposited coating. The residual oxide content of the coating was a result of the nature of the coating process. The coating microstructure, irrespective of the coating process, became homogeneous after in-situ annealing. The

oxides in the coating have been redistributed more uniformly, as seen in the cross-section microstructure (Fig. 4.27). The maximum heat treatment temperature is 1150 °C, which uniformly relaxes the coating strain to 0.1. Post in-situ HT-XRD heat treatment EDS analysis reveals the formation of excess oxides (NiO) increase after treatment for both DSC and APS coatings. The oxide formation can also be attributed to the increased lattice strain after the samples are cooled to the ambient condition. The DSC coating is more intact to the substrate, and the crystallite size is relatively low compared to the APS. The nature of in-flight oxidation, relatively stable microstructure at elevated temperatures, and comparable CTE of the DSC coating make it promising for TBC applications. Therefore, the selection of the coating process becomes more significant while depositing the bond coat for the TBC applications.

In-situ HT-XRD proved to be a quick way to measure the physio-thermal properties of the overlay coating without separating them from the substrate. Recrystallization after homogenization treatment will decide the kinetics of TGO formation (Kala et al. 2022). Besides, in-situ HT-XRD helps to understand the recrystallization of the as-processed coatings and would support the microstructural optimization of the bond coats for TBC applications. Thus, in-situ HT-XRD helps to understand the recrystallization of the as-processed coatings and would support the optimization of TBC.

Table 4. 14. Element contents (wt%) of APS and DSC sprayed Ni-5wt%Al coating.

Conditions	APS						DSC					
	Surface			Cross-section			Surface			Cross-section		
	Ni	Al	O	Ni	Al	O	Ni	Al	O	Ni	Al	O
As deposited	88.33	6.26	5.41	84.27	3.98	11.75	95.07	2.51	2.42	92.70	4.05	3.25
After HT-XRD	71.82	9.80	18.38	53	14.37	32	82.72	8.24	9.05	84.27	3.98	11.75

4.3. Effect of thermal expansion on the high temperature wear resistance of Ni-20%Cr detonation spray coating on IN718 substrate

4.3.1. In-situ high-temperature X-ray diffraction (HT-XRD)

4.3.1.1. Stacking and peak shift behaviour of a Ni-20%Cr coating

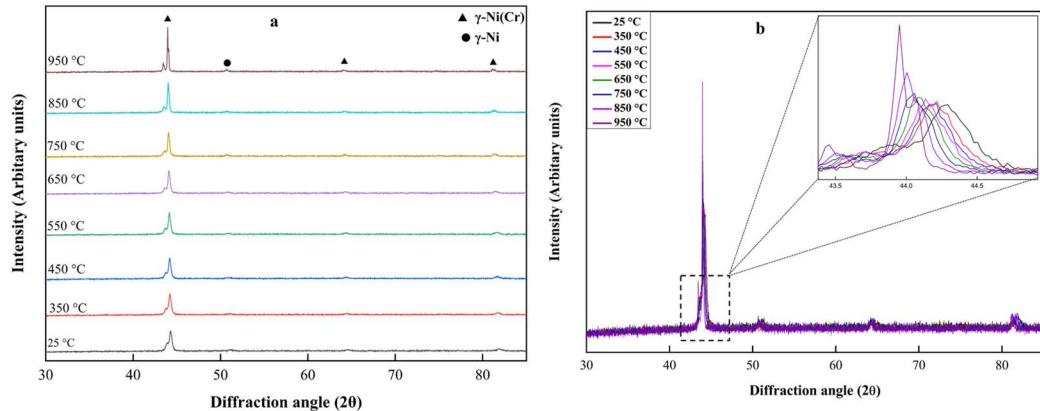


Fig. 4. 28. Stacking and Peak Shift During HT-XRD and the inset depicts the thermal expansion caused peak shifting phenomenon. (a) Diffraction peak stacking (b) Peak Shift phenomenon.

The diffraction patterns obtained at various temperatures were stacked and indexed, as shown in Fig. 4.28(a). According to the HT-XRD analysis, the intensity of the peaks recorded at high temperatures is much narrower than those recorded in as-deposited coatings, showing crystallinity and finer crystallite size. The broader peaks correspond to as-deposited coatings, showing that residual stress and strain hardening happened during deposition, which includes more kinetic energy (high spray particle velocity) than thermal energy. The Ni-20%Cr coating preserved the major phases seen at various elevated temperatures (25 °C - 950 °C). Significant phases in Ni-20%Cr coatings have FCC (solid solution crystal structure) structure, with only pure γ -Ni(Cr) (ICDD File no: 01-071-7597) dominant, and γ -Ni (ICDD File no: 01-071-4653) is the minor peak, with no other peaks visible from ambient temperature to 950 °C.

Fig. 4.28(b) shows the HT-XRD findings of a DSC sprayed Ni-20%Cr coating from room temperature (25 °C) to high temperature (950 °C). There was no significant difference in the room temperature XRD data acquired in a typical temperature versus a vacuum. As the temperature rises, the diffraction peaks move from the initial 2θ location to the lower diffraction angle side. The peak shift reflects residual stress

relaxation and lattice expansion (Kala et al. 2022). As a result, peaks at high temperatures are substantially sharper than at room temperature. Simultaneously, the strain relieving in the coating is seen as a result of the high-temperature exposure. Peak sharpening (Fig. 4.28) shows crystallite size and lattice strain in the coating. The shift in peak location in XRD patterns is responsible for developing new planes, phase changes, lattice strain effects, and other phenomena.

4.3.1.2. Measurement of coefficient of thermal expansion (CTE)

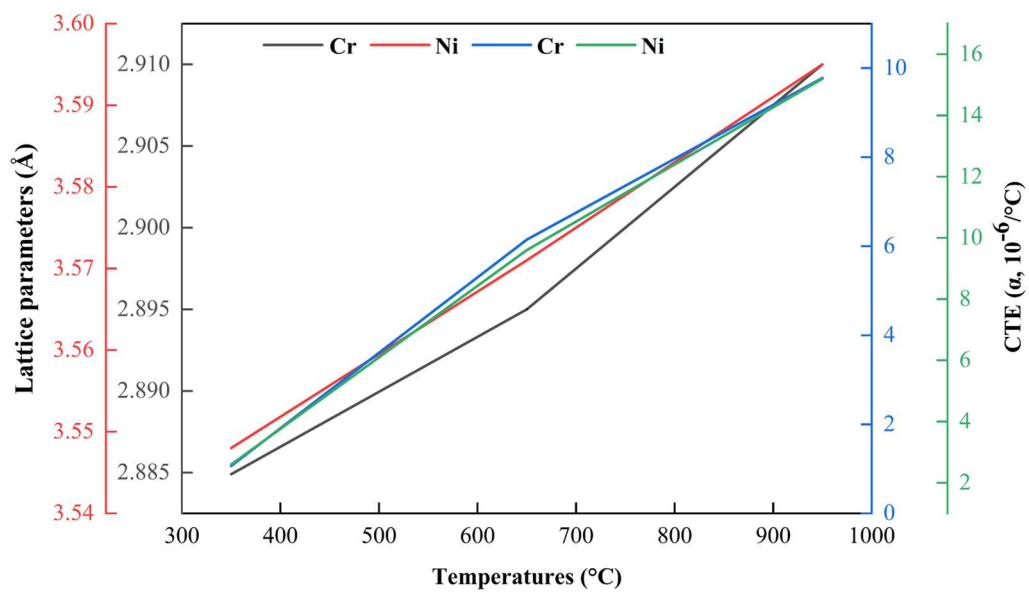


Fig. 4. 29. Lattice parameters and CTE vs. temperatures of DSC sprayed Ni-20%Cr coatings.

One of the most significant factors in predicting the lifespan of thermal spray coatings for high-temperature applications is thermal expansion. The CTE depends solely on the crystal structure and any phase transitions during heating. Thermal expansion studies were performed on a DSC sprayed Ni-20%Cr coating from room temperature (25 °C) to high temperature (950 °C). The HT-XRD lattice parameter determines the average linear coefficients of thermal expansion (CTEs) using eq (3.1).

Based on the γ -Ni(Cr) phase with FCC structure, typical in Ni-20%Cr coatings and superalloys with high Ni content, the lattice parameter from HT-XRD is used to compute the average linear coefficients of thermal expansion (CTEs). Fig. 4.29 shows the calculated value of lattice parameters of γ -Ni(Cr) phases vs. temperature, and CTE remains constant at $15.2 \times 10^{-6}/^{\circ}\text{C}$ from ambient temperature to 950 °C (Karunaratne et

al. 2016). As Cr is a major alloying element in Ni-20%Cr coatings, the α -Cr phase (BCC) may also dominate the thermal expansion and agrees with the reported result that CTE remains reasonably constant at $9.78 \times 10^{-6}/^\circ\text{C}$ from ambient temperature to 950°C (Karunaratne et al. 2016), (Fritscher et al. 1995).

The CTEs of Ni and Cr phases grow linearly over the temperature range as the crystal lattice vibration intensifies. The CTE of DSC Ni-20%Cr coating is higher and closer to the substrate. As a result, the thermal expansion mismatch at the coating-substrate interface is low. Because of the lower thermal stress generated at the interface, the coating and substrate will be more resistant to crack initiation and spallation, thereby ensuring superior wear resistance (Saladi et al. 2014).

4.3.1.3. Crystallite size and lattice strain

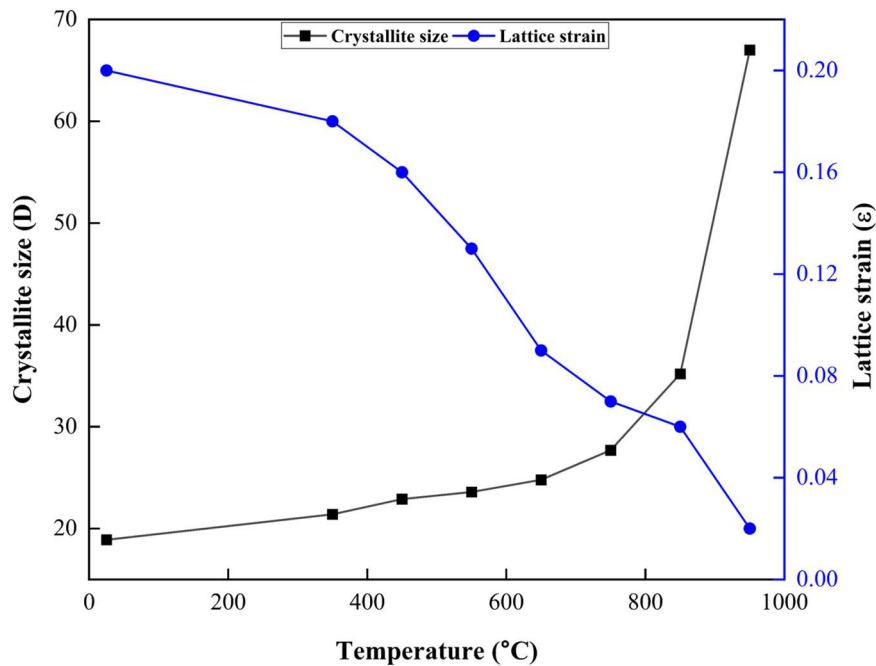


Fig. 4. 30. Variation of crystallite size (D) and lattice strain (ϵ) with annealing temperature of Ni-20%Cr coatings.

The crystallite size and lattice strain of Ni-20%Cr coatings at temperatures ranging from 25°C to 950°C were computed using W-H profiles and are shown in Fig. 4.30. At room temperature, no stress was noticed, and the average crystallite size and lattice strain was 18.9 nm and 0.2, respectively. Fig. 4.30 shows a gradual decrease in lattice strain (0.02) and a rise in crystallite size (65 nm) as temperature increases to 950

°C. The release of lattice strain at high temperatures (950 °C) can be ascribed to the driving force for recrystallization. The development of finer crystals was eventually influenced by temperature.

4.3.2. Tribological behaviour of Ni-20%Cr coating

4.3.2.1. Microstructural characterization of Ni-20%Cr coating

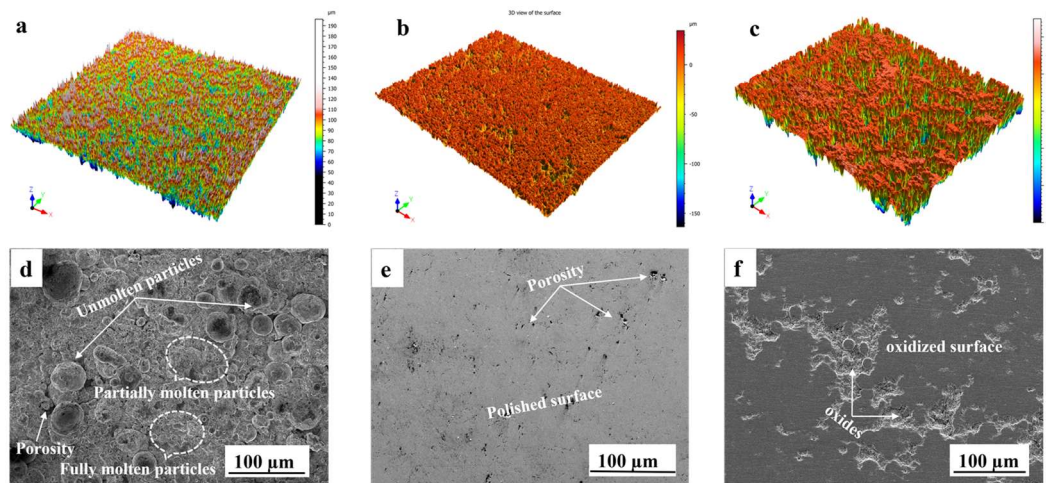


Fig. 4.31. 3D topographical and FESEM micrographs of Ni-20%Cr coating; (a, d) As-deposited (b, e) After polishing and 25 °C (c, f) after the wear test at 850 °C.

Fig. 4.31 displays 3D profilometry, FESEM pictures, and surface morphology and roughness evolution of Ni-20%Cr coating. As illustrated in Fig. 4.31(a, d), many partially/unmolten powder particles were entrapped to the as-deposited Ni-20%Cr sample surface, needle-like tips and deep pits be seen in Fig. 4.31(a), resulting in a high roughness of $12.23 \pm 1.68 \mu\text{m}$. Because of the extreme velocity of the impinging molten powder particles during the DSC, the coating had sparse porosity and a relatively homogenous microstructure, dense and well adhered to the substrate, with a thickness of $250 \pm 23 \mu\text{m}$. After metallography polishing, it can be noticed that the partially molten/unmolten particles disappeared significantly, and the sample surfaces are much smoother, more consistent, and brighter than the as-deposited coating surface. A long polishing time can influence substantially by enhancing the surface quality and decreasing roughness considerably to $3.27 \pm 0.72 \mu\text{m}$, as shown in Fig. 4.31(b, e). At the same time, a few burr-shaped asperities were observed on the Ni-20%Cr coating surface, increasing the surface roughness to $8.39 \pm 1.36 \mu\text{m}$ in Fig. 4.31(c, f). This is

because the polished coating was partially oxidized during sliding friction and wear experiments at 850°C, paving the way for a few oxide formations.

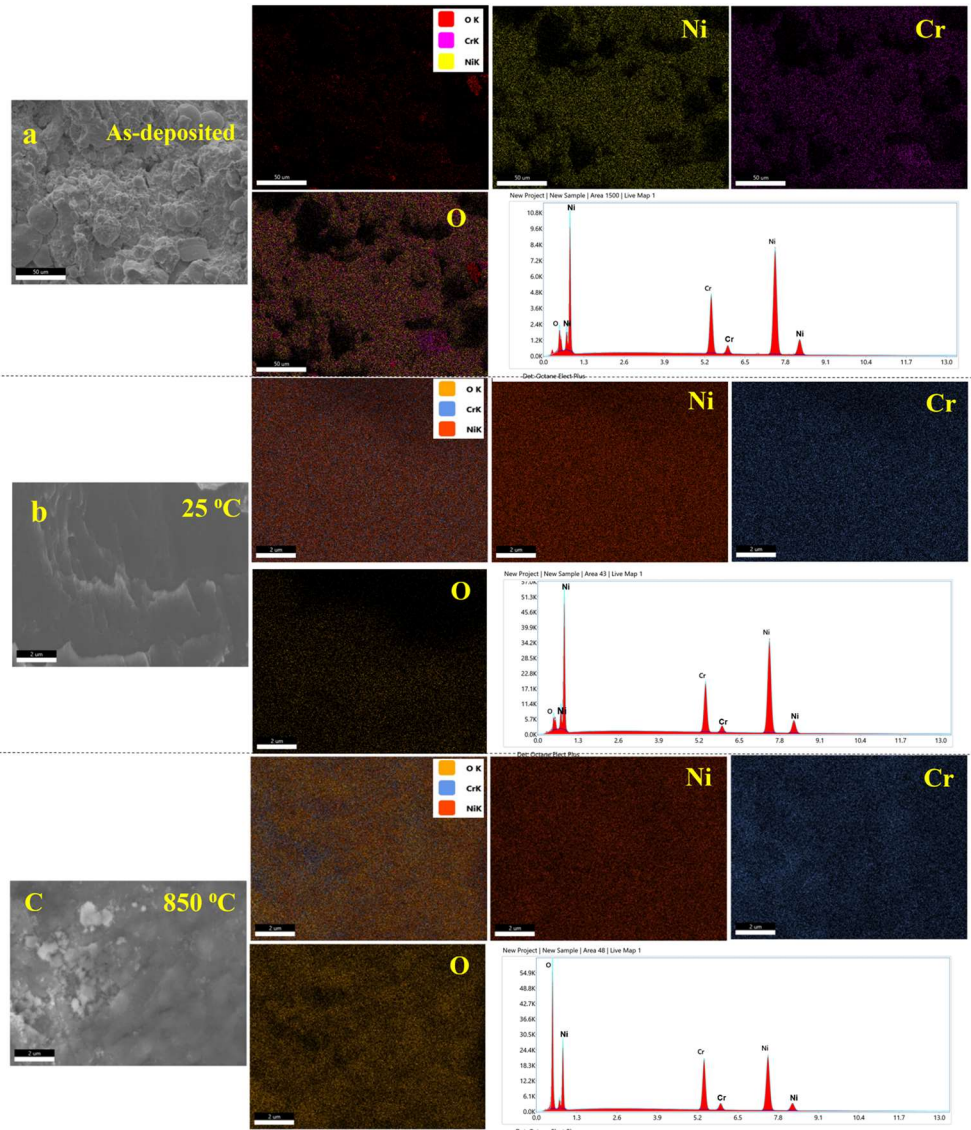


Fig. 4. 32. Elemental mapping analysis of Ni-20%Cr coating; (a) As-deposited (b and c) After the Wear at 25 °C and 850 °C.

Fig. 4.32 shows surface EDS elemental mapping of the Ni-20%Cr coating as as-deposited and after the wear at 25 °C and 850 °C. The oxidized surfaces EDS analyses revealed that the maps of chromium (Cr), oxygen (O), and nickel (Ni) are well matched. The chemical composition of the as-received powder is approximately 80% Ni and 20% Cr, almost identical to the theoretical value of Ni-20%Cr. Furthermore, the element composition of the as-deposited and 25 °C Ni-20%Cr coating is equivalent to feedstock powders. It also suggests that all materials are deposited homogeneously and without

evident segregation during the coating deposition. However, as the temperature rises from 25 °C to 850 °C, Ni and Cr decrease and increase O. It acts by increasing the concentration of oxygen (O) within the surface area, indicating the development of oxides at high temperatures (Shi et al. 2021), and Table 4.15 summarises the findings.

Table 4. 15. Surface roughness and EDS analysis of DSC sprayed Ni-20%Cr coating.

Coating	Temperature (°C)	Surface roughness (S _a , μm)	Chemical composition (wt%)		
			Ni	Cr	O
Ni-20%Cr	As-deposited	12.2±1.8	79.3±1.1	18.2±0.4	2.4±0.63
	25	3.2±0.7	78.4±0.5	18.4±0.2	3.2±0.3
	850	8.4±1.4	59.3±0.6	16.5±0.8	24.1±0.2

4.3.2.2. Microhardness evaluation of the Ni-20%Cr coating

Table 4.16 illustrates the Vickers microhardness indentations formed on the Ni-20%Cr coatings at the cross-section under the 200g applied load at different temperatures (after the wear test at 25 °C and 850 °C). The porosity and density of the coating influence the microhardness to a large extent (Du et al. 2011). The significant variation in microhardness values is caused by several factors that are affected by the coating deposition process and the presence of oxides and metallic phases. At 25 °C, the average micro-hardness of Ni-20%Cr coating was (332±47.63 HV_{0.2}) very high because of the significant residual stress generated by the faster cooling rate, presence of partial oxides, and metallic phases in the coating (Bai et al. 2011). After the wear test (850 °C) of an oxidizing medium, the microhardness was reduced to 267±28 HV_{0.2}. It can be attributed to the coatings further softening and annealing at the increased temperature by absorbing ambient and friction heat and releasing compressive stresses, resulting in finer grains, which lower shear strength and enhance plastic deformation (Hager et al. 2009). There is no indication of plastic or shear transformation zones from the corners of the indentations at 25 °C and 850 °C. This result reaffirmed the high mechanical toughness values and significant ductility in both conditions.

Table 4. 16. Microhardness values and standard deviations of Ni-20%Cr coatings after the wear test at 25 °C and 850 °C.

Coating	Hardness (HV _{0.2})	
	25 °C	850 °C
Ni-20%Cr	332±47.63	267±28

4.3.2.3. Dry sliding friction and wear behaviour of Ni-20%Cr coating

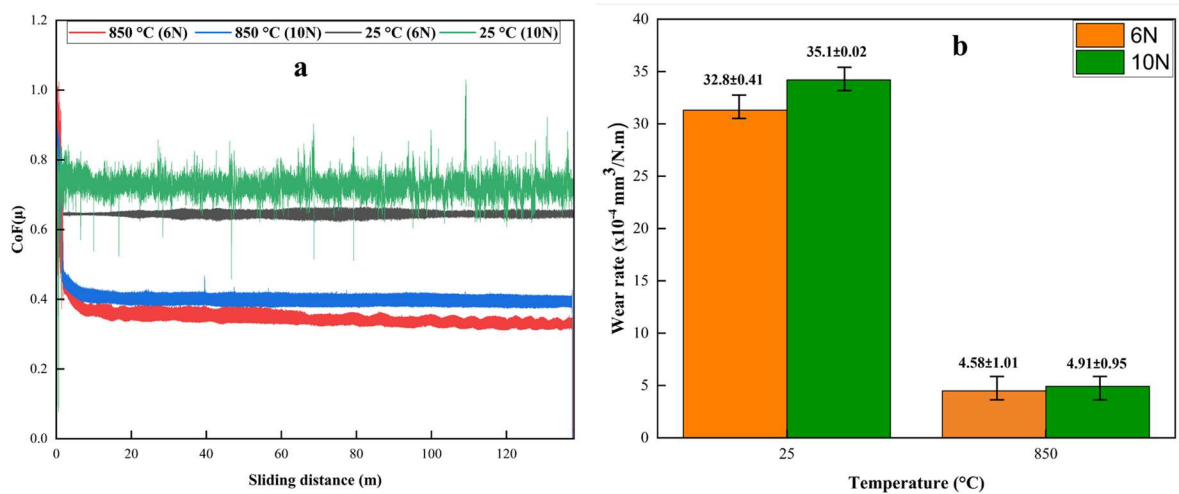


Fig. 4. 33. Depicts the dry sliding friction and wear behaviour of a Ni-20%Cr coating sliding against a ball in stagnant air evaluated at RT (25 °C) and HT (850 °C). (a) CoF vs. sliding distance (b) Wear rate vs. temperature.

Fig. 4.33(a) represents their frictional performances of Ni-20%Cr coating under different loads (6N & 10N) at elevated temperatures (25 °C and 850 °C) and exhibits some temperature-dependent characteristics for the two tribological pairs. The increasing operational temperatures decrease the CoF of the coating against the Al₂O₃ ball. The CoF at 25 °C for 6N and 10N loads is 0.65±0.03 and 0.72±0.07, respectively. CoF values were initially high because of the breaking of the surface and other partial oxide layers during the run-in. When the worn debris was compressed into the friction pair, they immediately reduced to low steady-states. At 850 °C, the CoF of Ni-20%Cr coatings for 6N and 10N becomes as low as 0.39±0.06 and 0.42±0.04, respectively (Medabalimi et al. 2021). It is evident that the CoF of Ni-20%Cr coating significantly reduced at 850 °C due to the formation of surface oxides, which eventually enhanced

the wear resistance. These findings imply that temperature-mediated frictional characteristics in coatings are essentially controlled by the generated tribolayer over the tribologically interacting surface (Novak and Polcar 2014) (Munagala et al. 2019). The formation of these protective glazed oxide layers and other intermetallic compounds enters the contact interface between the friction pair, reducing the adhesion phenomenon and ploughing on the coating.

At high temperatures, Ni-based coatings, deposited by thermal spray techniques, can form stable, protective oxides (NiO, Cr₂O₃, and NiCr₂O₄). These oxides can directly impact the wear behavior and contribute to reducing the friction coefficient and wear rate (Karaoglanli et al. 2017) (Medabalimi et al. 2021), (Kiryc et al. 2023), (Bolelli et al. 2020). The coefficient of friction (CoF) and wear rate in coatings and substrates decreased gradually as the temperature increased. While considering the wear rate of the DSC Ni-20%Cr coatings in the present study, the performance is on par with the high-velocity oxy-fuel (HVOF) sprayed MCrAlY coatings and atmospheric plasma sprayed Ni-20%Cr (Medabalimi et al. 2021), (Kiryc et al. 2023).

The dry sliding wear behaviour of Ni-20%Cr coating against a ceramic Al₂O₃ ball is also temperature dependent. Fig. 4.33(b) shows a gradual decrease from 25 °C to 850 °C, which agrees with unanticipated tribo-oxidation under friction, heat, and stressed-shearing conditions. This is explained by lower hardness, lower yield strength, and higher ductility. As a result, wear is not prevalent owing to the enhanced plastic deformation at 850 °C (Huang et al. 2016). On the other hand, the coating's wear rate, a compacted oxidation layer (Cr₂O₃ and NiO) with its self-lubricating effect, usually forms while sliding and is protective and resistant to friction and wear (Medabalimi et al. 2021). These oxides may be self-lubricating due to the tribolayer. More information is presented in the following sections.

4.3.2.4. Worn surface topography by 3D profilometer

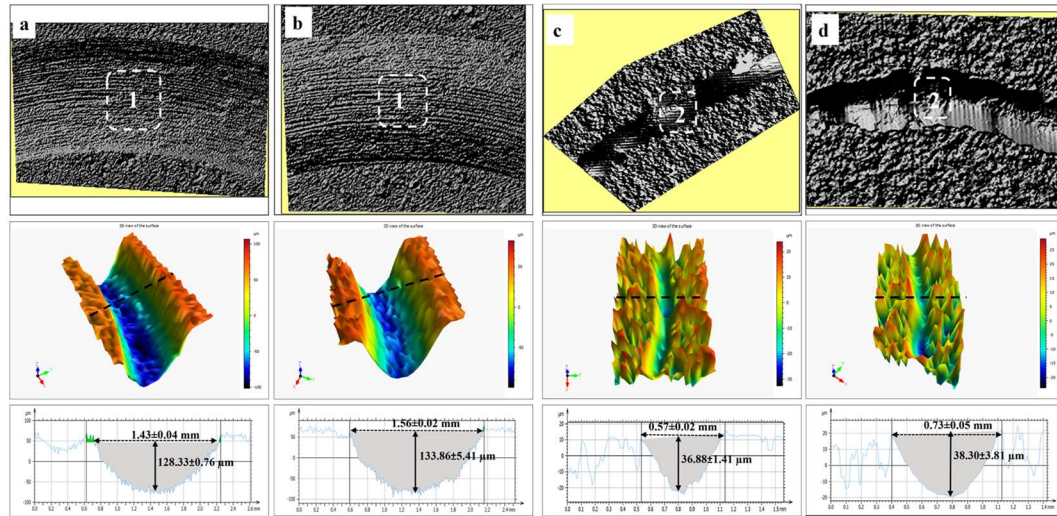


Fig. 4. 34. Non-contacting optical 3D profilometry of the 3D and 2D topographies of wear traces of Ni-20%Cr coating after dry sliding under different 6N and 10N loads. (a, b) RT (25 °C) and (c, d) HT (850 °C).

The 2D and 3D profiles and topographies of the worn surface of Ni-20%Cr coating after dry sliding at 25 °C and 850 °C are shown in Fig. 4.34 and Table 4.17. After a dry sliding friction test at 25 °C, the wear track of the as-polished surface has several parallel plough markings (marked as a region "1" in Fig. 4.34(a, b)). The hard-abrasive particles produced during friction cause the formation of parallel furrows. Increasing the surrounding temperature, the traces of abrasive wear (parallel grooves) of the coatings rubbing at 850 °C eventually disappear, as shown in Fig. 4.34(c, d). In contrast, the tracks of plastic deformation caused by adhesion wear (denoted by the region "2") become prominent. Because the Ni-20%Cr coating may be softened by absorbing ambient and frictional heat, the lower the hardness and the higher the ductility (Table 4.16). As a result of the thermal softening of the coating, it spread out along the sliding direction, resulting in plastic deformation (Hao et al. 2019).

Table 4. 17. Wear data with standard deviations of Ni-20%Cr coating at 25 °C and 850 °C temperatures.

Coating	Loads (N)	Width (mm)		Depth (μm)	
		25 °C	850 °C	25 °C	850 °C
Ni-20%Cr	6	1.43 ± 0.04	0.57 ± 0.02	128.33 ± 0.76	36.88 ± 1.41
	10	1.56 ± 0.02	0.73 ± 0.05	133.86 ± 5.41	38.30 ± 3.81

4.3.2.5. Temperature-mediated wear behaviors of Ni-20%Cr coatings

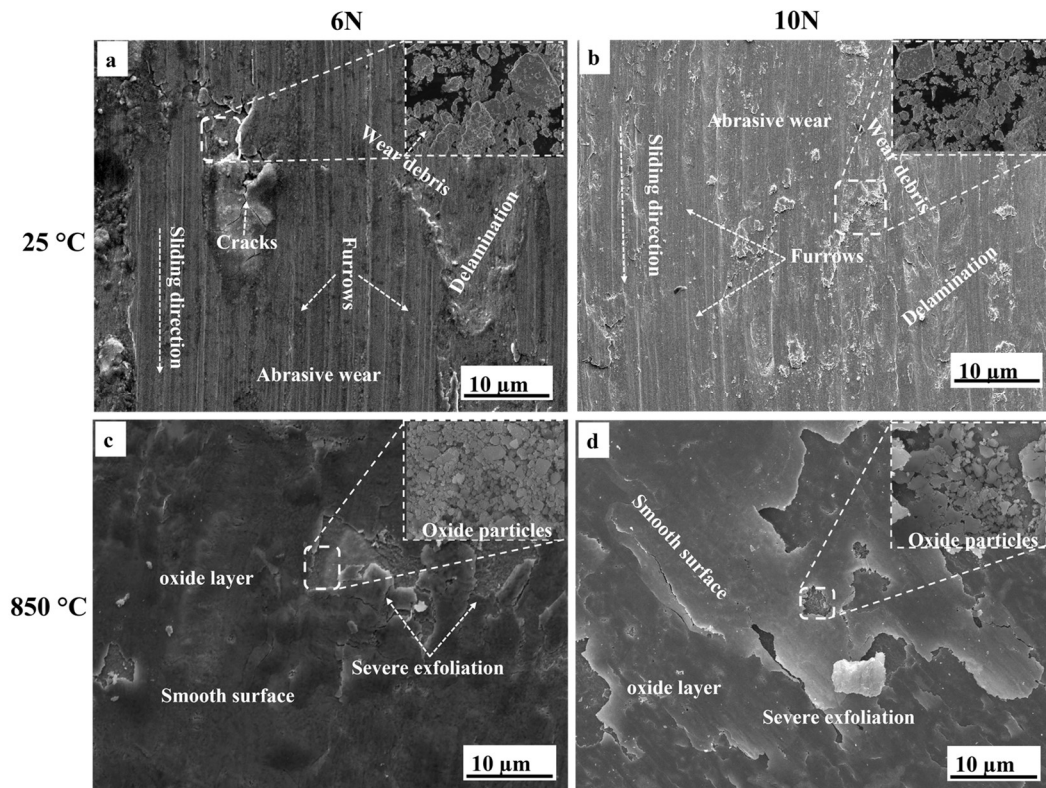


Fig. 4. 35. Worn surface morphologies of Ni-20%Cr coating (a, c) 6N (b, d) 10N loads at 25 °C and 850 °C.

The microstructural features of worn surfaces of Ni-20%Cr from 25 °C to 850 °C are depicted in Fig. 4.35(a-d). As seen in Fig. 4.35(a, b), the abrasion (parallel furrows and micro ploughing) and surface fatigue (micro-cracks and delamination) have been the primary wear mechanism, and the wear debris and accumulation of fragile particles (indicated as boxes in "a, b"). It can be incorporated in coatings and counterpart balls or function as loose particles between the two contacts, increasing friction between the rubbed contacts. This phenomenon is attributed to a three-body abrasion.

The wear characteristics of the Ni-20%Cr coating at 850 °C significantly differ from those at 25 °C, as illustrated in Fig. 4.35(c, d). At 850 °C, the dimensions of the wear scars decrease with increasing temperature. This relates to the self-lubricating characteristic of the progressively developing tribo-layer on coating and wear resistance. The coating's dominant wear mechanism includes agglomeration of oxide layers (oxidative wear) and fissures of the oxidized surfaces, as noticed from the severe

peeling of the oxide layer. The wear mechanism of Ni-20%Cr coating seems to be predominantly sticky with severe score marks (Fig. 4.35(c, d)). At 850 °C, smooth tribo-layers develop over the worn surfaces, and adhesive grooves are evident, suggesting adhesive wear. On the other hand, the oxide film (highlighted in boxes "c, d") offers more lubrication at higher temperatures. The significantly thin oxide layer in the coating acts as a barrier between the rubbing surfaces (friction pair) and improves the tribological properties.

4.3.2.6. SEM-EDS morphology of worn surfaces over Al₂O₃ counter material

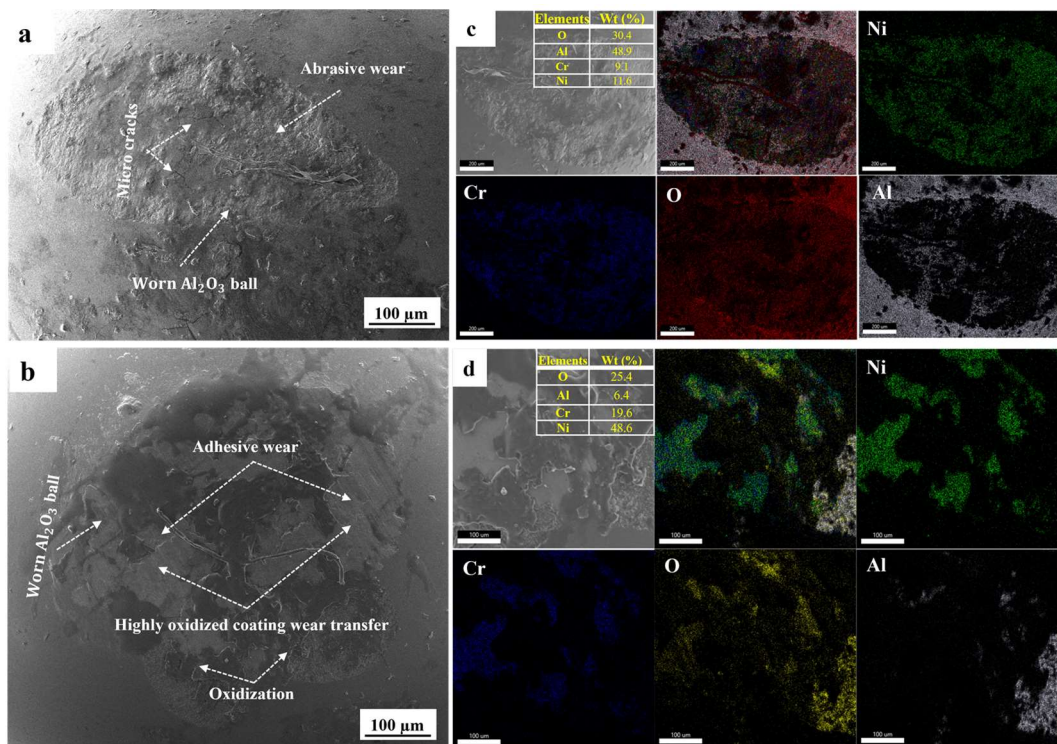


Fig. 4. 36. FESEM micrographs and Elemental mapping on the worn surface of Al₂O₃ ball at different temperatures. (a and c) 25 °C (b and d) 850 °C.

Fig. 4.36 illustrates the FE-SEM micrographs of worn surfaces of the counterpart (Al₂O₃) at average and high temperatures. The wear scar on the paired Al₂O₃ surface against Ni-20%Cr coating decreases with increasing temperatures, which is attributable to the self-lubricating behavior of the gradually expanding tribo-layer on the paired Al₂O₃ surface, and therefore, wear resistance increases gradually. Fig. 4.36(a) shows grooves and delamination at room temperature. The stress concentration in the contact area encourages the formation of microcracks, which promotes crack development and interaction along the sliding direction, implying abrasive and surface

fatigue wear. Wear scar is relatively rough, and some debris clumps together. Countless single particles are scattered throughout the worn surface. Fig. 4.36(c) shows that in the EDS elemental mapping analysis of worn surfaces of the counter material, Al and O concentration is higher, representing that no coating is transferred to the counter material and suggesting abrasive and surface fatigue wear.

Nonetheless, the worn micrographs of the Al₂O₃ ball at 850 °C are significantly different from those at room temperature. Due to the highly oxidized coating transfer to counter material and tribo-oxide film with lubrication ability. Small wear debris particles are sticking on the worn surface (The gray colour region in "b"). Another notable aspect is the increased Ni and Cr concentrations adhering to the worn region (seen in "d"), indicating that nickel and chromium oxides considerably contribute to frictional decrement at elevated temperatures. However, wear is minimal, and smooth tribo-layers are produced over the worn surface of the coating. This thin layer reduces friction and wear as a barrier between the rubbing surfaces.

4.3.2.7. SEM/EDS elemental line analyses of worn surfaces

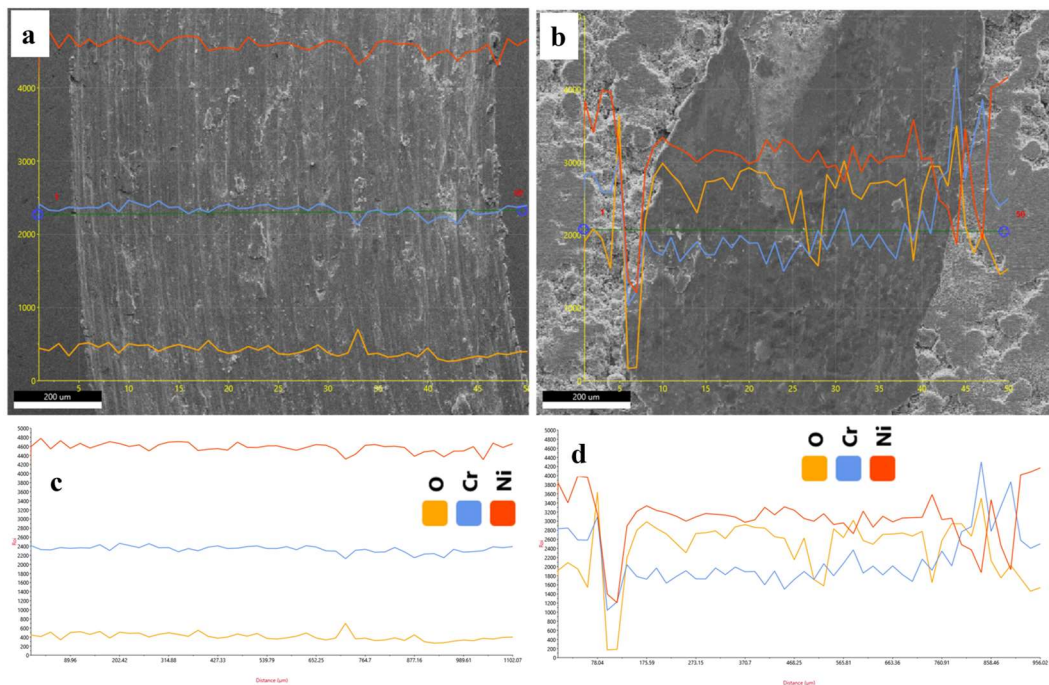


Fig. 4. 37. EDS line analysis of element content on the coating cross-sections at (a, c) 25 °C and (b, d) 850 °C for Ni-20%Cr coating.

Fig. 4.37(a&b) illustrates EDS line analyses over the worn surfaces of Ni-20%Cr coating at 25 °C and 850 °C after rubbing the Al₂O₃ counterpart. At 25 °C, Fig. 4.37(a&c) exhibits small oxide peaks noticed within the worn surface. The abrasion mechanism decreases as temperature increases to 850 °C. In contrast, as shown in Fig. 4.37(b&d), it acts as a careful examination of the oxygen (O), nickel (Ni), and chromium (Cr) element intensities, suggesting that the tribo-layer has been composed of the mixed oxides of both Ni and Cr.



As shown in the above equations, the formation of NiO and Cr₂O₃ is usually well-known in Ni-20%Cr. The proportion of each oxide and its growth depends on thermodynamics and kinetics. This proves that the sliding wear response of Ni-20%Cr coating is temperature-dependent as the composition of Ni and Cr plays a crucial role in developing a lubricating surface, as seen in Table 4.18.

It denotes that the adhesion layer is formed due to a chemical reaction mediated by in-situ frictional heating. Due to continuous friction, the grains are refined and recrystallized in the oxide layer. The friction coefficient of the coating improves from this refined and recrystallized grain. Many distinct grain boundaries formed during recrystallization may relieve local tensile stress, contributing significantly to anti-wear and tribological superiority (Hao et al. 2019).

Table 4. 18. EDS line analysis of the elemental composition of Ni-20%Cr coating at different temperatures.

Coating	Temperatures (°C)	Elemental composition (wt%)		
		Ni	Cr	O
Ni-20%Cr	25	78.5	18.6	2.9
	850	52.3	17.7	30

4.3.2.8. Post wear test tribo-layer analysis

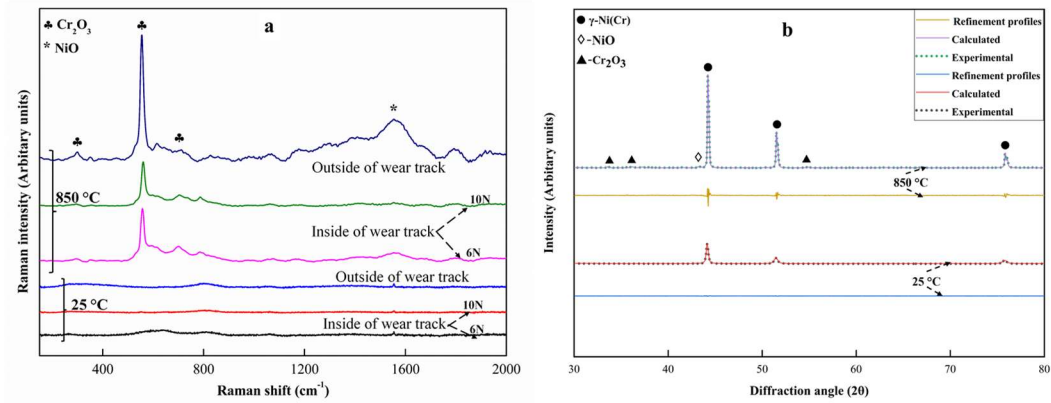


Fig. 4. 38. Post wear track of Ni-20%Cr coatings after the ball-on-disc sliding test at 25 °C and 850 °C. (a) Raman spectra, (b) XRD analysis.

Following the 25 °C sliding wear, no metal oxide peaks were observed in the Raman spectra performed inside and outside the wear track. Ni and Cr oxidize under strained shearing and temperature environments, and the formation of the glazing layer is crucial for friction and wear resistance due to its lubricious nature. However, these peaks remain visible in the worn inner surface area (Fig. 4.38(a)) and become more prominent and intense at the outer sides away from the wear tracks. This indicates the removal of the oxide layer/tribo-layer from the contact region due to the continuous rubbing action. At 850 °C, the Cr₂O₃ layer inside the wear track should have formed before the sliding wear test.

It should be noted that the holding time is about 1 hr at 850 °C before the sliding starts (as stated in the experimental section 2.2). Therefore, the Cr₂O₃ layer can be formed well earlier before the sliding starts. The worn surface area generates a NiO and Cr₂O₃ glaze layer. Peaks at 1500 cm⁻¹ are attributed to NiO (Shi et al. 2020), whereas peaks around 548 cm⁻¹ and 685 cm⁻¹ are attributed to Cr₂O₃ (Hao et al. 2018). The prominent peak of Cr₂O₃ inside the wear track even after the removal of the oxides reveals that the Cr₂O₃ offers excellent protection than NiO (Li et al. 2014). The dominating development of the Cr₂O₃ layer is the primary cause of the decreased friction and wear, resulting in a significant improvement in tribological properties.

As illustrated in Fig. 4.38(b), XRD patterns collected at various temperatures (25 °C and 850 °C) were stacked and indexed. According to the XRD investigation, the intensity of the peaks recorded at 850 °C is highly crisp, clear, and narrow compared to 25 °C coatings, indicating crystallinity and coarser crystallite size. The Rietveld refinement analysis revealed that the phase quantification and refinement plots (Table 4.19) were refined with the help of shifted anchor scan background data. It can be seen that only pure NiCr is the dominant phase crystalline, and no other diffraction peaks are found at 25 °C. But, at 850 °C, Ni and Cr react with oxygen (O) during the friction and wear test. As a result, the NiO (ICDD File no: 00-047-1049) and Cr₂O₃ (ICDD File no: 01-073-6214) have been formed as a minor phase, as shown in Fig. 4.38(b). The dominating development of the Cr₂O₃ and NiO oxide layers are the primary cause of the decreased friction and wear.

Table 4. 19. Rietveld refinement analysis of Ni-20%Cr coatings.

Coating	Temperature (°C)	Refinement data		Phase quantification (wt%)		
		Goodness of fit	R _{wp}	NiCr	Cr ₂ O ₃	NiO
Ni- 20%Cr	25	1.263	7.094	100	--	--
	850	1.599	10.46	8	90	2

4.3.2.9. Recrystallization

The crystallite size and lattice strain of Ni-20%Cr coatings at 25 °C and 850 °C were calculated using the W-H method. The crystallite size and lattice strain values at each stage are computed from these diffraction peaks (Fig. 4.38(b)). At ambient temperature, the average crystallite size and lattice strain are 56.3 and 224.5 nm and 0.196 and 0.08, respectively. A gradual decrease in lattice strain and increase in crystallite size with temperature is evident. At high temperatures (850 °C), the release of the micro-strain can be attributed to the driving force for the recrystallization. The temperature eventually affected the formation of finer crystals. As a result, refined and

recrystallization grains play an essential role in anti-wear and increasing tribological superiority.

4.3.2.10. Cross-sectional analysis of a Ni-20%Cr coating

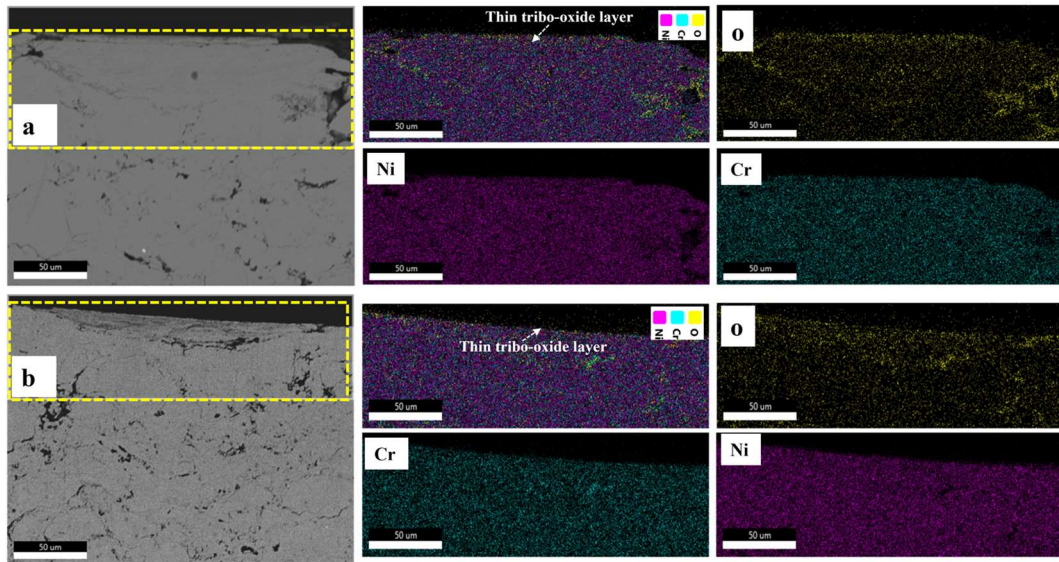


Fig. 4. 39. BSE micrographs and corresponding EDS element mappings of the cross-sections of the worn surface of Ni-20%Cr coating at 850 °C. (a) 6N (b) 10N.

Under frictional conditions, fracture initiation and propagation occur in material peeling from the Ni-20%Cr layer and are usually followed by contact fatigue fractures because of the stress concentration. When the fissure or a sub-surface crack caused the material to break through, shear stress induced by friction peeled the material's surface layer from the Ni-20%Cr coating.

The cross-section FE-SEM morphology of the after 850 °C wear coating is shown in Fig. 4.39. It demonstrates that the homogenous and dense oxidative layer, with a thickness of around 3-5 µm, is effectively bonded to the coating. For instance, Cr₂O₃ was found to be homogeneously distributed throughout the Ni-20%Cr treatment at 850 °C. Fig. 4.39 and Table 4.20 show that following friction testing at 850 °C, Cr, Ni, and O elements developed over the worn surface. Temperature also increased the chemical affinity of Ni-20%Cr and NiO, and the lubricating layer was continuously compact and intact. These boundary oxides might refine the grain size of the coating, which is beneficial for decreasing internal stress. It may successfully improve adhesion

to prevent oxidative layer exfoliation from the coating, resulting in enhanced wear and friction at 850 °C.

Table 4. 20. EDS elemental mapping analysis of the elemental composition of Ni-20%Cr coating at 850 °C.

Coating	Loads (N)	Elemental composition (wt%)		
		Ni	Cr	O
Ni-20%Cr	6	77.7	16.8	5.5
	10	76.7	15.9	7.3

4.3.2.11. The effect of temperature on the wear behaviour of Ni-20%Cr

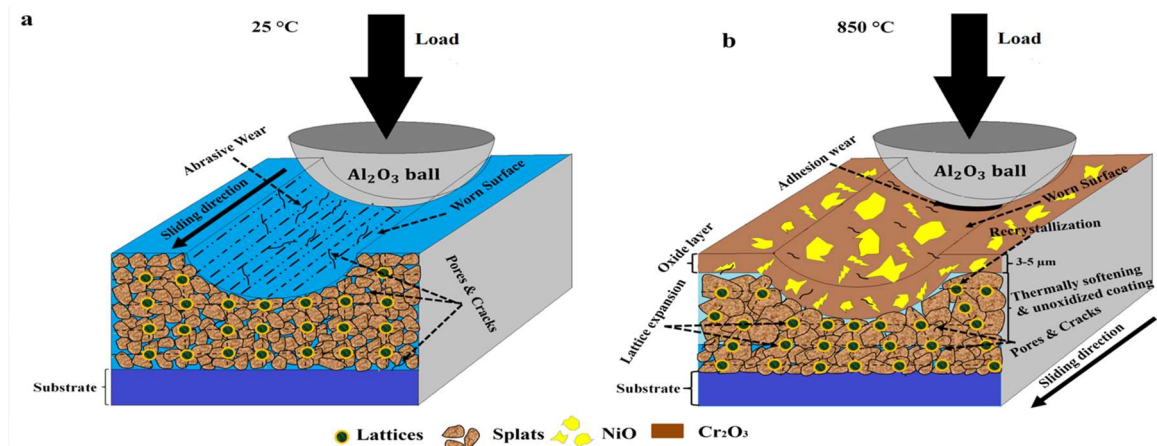


Fig. 4. 40. Schematic diagram of tribological evolution of Ni-20%Cr coating at 25 °C & 850 °C.

A physical schematic has been proposed to understand the tribological behavior of the Ni-20%Cr coating at 25 °C and 850 °C. Under typical loads, a contact layer with depth was generated on the surface of the specimen, as illustrated in Fig. 4.40. The stress concentration in this contact area initiates the nucleation of microcracks, which promotes the propagation of crack growth and interaction, resulting in crack coalescence with one another under ambient temperatures. The materials removal and loose particles/debris due to some abrasion scars; the abrasion and surface fatigue are the dominant wear mechanisms, which is typical for a substantial measure and development of wear debris.

Thermal expansion, stress relieving, recrystallization, and oxidation are dominant phenomena occurring at elevated temperatures in metallic coatings. The influence of thermal expansion on high-temperature wear properties has been seen as positive as well as negative (Barber 1967), (Hahn and Kettleborough 1968), (Grigoriev et al. 2020). According to the present study, stress relieving has been considered the first high-temperature effect on wear resistance. Detonation spray coating (DSC) is known for inducing compressive residual stresses during the coating process due to its intermittent nature of spraying partially molten particles with the peening effect (Wang et al. 2012), (Rajasekaran et al. 2008). The compressive stress is expected to improve the wear resistance of the overlay coating in ambient conditions. Compressive residual stress has also been crucial in high temperatures before the complete stress relieving. When the residual stress is reduced completely, the recrystallization dominates with thermal expansion, as observed from the HT-XRD results. Recrystallization improves the ductility and thereby plastically deforms the contact area, eventually increasing the wear resistance. It is also well known that thermal expansion will create many vacancies in the lattice and pave the way for external oxygen to diffuse quickly.

Together with the low free energy Cr_2O_3 formation (-229.74 KJ/mol), the thermal expansion is expected to aggravate the oxidation of Cr into Cr_2O_3 , forming the protective tribo-layer. Even though the continuous rubbing relatively at a higher normal load (10N) did not remove the protective Cr_2O_3 tribo-layer (inside the wear track), as evidenced by Raman spectra. The layer underneath the very thin protective Cr_2O_3 tribo-layer will sufficiently expand thermally and provide the load-bearing ability, enhancing the sliding wear resistance of detonation sprayed Ni-20%Cr coating. Ni joins with Cr and oxidizes at 850 °C. The formation of the glazed oxide layer (Cr_2O_3 , NiO) is significant for friction and wear resistance because of its lubricious nature (Medabalimi et al. 2021). This low tolerance is an inside attack of oxygen and Cr ions' reduced outward diffusion rate. The results of this experiment were consistent with the continuous friction, as the grains refine and recrystallize in the oxide layer. The thermal expansion at 850 °C and recrystallization relieve the local tensile residual stress and contribute considerably to anti-wear and tribological superiority.

4.4 Dry sliding friction and wear behaviour of DSC sprayed Ni-based coatings with different compositions at elevated temperatures

4.4.1. Microstructural and Microhardness evolution of coatings

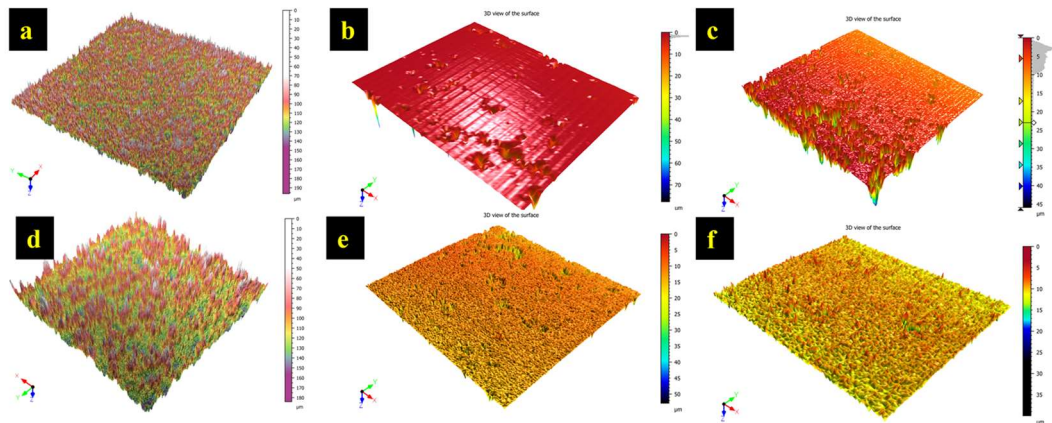


Fig. 4. 41. 3D profilometry topographs of DSC sprayed Ni-5wt%Al and Ni-20%Cr coatings. (a&d) As-deposited, (b&e) Polished surfaces, (c&f) After the wear test at 850 °C.

Fig. 4.41 depicts surface roughness's evolution in 3D topography under different conditions. Many semi-melted and unmelted powder particles were entrapped on the surface of the as-deposited coatings, resulting in a rough structure with needle-like points and deep pits, as well as a high peak and less densely packed roughness, as seen in Fig. 4.41(a&d). The partially melted/unmelted particles have been removed by metallography polishing. The sample surfaces are substantially smoother, more uniform, and brighter than the as-deposited coatings, as shown in Fig. 4.41(b&e). The coating surfaces were somewhat oxidized during dry sliding friction and wear experiments at 850 °C, enabling a few oxides to form. In Fig. 4.41(c&f), the coatings have a few burr-shaped bulges on the polished surface, increasing the roughness. These observations are seen in Table 4.21.

The Microhardness is significantly influenced by the porosity and density of the coating (Du et al. 2011). It is determined not only by the coating deposition techniques but also by its chemical composition and microstructure, as well as the presence of oxides and metallic phases. Table 4.21 shows the Vickers microhardness indentations made on the cross-section under the 200g applied loads and 15 sec dwell time. Partially oxide and metallic phases in the coating deposition may all be ascribed to increased

microhardness at 25 °C due to the rapid cooling rate, high strain hardening, and rapid solidification (Bai et al. 2011). Chromium is a hardening element, which means that it can increase the strength and hardness of the material through solid solution strengthening and precipitation hardening mechanisms, which increases the microhardness of Ni-20%Cr coatings more than Ni-5%Al coatings. Coatings soften during the wear test at 850 °C by absorbing ambient and friction heat and releasing compressive stresses, resulting in smaller grains, which lower shear strength, increase plastic deformation, and decrease microhardness, as shown in Table 4.21 (Hager et al. 2009).

Table 4. 21. Surface roughness (S_a) and roughness ($HV_{0.2}$) of DSC sprayed coating.

Coatings	Surface roughness (S_a)			Hardness ($HV_{0.2}$)	
	As-sprayed	After polishing	850 °C	25 °C	850 °C
Ni-5wt%Al	12.2±0.9	1.8±0.1	8.4±0.2	285±8.4	254±6.7
Ni-20%Cr	13.8±1.6	2.1±0.7	9.3±1.2	326±4.6	265±9.2

4.4.2. Dry sliding friction and wear behaviour

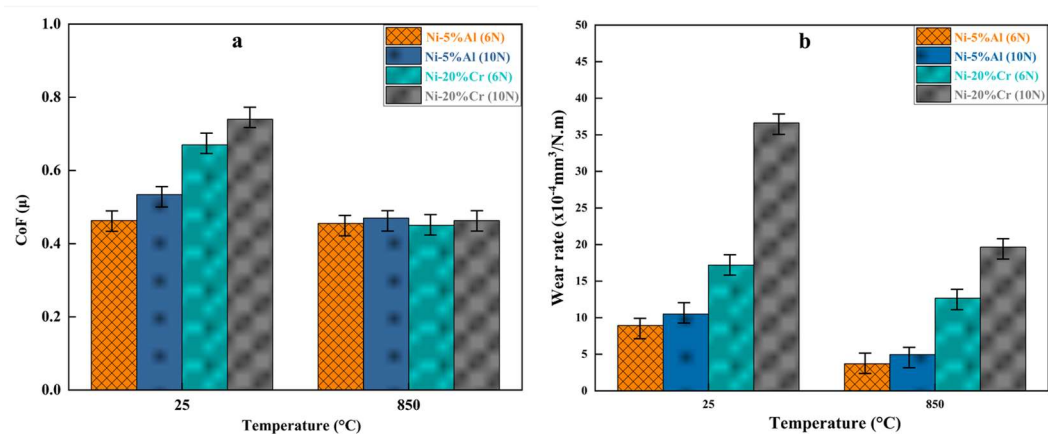


Fig. 4. 42. Depicts the dry sliding friction and wear behaviour of Ni-5wt%Al and Ni-20%Cr coatings under the 6N and 10N loads at 25 °C and 850 °C. (a) CoF vs. sliding distance; (b) Wear rate vs. temperature.

4.4.2.1. Effect of normal loads (N) on friction and wear behavior

Fig. 4.42 shows the dry sliding friction and wear behaviour of Ni-5wt%Al and Ni-20%Cr coatings against the Al₂O₃ counter material under varied loads (6N and 10N) at elevated temperatures (25 °C and 850 °C). Alfred explored the correlation between wear, friction, and frictional heat developed between the frictional pair; with increased loads, the frictional force increases, generating more frictional heat and increasing the contact area, resulting in significant plastic deformation. The energy is released as heat when the material is removed from the stretched condition of the frictional contacts. The observed properties might be related to plastic deformation, including micro-cracks and delamination (Zmitrowicz 1987). Additionally, Ni-20%Cr coatings have a higher CoF (Fig. 4.42(a)) and more wear debris on the worn surface than Ni-5wt%Al coatings due to the coarser surface texture and higher interfacial pressure between the frictional pairs.

4.4.2.2. Effect of temperature on friction and wear behaviour

At room temperature, the partially oxidized coatings comprise oxidized layers and splats. The partly oxidized coatings deform due to brittle fractures and the splat boundary contact, resulting in many third bodies (wear debris) and a higher wear rate. When the coating is exposed to high temperatures (850 °C), these oxidized splats deform and connect with partially oxidized splats to form an oxide layer. Furthermore, when the wear debris (oxide particles) was compacted into a homogenous oxide film, the development of these protective glaze oxide layers and other intermetallic compounds enters the friction pair, reducing adhesion and ploughing on the coating, resulting in a lower CoF and wear rate (Munagala et al. 2019)(Novak and Polcar 2014)(Jiang et al. 1998)(Stott 2002).

4.4.2.3 Wear rate (ω)

The wear rates of the coatings are shown in Fig. 4.42(b) under different loads (6N and 10N) at 25 °C and 850 °C. Many third bodies (or tribo-material) are generated during dry sliding wear, but only a portion is evacuated from the system. The remains may even act as a solid or liquid lubricant, allowing for decreased material loss rates. Wear scar is used for analyzing and evaluating volume loss (Fillot et al. 2007).

At room temperature, high shear stresses between the splats cause material deformation and increase the wear rate in partly oxidized coatings. Ni-5%Al coatings have a finer microstructure, allowing them to deform and reduce wear rates. As a result, Ni-20%Cr coatings have more excellent wear rates because they are more prone to breaking and cracking during sliding or abrasive wear. At high temperatures (850 °C), the oxide layers (NiO, Cr₂O₃) may be self-lubricating protective layers to minimize frictional pair contact. As a result, both coatings have a decreased wear volume and wear rate. More information is discussed about the tribo-layer formation in the following sections.

4.4.3. Topographical evolution of the worn surface of coatings

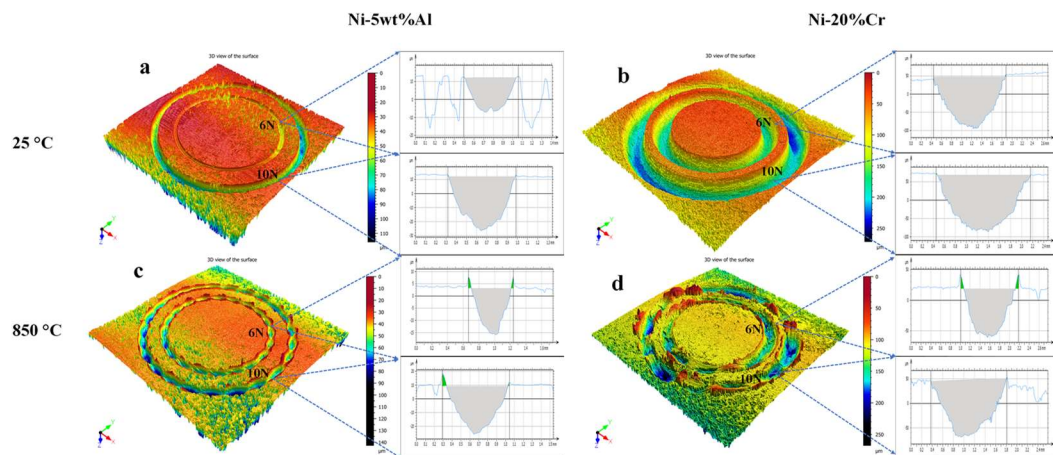


Fig. 4. 43. 3D topographies and depth profiles of wear tracks of the coatings after dry sliding friction and wear under different 6N and 10N loads. (a&b) 25 °C and (c&d) 850 °C.

Fig. 4.43 displays the 3D topographies and 2D depth profiles of wear tracks following dry sliding friction and wear at 25 °C and 850 °C under varied loads of 6N and 10N. The amount of material lost for each sample was determined using the depth and width of the wear tracks measured by the confocal 3D optical microscope. The test results showed that wear tracks are strongly linked with sample wear profiles at a sliding distance of 138m. At 25 °C, more material is removed from the disc samples (Ni-based coatings), increasing the depth and width of wear tracks, as seen in Fig. 4.43(a&b) and Table 4.22. Compared to Ni-20%Cr coatings, Ni-5%Al coatings usually have a smaller breadth and depth, allowing less material to be removed. It shows an increase in CoF and wear rate resistance. The oxide scale forms and expands on the

coated surfaces when the surrounding temperature increases to 850 °C. Because of the high shearing action of friction, the spreading oxide layer peels off the worn surface more quickly. The entrapment of oxide particles may reduce contact between the disc and the counter material (Fig. 4.35(c&d)), hence minimizing wear damage (Hao et al. 2019).

Table 4. 22. Wear data with standard deviations of coatings at 25 °C and 850 °C.

Coating	Loads (N)	Width (mm)		Depth (µm)	
		25 °C	850 °C	25 °C	850 °C
Ni-5wt%Al	6	0.62±0.01	0.56±0.08	29.7±0.4	22±7.4
	10	0.75±0.02	0.63±0.07	33±1.1	29±2.4
Ni-20%Cr	6	1.52±0.10	1.14±0.04	133±3.6	69±6.3
	10	1.72±0.03	1.45±0.01	142±6.8	98±4.2

4.4.4. Temperature-mediated wear behaviors of coatings

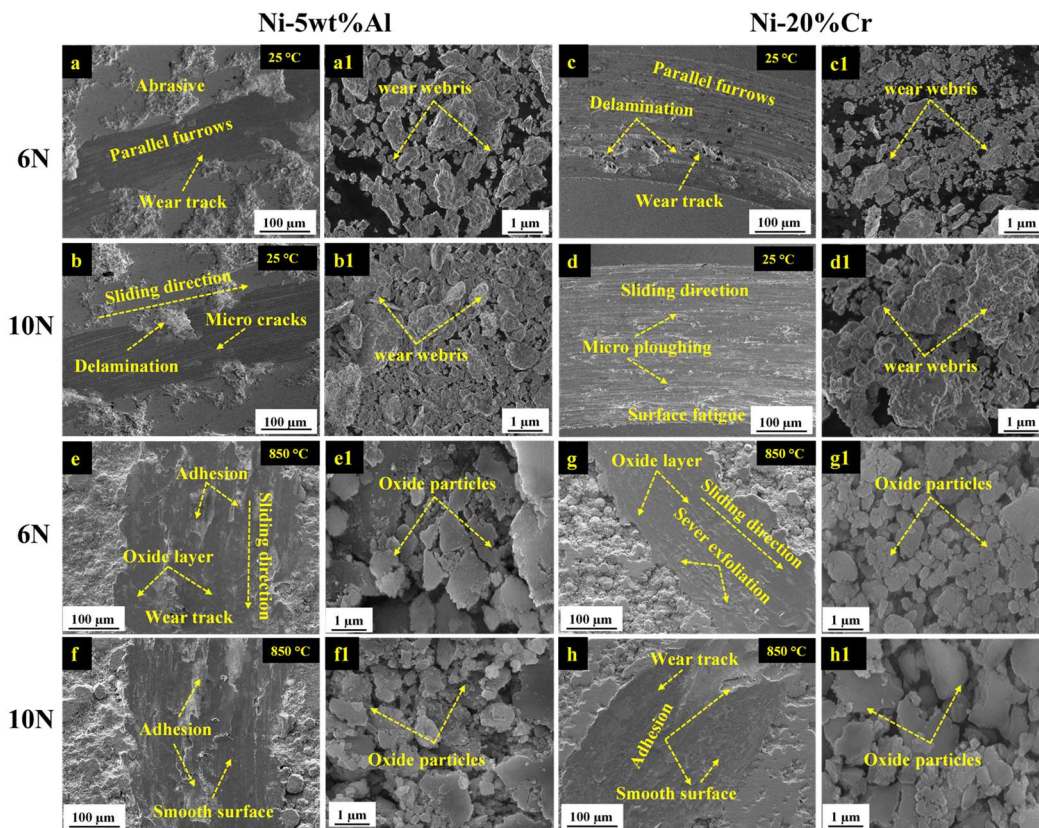


Fig. 4. 44. Worn surface morphologies of coatings (a-b) 6N (c-d) 10N loads at 25 °C and (e-f) 6N (g-h) 10N loads at 850 °C.

The FESEM technique was used to examine the wear scar of coatings, showing the primary mechanisms and sub-mechanisms associated with temperatures (25 °C and 850 °C) and loading (6N and 10N) conditions. Fig. 4.44(a-d) depicted the abrasive wear represented by parallel furrows with micro-ploughing along the sliding direction. Due to continuous dry sliding, stress can develop in or near the coating surface, and cracks will grow, expand, and connect, causing delamination known as Surface fatigue (Fischer et al. 2018). Abrasive debris (Fig. 4.44(a1-d1)) was formed during the continuous sliding wear. It can adhere to the counter material or act as loose particles between the friction pair, developing a three-body abrasive (Zum Gahr 1987). Coating wear rate and coefficient of friction values are significantly influenced by partly oxidized coating. High shear Stress between oxidized and partially oxidized splats generates microcracks, which increase the wear rate at ambient temperature (Parthasarathi et al. 2012).

When the surrounding temperature rises to 850 °C, tribo-chemical reactions increase the percentage of oxygen in the partially oxidized coating, developing the oxide layer. This is attributed to self-lubricating ability on coating and wear resistance. The wear process appears to be primarily sticky with severe score marks (Fig. 4.44(e-h)), and material is transferred to counter material showing adhesive grooves, indicating adhesive wear (Shi et al. 2020). On the other hand, the oxide film (Fig. 4.44(e1-h1)) provides more excellent lubrication, works as a barrier between the rubbing surfaces (Friction pair), and enhances tribological performances at high temperatures.

Table 4. 23. Primary wear and Sub-wear mechanisms of Ni-based coatings at different temperatures.

Temperature (°C)	Main wear mechanism	Sub wear mechanism
25	Abrasive	Micro-Ploughing
	Surface fatigue	Delamination
	Adhesion	Material transfer
850	Tribo- Chemical reactions	Tribo-Oxidation

4.4.5. SEM/EDS elemental mapping analyses of worn surfaces

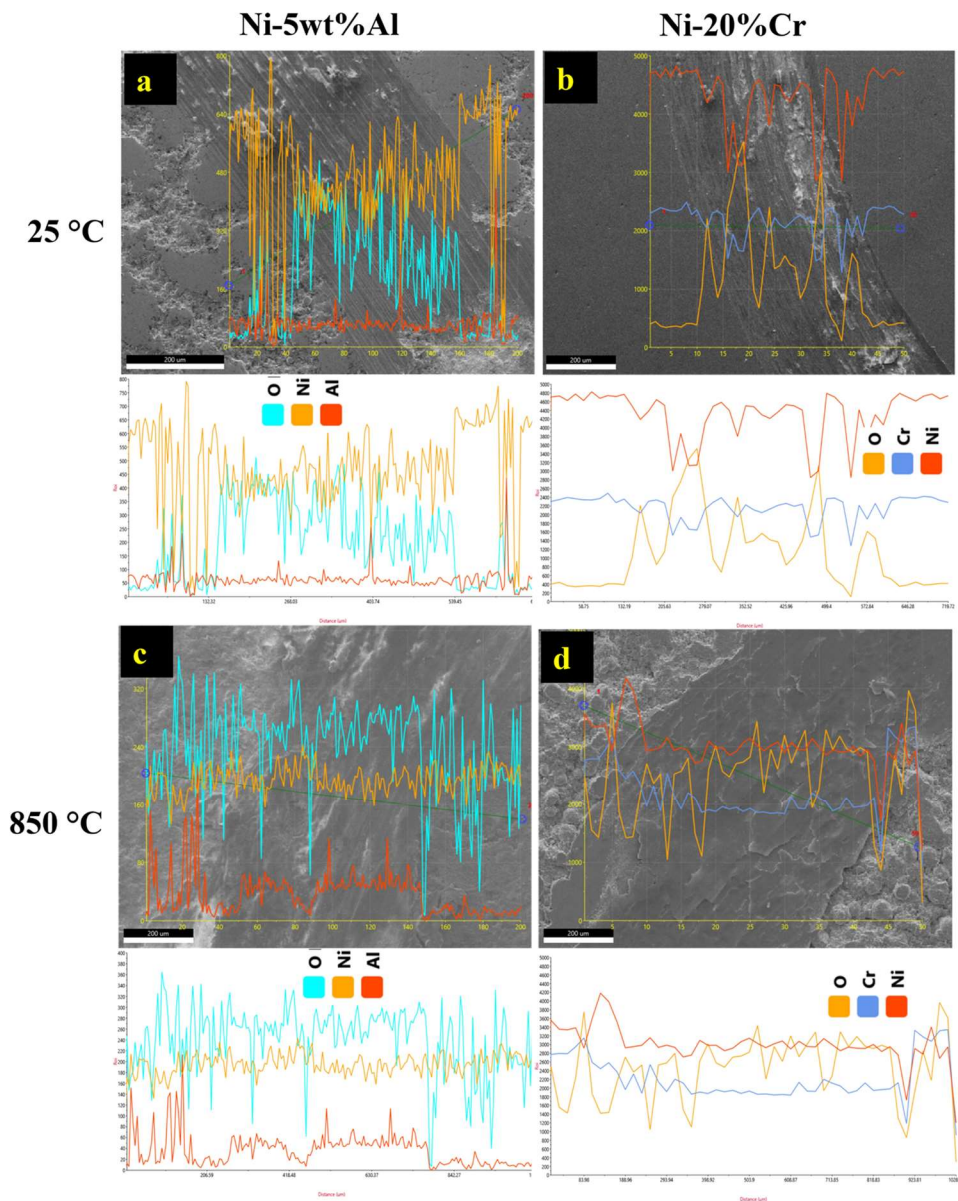


Fig. 4. 45. EDS line analysis of element composition on coating cross-sections at (a, c) 25 °C and (b, d) 850 °C.

After the dry sliding friction and wear test, the green line was drawn along the worn surface of the wear track to evaluate the elemental composition of coating at different temperatures (25 °C and 850 °C), is shown in Fig. 4.45. The concentration of oxygen (O) peaks inside the worn surface is approximately similar to the composition of the as-deposited coatings. Fig. 4.45(a&b) indicates that no oxides are formed at 25 °C. During high-temperature wear experiments, the oxygen concentration on the worn surface of partially oxidized splats increases, and a well-adjacent oxide layer equivalent

to a glazing layer (Bolelli et al. 2020)(Stott et al. 1973) is observed in Table 4.24. Fig. 4.45(c&d) indicates that the tribo-layer is made up of nickel (Ni), chromium (Cr), and oxygen (O) oxides.



According to the above equations, the Ni and Cr elements oxidized and encouraged to form protective layers (NiO and Cr₂O₃) and play an essential role in developing a lubricating surface. These defensive oxide phases are a barrier between the frictional pairs, reducing friction and wear at higher temperatures. The grains in the oxide layers are refined and recrystallized by continuous dry sliding friction. Many unique grain boundaries generated after recrystallization may relieve local tensile stress, considerably contributing to anti-wear and tribological superiority (Hao et al. 2019). It reveals that the sliding wear response of coatings is temperature-dependent.

Table 4. 24. EDS line analysis of the elemental composition of coatings at different temperatures.

Coating	Temperatures (°C)	Elemental composition (wt%)			
		Ni	Cr	Al	O
Ni-5wt%Al	25	79.4±2.2	--	5.6±0.3	13.9±0.6
	850	64.9±1.6	--	5.1±0.2	30±1.3
Ni-20%Cr	25	71.5±0.6	18.1±0.3	--	10.4±0.4
	850	52.2±1.2	18.2±0.6	--	29.6±0.2

4.4.6. Post-wear test tribo-layer analysis

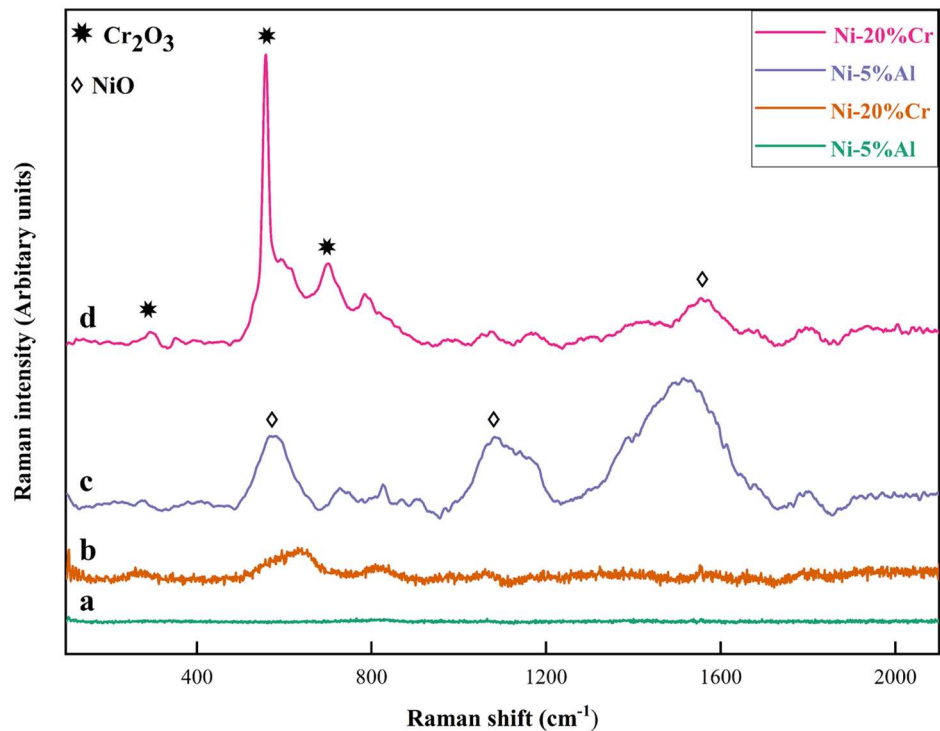


Fig. 4. 46. Raman spectra of wear tracks after the ball-on-disc sliding wear at different temperatures. (a and b) 25 °C, (c and d) 850 °C.

By evaluating the coated surfaces, Raman spectra were also obtained to identify the different phase chemical compositions based on raman shifts and intensities. The Raman spectra showed the absence of metal oxide peaks (Fig. 4.46(a&b)), indicating no oxides formed during sliding wear at 25 °C. The oxide peaks remained visible on the worn surface, and the wear tracks became more intense and prominent (Fig. 4.46(c&d)). It represents the protective oxide phases performed at 850 °C, reducing friction and wear.

The worn surface produces a NiO and Cr₂O₃ glazing layer at high temperatures. Raman peaks at 1500 cm⁻¹ are attributed to NiO (Shi et al. 2020), whereas peaks at 548 cm⁻¹ and 685 cm⁻¹ are attributed to Cr₂O₃ (Hao et al. 2018). A significant peak of Cr₂O₃ provides better protection than NiO (Li et al. 2014). The dominant growth of the Cr₂O₃ and NiO layer are the primary reason for the reduced friction and wear, leading to a substantial improvement in tribological performance.

4.4.7. X-ray diffraction and Recrystallization

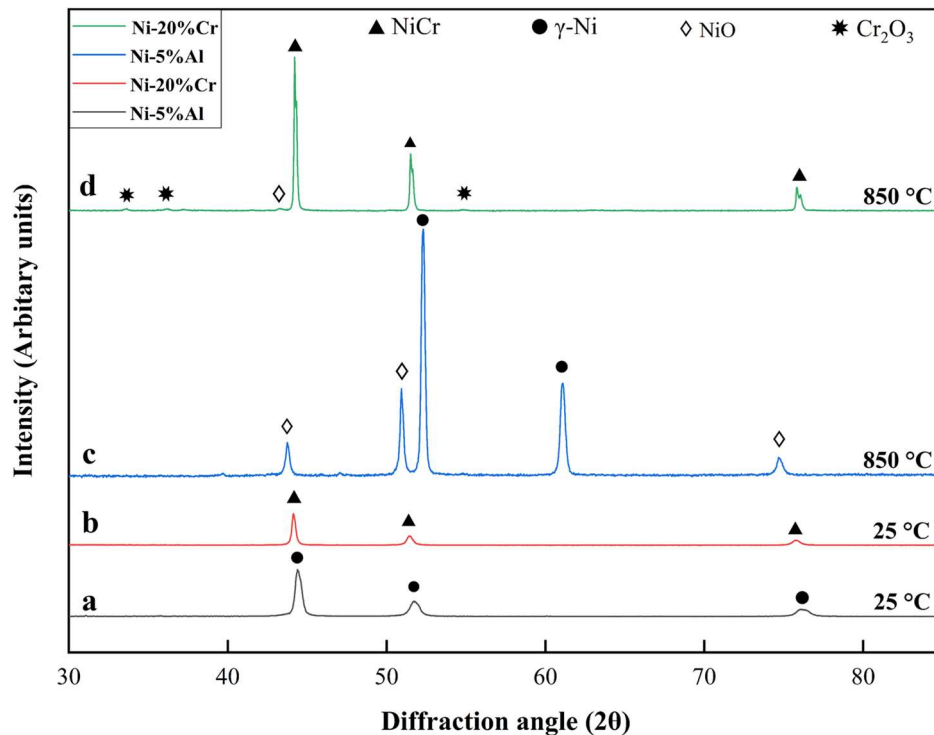


Fig. 4. 47. Stacking of XRD diffraction patterns at various temperatures. (a&b) Ni-5wt%Al, (c&d) Ni-20%Cr at 25 °C and 850 °C.

After the dry sliding wear test at 25 °C and 850 °C, the diffraction patterns were stacked and indexed, as shown in Fig. 4.47. According to the XRD analysis, the diffraction peaks are intense, crisp, clear, and narrow, suggesting crystallinity and coarser crystallite size. The peaks at 25 °C indicate the γ -Ni and γ -NiCr phases with face-centered cubic (FCC) structures. After the wear test at 850 °C, NiO and Cr₂O₃ developed as minor phases with the γ -Ni and γ -NiCr phases in the Ni-5%Al and Ni-20%Cr coatings, respectively.

At high temperatures (850 °C), the strain relieving in the coating and peak broadening (peak sharpening) increase with temperature. The driving force for recrystallization can be attributed to the release of micro-strain. The Scherrer equation (Eq 3.2) was used to calculate the crystallite size variation (Kala et al. 2022). The temperature eventually affected the formation of more fine crystals. A gradual increase in crystallite size with temperature is evident in Table 4.25. As a result, refined and

recrystallization grains in the oxide layers (Cr_2O_3 and NiO) play an essential role in anti-wear and increasing tribological superiority.

Table 4. 25. Crystallite size of coatings at different temperatures.

Temperature ($^{\circ}\text{C}$)	Crystallite size (D, nm)	
	Ni-5%Al	Ni-20%Cr
25	15.23 \pm 1.4	26.1 \pm 1.7
850	39.6 \pm 2.6	50.3 \pm 3.1

4.4.8. Quantitative depth profiling analysis by glow discharge optical emission spectroscopy (GD-OES)

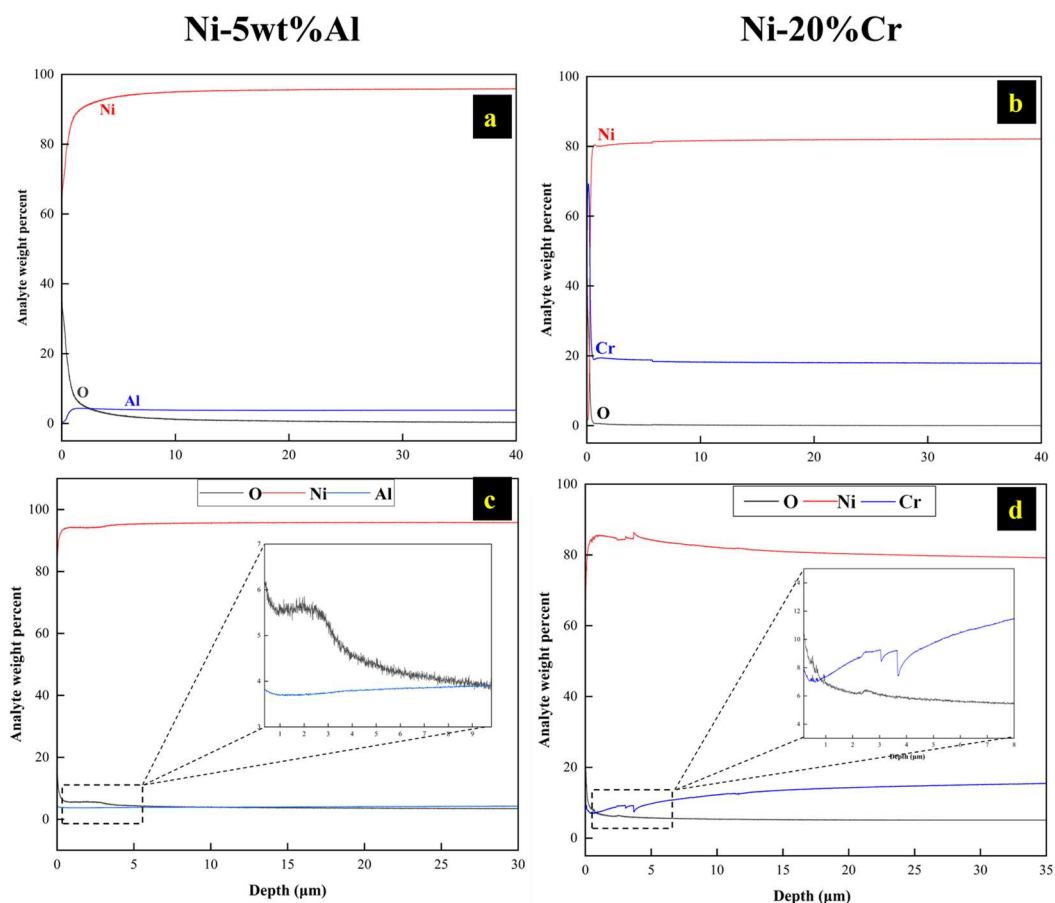


Fig. 4. 48. Quantitative elemental depth profiles of Ni-based coatings at various temperatures. (a and b) 25 $^{\circ}\text{C}$, (c and d) 850 $^{\circ}\text{C}$.

The quantitative elemental depth profiles were measured using a GD-OES analysis, carefully considering glow discharge parameters such as voltage, current, and calibration and recalibration sample factors. A multi-matrix calibration was carried out using a wide range of verified reference materials. Fig. 4.48 illustrates quantitative elemental depth profiling of nickel, chromium, and oxygen concentrations in GD-OES spectra of coatings at temperatures ranging from 25 to 850 °C. The light sputtered 30-40 μm into the coatings in 12 minutes.

After the wear test at 25 °C, the coating has no oxygen concentration peaks (Fig. 4.48(a&b)) nearly equivalent to the as-deposited coating composition. It indicates that no oxide layer has developed on the surface. Nevertheless, when the temperature rises from 25 °C to 850 °C, Ni and Cr concentrations decrease with increasing oxygen (O). Ni and Cr react with oxygen (O) to develop the oxide layers (NiO and Cr₂O₃) up to 3-5 μm on the coating surface (Fig. 4.48(c&d)). These oxide layers act as a lubricant between the frictional contacts, reducing the CoF and wear rate at high temperatures.

4.4.9. Counterpart analysis

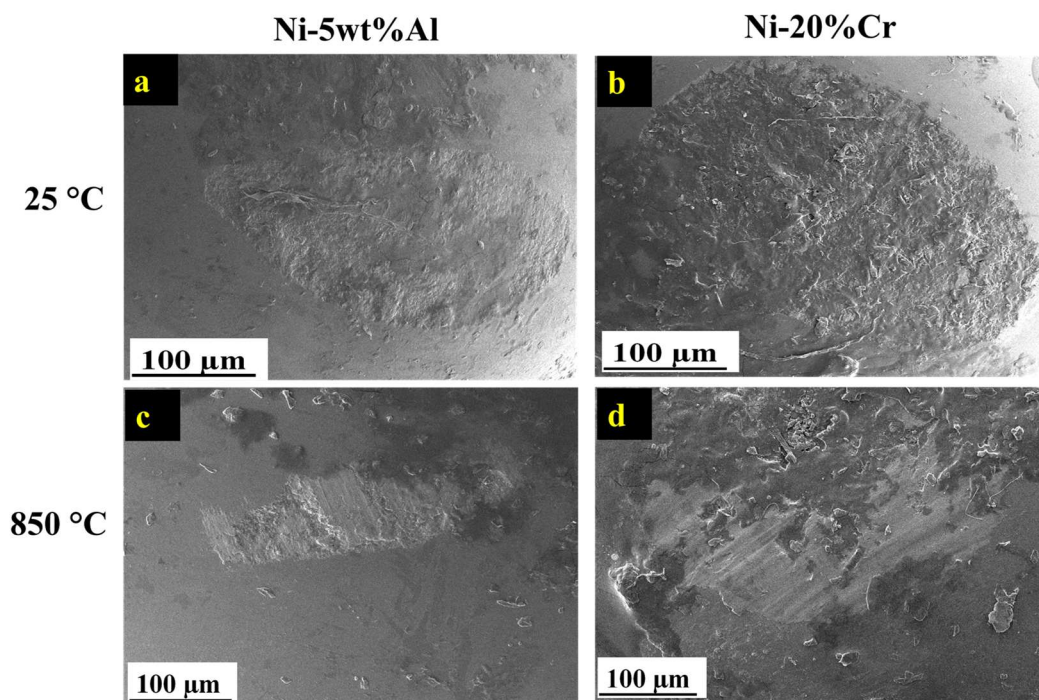


Fig. 4. 49. Worn surface morphologies of Al₂O₃ counter material. (a & b) 25 °C and (c & d) 850 °C.

FE-SEM examines the micrographs of an Al₂O₃ counter material sliding against coatings at elevated temperatures (25 °C to 850 °C). At 25 °C, the worn surface of the counter material has wear debris, micro-ploughing, and delamination with sliding direction, indicating abrasive and surface fatigue wear (Fig. 4.49(a&b)). Although some worn debris is clumped together, small particles are spread throughout the worn-out surface. However, the surface morphologies of the Al₂O₃ ball significantly differ at 850 °C. The diameters of the wear scars on the counter material decrease with increasing temperature due to the formation of tribo-layer on the paired surface, which reduces contact between these two. Because the highly oxidized coating material is transferred and stick to the Al₂O₃ counter material (a grey colour region in " (Fig. 4.49(c & d))" and this tribo-oxide film acts as a lubricant. This thin layer is a barrier between rubbing surfaces, reducing friction and wear rate. Due to severe oxidation at 850 °C, EDS mapping of an Al₂O₃ counter material revealed that a large amount of the coating material (Ni and Cr) transfer and dense tribo-oxide layer forms on the Al₂O₃ surface becomes too thick is noticeable in Table 4.26 and Fig. 4.50. Which reduces friction and increases wear resistance (Sun et al. 2021).

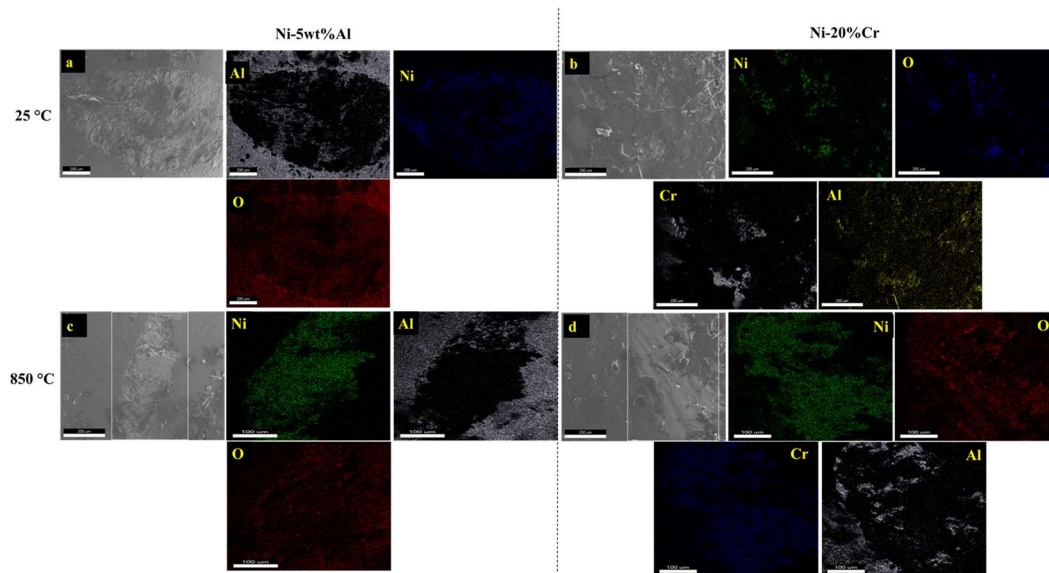


Fig. 4. 50. EDS element mapping analysis of counter material at 850 °C.

Table 4. 26. Elemental mapping analysis of counter material at different temperatures.

Coating	Temperatures (°C)	Elemental composition (wt%)			
		Ni	Cr	Al	O
Ni-20%Cr	25	14.9±1.2	8.6±0.5	41.4±2.3	35.1±1.7
	850	63.4±2.8	13.9±0.3	12.0±0.6	10.7±0.2
Ni-5wt%Al	25	6.4±0.6	--	47.0±1.9	46.6±1.3
	850	46.1±2.2	--	35.2±1.2	18.7±0.5

4.4.10. Wear rate coefficient (ω)

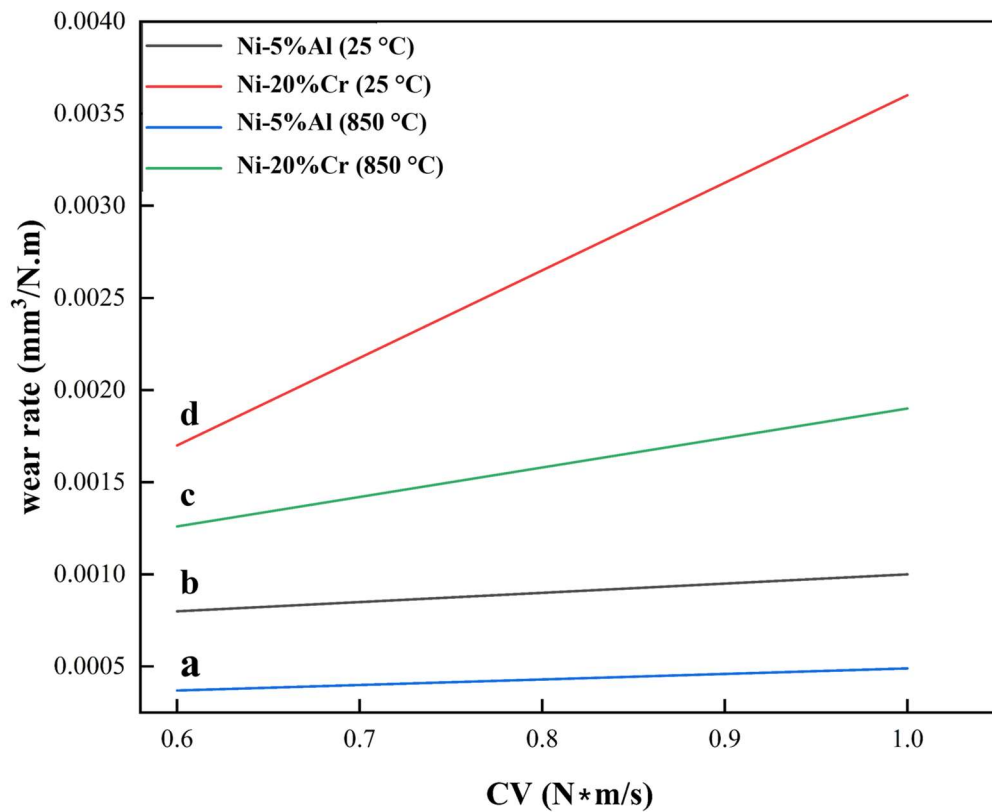


Fig. 4. 51. Wear rate vs. CV of Ni-based coatings at different temperatures. (b & d) 25 °C, (a & c) 850 °C.

The tribological performance of coatings against a ceramic Al_2O_3 counter material is also temperature dependant. The wear rate coefficient measures coating quality, with a lower value indicating higher quality (Fernández et al. 2005). It is calculated by dividing the wear rate (k) by the product of applied load (C) and sliding velocity (V). A study found that the wear rate coefficient was lower at 850 °C than at 25 °C, as shown in Fig 4.51. This relates to unanticipated tribo-oxidation under friction heat and stressed-shearing conditions. On the other hand, a compacted oxidation layer (Cr_2O_3 and NiO), with its self-lubricating action, usually develops while sliding and is protective and resistant to friction and wear (Torgerson et al. 2018).

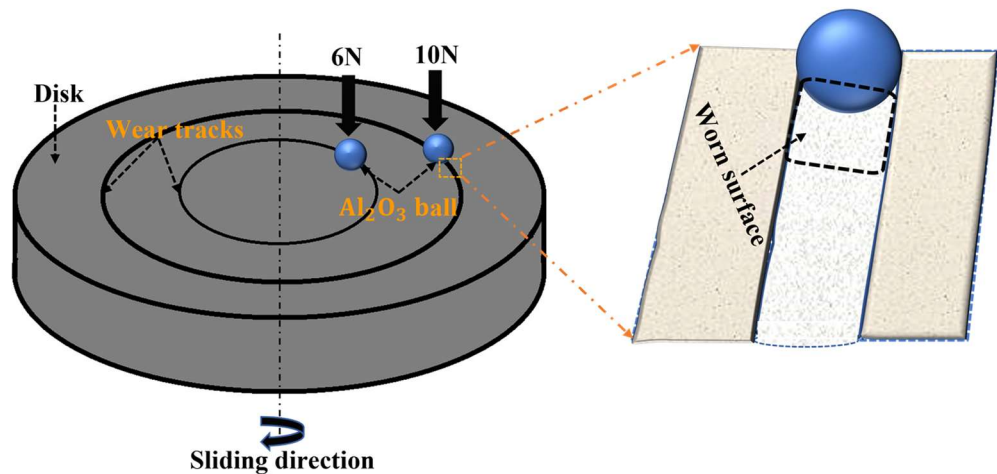


Fig. 4. 52. A schematic representation of the tribological behavior of Ni-based coatings under various loads (6N & 10N).

To explain the tribological behavior of Ni-based coatings under typical loads of 6N and 10N, a physical schematic has been developed in Fig. 4.52. When two bodies rub against each other, it generates heat due to friction. As the load increases, so does the frictional force and heat produced. This also leads to plastic deformation and energy release as heat when the material is removed from the contact area. The high shear stresses between splats at 25 °C cause brittle fracture and material deformation, increasing wear track depth and width in partially oxidized coatings. Parallel furrows with micro-ploughing along the sliding direction conformed to abrasive wear. Stress can develop on or near the coated surface due to continuous dry sliding, and cracks can develop, expand, and connect, causing delamination, known as surface fatigue.

When the ambient temperature increases to 850 °C, tribo-chemical interactions increase the percentage of oxygen, forming the oxide layer. It is self-lubricating and acts as a barrier between the rubbing surfaces (friction pair) to provide wear resistance. The wear process appears to be primarily sticky, with severe score marks, and material is transferred to the counter material, indicating adhesive wear. On the other hand, the grains in the oxide layers are refined and recrystallized during continuous friction. Its refined and recrystallized grain improves tribological performance at high temperatures.

CHAPTER 5

CONCLUSIONS

5.1 Conclusions of proposed research work

This study used the detonation spray method to deposit Ni-based coatings. The structural characterization of as-deposited coatings was carried out using SEM, EDS, and XRD. The mechanical characteristics of as-deposited and after-wear coatings were studied. The frictional and wear behaviour of Ni-based coatings was investigated under various loads and temperatures. The effect of temperature-dependent material characteristics (Stress relieving, Recrystallization, Thermal expansion) on the dry sliding wear resistance of a DSC sprayed Ni-based coating has been investigated. SEM, EDS, XRD, GD-OES, non-contact optical 3D profilometry, and Raman spectroscopy were used to examine the wear maps and mechanisms and the composition of tribo-chemical reaction layers on the worn surfaces. The detailed study of wear surfaces and debris has contributed to understanding wear mechanisms, tribo oxidation effects, and phase composition of tribo chemical reaction films.

5.1.1 Coating characterization

The detonation spray coating (DSC) technology was used to successfully deposit Ni-based composite (Ni-20%Cr and Ni-5%Al) coatings on Inconel 718 (IN718) substrate. The coatings had a typical lamellar microstructure with a thickness of around 250 ± 25 μm . According to XRD and EDS examination, as-deposited coatings are deposited without oxidation or disintegration under the investigated spraying constraints, and solid lubricants are present in the coatings. Ni-based coatings deposited by DSC, a kinetic energy-dominated process, were relatively homogeneous, highly strain-hardened, and denser microstructure than others.

Due to partially/unmolten powder particles entrapped on the as-deposited coating surface showing high surface roughness with needle-like tips and deep pits. After metallography polishing, the sample surfaces are substantially smoother, more uniform, and brighter, reducing surface roughness. Simultaneously, a few burr-shaped asperities were observed on the coating surface, increasing the surface roughness. This

is because of paving the way for a few oxide forms at 850 °C during the tribological testing.

The hardness of the coatings has been found to decrease with increasing temperatures. The As-deposited Ni-based coating has relatively higher micro-hardness values. The high-strain hardening, rapid solidification, presence of partial oxides, and metallic phases in the coating deposition may all be attributed to the enhanced microhardness of the coating. After the high-temperature wear test, the microhardness of the coatings was reduced significantly due to the softening and annealing effect, resulting in coarser grains that reduce shear strength, which may encourage plastic deformation. The residual stress induced during thermal spraying and reliving is visible during thermal softening.

5.1.2 Dry sliding friction and wear behaviour of coatings

5.1.2.1 Sliding Wear Behaviour of Ni-5%Al Coating Deposited by Detonation Spray on IN718

In this study, Ni-5%Al overlay coating was deposited on the IN718 substrate using a DSC process. The average coating thickness was about 250 ± 28 μm , and the crystallite size of the coating was 15 nm, measured using a Scherrer formula. The microhardness test showed that the coated sample exhibited a better hardness value of 305 HV_{0.2}. The sliding wear test demonstrated the potential of the Ni-5%Al coating to enhance the wear resistance capability due to its microstructure, surface morphology, and better microhardness. The coefficient of friction (CoF) between Al₂O₃ and Ni-5%Al coating surface was low at around 0.47 and showed excellent wear resistance. At the same time, uncoated IN718 resulted in a high CoF of about 0.719. 3D non-contact profilometry was a beneficial tool for qualitative assessment, such as effective contact area between contact pairs and supporting the calculation of volume loss and wear rate. The worn surface morphology correlated well with the obtained wear and friction results. Though the abrasion-induced plowing was identified as the primary wear mechanism of bare IN718 and Ni-5%Al coating, the coating's vulnerability to wear seemed to be lesser because of the lesser effective contact area.

5.1.2.2 High temperature sliding wear behaviour of detonation sprayed Ni-5wt%Al coating.

The role of thermal expansion on the dry sliding behavior of DSC Ni-5wt%Al coating was examined at room temperature (25°C), and high temperature (850°C), and the following conclusions were achieved:

1. At ambient conditions (25°C), the inherent microstructure of Ni-5wt%Al, partially oxidized during thermal spraying (in-flight oxidation), provides excellent wear resistance. The predominant wear mechanisms are abrasion, surface fatigue with parallel furrows, and delamination.
2. The wear resistance of the coating improves further at elevated temperatures (850 °C) due to the excessive plastic deformation accompanied by the recrystallization and the formation of tribo-layer with self-lubricating behavior. At higher temperatures, CoF steadily decreases, and the wear process shifts from abrasive and surface fatigue to adhesion wear and oxidative wear.
3. In-situ HT-XRD revealed the high thermal expansion of Ni-5wt%Al coating and the relaxation of residual stresses (micro-strain), while relaxation and recrystallization are prominent above 800 °C.
4. Thermal expansion has been seen as one of the prominent reasons for improving wear resistance. Thermal expansion plays an important role in the change in wear mechanism and stress relaxation.

5.1.2.2.1 In-situ high temperature X-ray diffraction study on atmospheric plasma and detonation sprayed Ni-5wt%Al coatings

Thermal expansion and recrystallization characteristics of Ni-5wt%Al coatings deposited on IN718 using atmospheric plasma spraying and detonation spray methods were examined under in-situ HT-XRD in a controlled atmosphere (10^{-4} mbar) at different temperatures: 25 °C (Before heating), 950 °C, 1050 °C, 1150 °C, and the following conclusions were:

- (1) Ni-5wt%Al coating deposited by DSC, a kinetic energy-dominated process, was relatively dense, highly strain-hardened, and exhibited finer crystallite size.

While APS coating, a thermal energy-dominated process, showed high porosities and oxidized interlamellar. The γ -Ni (FCC) was the primary phase in APS and DSC Ni-5wt%Al coatings. However, APS coatings resulted in the formation of nickel oxide (NiO) as a minor phase due to the nature of the process.

- (2) Recrystallization and lattice strain release of APS and DSC coatings calculated from Williamson-Hall plots through UDM from the XPPA analysis are very much inter-correlated. The crystallite size of the as-deposited APS and DSC coating is 65.7 nm and 27.5 nm, respectively. The in-situ HT-XRD annealing increases crystallite size to 78.0 nm and 53.2 nm for APS and DSC, respectively. The DSC process leads to finer crystallite size. It helps to retain the feedstock characteristic, and, at the same time, the DSC was more stable as the crystallite size was relatively finer before and after heat treatment. The relatively low oxygen pick-up observed by the EDS after the heat treatment was evidence of thermal stability.
- (3) The precise evaluation of the thermal expansion of the thermal spray coatings with the substrates is realized using the in-situ HT-XRD in a controlled atmosphere. The CTE has been linear across the entire temperature range. At 1150 °C, the expansion coefficient of the APS Ni-5wt%Al coatings ($11.0 \times 10^{-6}/^{\circ}\text{C}$) is significantly lower than that of DSC ($17.4 \times 10^{-6}/^{\circ}\text{C}$) due to the presence of the NiO minor phase in APS coatings.
- (4) In-situ HT-XRD in a controlled atmosphere accomplished by the Williamson-Hall calculation route is a practical methodology for assessing the physio-thermal properties and microstructure evolution of as-deposited thermal spray coatings.

5.1.2.3 Effect of thermal expansion on the high-temperature wear resistance of Ni-20%Cr detonation spray coating on IN718 substrate

The high-temperature tribological properties of detonation sprayed Ni-20%Cr coating was studied, and the following conclusions were drawn:

1. The temperature-dependent material properties such as stress relieving, recrystallization, thermal expansion, and oxidation strongly influence the dry sliding wear resistance of detonation sprayed Ni-20%Cr coating.
2. The high-temperature wear resistance of the coating has been influenced by the stress relieving, recrystallization, and thermal expansion of overlay coatings, as examined by in-situ HT-XRD.
3. Thermal expansion of the Ni-20%Cr coating has been seen as a beneficial high-temperature material property that strongly influences the protective layer formation and load-bearing ability.
4. At 850 °C, the glazed oxide layer (Cr_2O_3 , NiO) formation is significant for friction and wear resistance because of its lubricious nature. The continuously intact layers produced by the tribo-induced oxidation justify the superior tribological characteristics over a wide operating temperature range, resulting in decreased friction and wear rate.

5.1.2.4 Dry sliding friction and wear behaviour of DSC sprayed Ni-based coatings with different compositions at elevated temperatures

Comparison tribological behaviour of detonation sprayed (DSC) Ni-based coatings with different compositions was studied, and the following conclusions were drawn:

1. DSC was used to deposit NiAl and NiCr thermal spray powders on Ni-based (IN718) substrates with a thickness of 250 ± 25 μm . Because of partial oxidation, Ni-based coatings are hard and adhere well to substrates.
2. Ni-20%Cr coatings have a brittle and coarser microstructure, high hardness, and self-healing properties at 25 °C, which makes them more prone to cracking and breaking during sliding or abrasive wear, resulting in high CoF and wear rates.

The wear processes include abrasive (micro-ploughing) and surface fatigue (Delamination).

3. The CoF and wear rate decrease at 850 °C due to temperature-dependent material properties such as recrystallization and tribo-oxidation. The wear mechanisms change to adhesion (material transfer) and Tribo-chemical reactions (tribo-oxidation), enhancing tribological characteristics.

Compared to Ni-20%Cr coatings, Ni-5%Al overlay coatings improve dry sliding friction and wear resistance in high-temperature sectors and enhance component lifespan in technical applications.

5.2 Recommendations for future work

The current work has provided significant insight into the wear mechanisms and operating the tribological behavior of Ni-based coatings at elevated temperatures, especially the formation of tribo-layers.

- Future work will focus on understanding their morphology and mechanical properties. Detailed studies will be conducted using scanning electron microscopy coupled with a focussed ion beam (FIB-SEM), transmission electron microscopy (TEM), and high-temperature nano-indentation.
- To investigate the effect of temperature-dependent properties on dry sliding friction and wear behaviour of coatings with varying sliding velocities, distance, and loads at elevated temperatures.
- It would be recommended to optimize the coating parameters further so that the (DSC) Ni-based coating can withstand higher temperatures, use the coating pins or ball-like geometry made up of similar materials, and employ suitable post-processing treatments.

REFERENCES

- Abhijith Vijay, V., Santhy, K., Sivakumar, G., and Rajasekaran, B. (2023). "Thermal expansion and microstructure evolution of atmospheric plasma sprayed NiCrAlY bond coat using in-situ high temperature X-ray diffraction." *Surf. Coatings Technol.*, 452, 129132.
- Andersson, J. O., Helander, T., Höglund, L., Shi, P., and Sundman, B. (2002). "ThermoCalc & DICTRA, computational tools for materials science." *Calphad Comput. Coupling Phase Diagrams Thermochem.*, 26(2), 273–312.
- Antonov, M., Hussainova, I., Veinthal, R., and Pirso, J. (2012). "Effect of temperature and load on three-body abrasion of cermets and steel." *Tribol. Int.*, 46(1), 261–268.
- Badisch, E., Katsich, C., Winkelmann, H., Franek, F., and Roy, M. (2010). "Wear behaviour of hardfaced Fe-Cr-C alloy and austenitic steel under 2-body and 3-body conditions at elevated temperature." *Tribol. Int.*, 43(7), 1234–1244.
- Bai, Y., Han, Z. H., Li, H. Q., Xu, C., Xu, Y. L., Wang, Z., Ding, C. H., and Yang, J. F. (2011). "High performance nanostructured ZrO₂ based thermal barrier coatings deposited by high efficiency supersonic plasma spraying." *Appl. Surf. Sci.*, 257(16), 7210–7216.
- Baicheng, Z., Xiaohua, L., Jiaming, B., Junfeng, G., Pan, W., Chen-nan, S., Muiling, N., Guojun, Q., and Jun, W. (2017). "Study of selective laser melting (SLM) Inconel 718 part surface improvement by electrochemical polishing." *Mater. Des.*, 116, 531–537.
- Bakshi, S. Das, Sinha, D., and Ghosh Chowdhury, S. (2018). "Anisotropic broadening of XRD peaks of α' -Fe: Williamson-Hall and Warren-Averbach analysis using full width at half maximum (FWHM) and integral breadth (IB)." *Mater. Charact.*, 142, 144–153.
- Balint, D. S., and Hutchinson, J. W. (2003). "Undulation instability of a compressed elastic film on a nonlinear creeping substrate." *Acta Mater.*, 51(13), 3965–3983.

- Bano, N., and Nganbe, M. (2013). "Modeling of thermal expansion coefficients of Ni-based superalloys using artificial neural network." *J. Mater. Eng. Perform.*, 22(4), 952–957.
- Barber, J. R. (1967). "The influence of thermal expansion on the friction and wear process." *Wear*, 10(2), 155–159.
- Bhushan B, Author, and Ko Pak Lim, Reviewer. (2003). "Introduction to Tribology." *Appl. Mech. Rev.*, 56(1), B6–B7.
- Biermann, H., Strehler, M., and Mughrabi, H. (1996). "High-temperature measurements of lattice parameters and internal stresses of a creep-deformed monocrystalline nickel-base superalloy." *Metall. Mater. Trans. A* 1996 274, 27(4), 1003–1014.
- Biju, V., Sugathan, N., Vrinda, V., and Salini, S. L. (2008). "Estimation of lattice strain in nanocrystalline silver from X-ray diffraction line broadening." *J. Mater. Sci.*, 43(4), 1175–1179.
- Bindu, P., and Thomas, S. (2014). "Estimation of lattice strain in ZnO nanoparticles: X-ray peak profile analysis." *J. Theor. Appl. Phys.*, 8(4), 123–134.
- Blau, P. J. (2010). "Elevated-temperature tribology of metallic materials." *Tribol. Int.*, 43(7), 1203–1208.
- Bochenek, K., and Basista, M. (2015). "Advances in processing of NiAl intermetallic alloys and composites for high temperature aerospace applications." *Prog. Aerosp. Sci.*, 79, 136–146.
- Bolelli, G., Candeli, A., Lusvarghi, L., Ravaux, A., Cazes, K., Denoirjean, A., Valette, S., Chazelas, C., Meillot, E., and Bianchi, L. (2015). "Tribology of NiCrAlY+Al₂O₃ composite coatings by plasma spraying with hybrid feeding of dry powder+suspension." *Wear*, 344–345, 69–85.

Bolelli, G., Vorkötter, C., Lusvarghi, L., Morelli, S., Testa, V., and Vaßen, R. (2020). “Performance of wear resistant MCrAlY coatings with oxide dispersion strengthening.” *Wear*, 444–445, 203116.

Cemal Kushan, M., Uzunonut, Y., Fehmi Diltemiz, S., Cevik Uzgur, S., and Diltemiz, F. (n.d.). “ALLVAC 718 Plus Superalloy for Aircraft Engine Applications Experimental investigation of ultrasonic assisted turning process View project Call for Book Chapters: Composite Laminates View project 4 ALLVAC 718 Plus™ Superalloy for Aircraft Engine Applicat.”

Chan, K. S., Pan, Y. M., and Lee, Y. Der. (2006). “Computation of Ni-Cr phase diagram via a combined first-principles quantum mechanical and CALPHAD approach.” *Metall. Mater. Trans. A Phys. Metall. Mater. Sci.*, 37(7), 2039–2050.

Chavana, N., Bhajantri F, V., and Jambagi, S. C. (2022). “Improvement in Slurry Erosion and Corrosion Resistance of Plasma-Sprayed Fly Ash Coatings for Marine Applications.” *ACS Omega*, 7(36), 32369–32382.

Cheng, X., Jiang, Z., Wei, D., Wu, H., and Jiang, L. (2019). “Adhesion , friction and wear analysis of a chromium oxide scale on a ferritic stainless steel.” *Wear*, 426–427(January), 1212–1221.

Chien, S. Y., and Cramer, M. S. (2019). “Pressure, temperature, and heat flux in high speed lubrication flows of pressurized gases.” *Tribol. Int.*, 129, 468–475.

Choudhury, M. S. H., Alam, M. S., Mizanul Islam, M., Soga, T., Shafiul Alam, M., and Islam, M. R. (2018). “Determining Crystallite Parameters of ZnO Nanoparticles Using Various Peak Profile Analysis.” *2018 Int. Conf. Innov. Sci. Eng. Technol. ICISSET 2018*, (October), 257–261.

Du, L., Huang, C., Zhang, W., Li, T., and Liu, W. (2011). “Preparation and wear performance of NiCr/Cr₃C₂–NiCr/hBN plasma sprayed composite coating.” *Surf. Coatings Technol.*, 205(12), 3722–3728.

- Evans, A. G., Mumm, D. R., Hutchinson, J. W., Meier, G. H., and Pettit, F. S. (2001). "Mechanisms controlling the durability of thermal barrier coatings." *Prog. Mater. Sci.*, 46(5), 505–553.
- Fernández, E., Cadenas, M., González, R., Navas, C., Fernández, R., and Damborenea, J. De. (2005). "Wear behaviour of laser clad NiCrBSi coating." *Wear*, 259(7–12), 870–875.
- Fillot, N., Iordanoff, I., and Berthier, Y. (2007). "Wear modeling and the third body concept." *Wear*, 262(7–8), 949–957.
- Fischer, A., Dudzinski, W., Gleising, B., and Stemmer, P. (2018). "Analyzing Mild- and Ultra-Mild Sliding Wear of Metallic Materials by Transmission Electron Microscopy." Springer International Publishing, 29–59.
- Fotovvati, B., Namdari, N., and Dehghanghadikolaei, A. (2019). "On coating techniques for surface protection: A review." *J. Manuf. Mater. Process.*, 3(1).
- Fritscher, K., Leyens, C., and Peters, M. (1995). "Development of a low-expansion bond coating for Ni-base superalloys." *Mater. Sci. Eng. A*, 190(1–2), 253–258.
- Gahr, K.-H. Zum. (1987). *Microstructure and wear of materials*. Elsevier.
- Gautam, R. K. S., Rao, U. S., and Tyagi, R. (2019). "High temperature tribological properties of Ni-based self-lubricating coatings deposited by atmospheric plasma spray." *Surf. Coatings Technol.*, 372, 390–398.
- Grigoriev, A. S., Shilko, E. V., Dmitriev, A. I., and Tarasov, S. Y. (2020). "Suppression of wear in dry sliding friction induced by negative thermal expansion." *Phys. Rev. E*, 102(4), 42801.
- Grzesik, W., Niesłony, P., Habrat, W., Sieniawski, J., and Laskowski, P. (2018). "Investigation of tool wear in the turning of Inconel 718 superalloy in terms of process performance and productivity enhancement." *Tribol. Int.*, 118, 337–346.

- Günen, A. (2020). “Properties and High Temperature Dry Sliding Wear Behavior of Boronized Inconel 718.” *Metall. Mater. Trans. A*, 51(2), 927–939.
- Habib, K. A., Cano, D. L., Alvaro, J. A. H., Serrano-Mira, J., Llopis, R., Moreno, D. L., and Mohammed, S. S. (2022). “Effects of thermal spraying technique on the remelting behavior of NiCrBSi coatings.” *Surf. Coatings Technol.*, 444, 128669.
- Hager, C. H., Hu, J., Muratore, C., Voevodin, A. A., and Grandhi, R. (2010). “The mechanisms of gross slip fretting wear on nickel oxide/Ti6Al4V mated surfaces.” *Wear*, 268(9–10), 1195–1204.
- Hager, C. H., Sanders, J., Sharma, S., Voevodin, A., and Segall, A. (2009). “The effect of temperature on gross slip fretting wear of cold-sprayed nickel coatings on Ti6Al4V interfaces.” *Tribol. Int.*, 42(3), 491–502.
- Hahn, E. J., and Kettleborough, C. F. (1968). “The effects of thermal expansion in infinitely wide slider bearings-free thermal expansion.” *J. Tribol.*, 90(1), 233–239.
- Hao, E., An, Y., Zhao, X., Zhou, H., and Chen, J. (2018). “NiCoCrAlYTa coatings on nickel-base superalloy substrate: Deposition by high velocity oxy-fuel spraying as well as investigation of mechanical properties and wear resistance in relation to heat-treatment duration.” *Appl. Surf. Sci.*, 462, 194–206.
- Hao, E., Zhao, X., An, Y., Deng, W., Zhou, H., and Chen, J. (2019). “The effect of pre-oxidation on microstructure, mechanical properties and high-temperature tribological behaviors of HVOF-sprayed NiCoCrAlYTa coating.” *Appl. Surf. Sci.*, 489, 187–197.
- Haynes, J. A., Pint, B. A., Porter, W. D., and Wright, I. G. (2004). “Comparison of thermal expansion and oxidation behavior of various high-temperature coating materials and superalloys.” *Mater. High Temp.*, 21(2), 87–94.
- Haynes, J. A., Pint, B. A., Porter, W. D., and Wright, I. G. (2014). “Materials at High Temperatures Comparison of thermal expansion and oxidation behavior of various high-temperature coating materials and superalloys.”

- Hazotte, A., Bellet, D., Ganghoffer, J. F., Denis, S., Bastie, P., and Simon, A. (1992). "On the contribution of internal mismatch stresses to the high-temperature broadening of gamma-ray diffraction peaks in a ni-based single crystal." *Philos. Mag. Lett.*, 66(4), 189–196.
- Holmberg, K., and Erdemir, A. (2017). "Influence of tribology on global energy consumption, costs and emissions." *Friction*, 5(3), 263–284.
- Hou, G., An, Y., Zhao, X., Zhou, H., and Chen, J. (2015). "Effect of alumina dispersion on oxidation behavior as well as friction and wear behavior of HVOF-sprayed CoCrAlYTaCSi coating at elevated temperature up to 1000 °C." *Acta Mater.*, 95, 164–175.
- Hsiao, W. T., Su, C. Y., Huang, T. S., and Liao, W. H. (2013). "Wear resistance and microstructural properties of Ni–Al/h-BN/WC–Co coatings deposited using plasma spraying." *Mater. Charact.*, 79, 84–92.
- Huang, C., Zou, B., Liu, Y., Zhang, S., Huang, C., and Li, S. (2016). "Study on friction characterization and wear-resistance properties of Si₃N₄ ceramic sliding against different high-temperature alloys." *Ceram. Int.*, 42(15), 17210–17221.
- Inman, I. A., Datta, P. K., Du, H. L., Burnell-Gray, J. S., Pierzgalski, S., and Luo, Q. (2005). "Studies of high temperature sliding wear of metallic dissimilar interfaces." *Tribol. Int.*, 38(9), 812–823.
- Inman, I. A., and Datta, P. S. (2008). "Development of a simple 'temperature versus sliding speed' wear map for the sliding wear behaviour of dissimilar metallic interfaces II." *Wear*, 265(11–12), 1592–1605.
- Jackson, R. W., Titus, M. S., Begley, M. R., and Pollock, T. M. (2016). "Thermal expansion behavior of new Co-based alloys and implications for coatings." *Surf. Coatings Technol.*, 289, 61–68.
- Jiang, J., Stott, F. H., and Stack, M. M. (1998). "The role of triboparticulates in dry sliding wear." *Tribol. Int.*, 31(5), 245–256.

Jones, L. C., and Llewellyn, R. J. (2009). "Sliding abrasion resistance assessment of metallic materials for elevated temperature mineral processing conditions." *Wear*, 267(11), 2010–2017.

Kala, V., Santhy, K., Sivakumar, G., and Rajasekaran, B. (2022). "Understanding the initial stage oxidation and microstructural evolution of detonation sprayed NiCoCrAlY bond coat using in-situ high-temperature X-ray diffraction." *Corros. Sci.*, 207, 110521.

Kamal, S., Jayaganthan, R., and Prakash, S. (2009). "High temperature oxidation studies of detonation-gun-sprayed Cr₃C₂-NiCr coating on Fe- and Ni-based superalloys in air under cyclic condition at 900 °C." *J. Alloys Compd.*, 472(1–2), 378–389.

Karaoglanli, A. C., Caliskan, H., Gok, M. S., Erdogan, A., Turk, A., Caliskan, H., Gok, M. S., Erdogan, A., Turk, A., Karaoglanli, A. C., Caliskan, H., Gok, M. S., Erdogan, A., and Turk, A. (2014). "A Comparative Study of the Microabrasion Wear Behavior of CoNiCrAlY Coatings Fabricated by APS , HVOF , and CGDS Techniques A Comparative Study of the Microabrasion Wear Behavior of CoNiCrAlY Coatings Fabricated by APS , HVOF , and CGDS Techniques." 2004.

Karaoglanli, A. C., Oge, M., Doleker, K. M., and Hotamis, M. (2017). "Comparison of tribological properties of HVOF sprayed coatings with different composition." *Surf. Coatings Technol.*, 318, 299–308.

Karunaratne, M. S. A., Kyaw, S., Jones, A., Morrell, R., and Thomson, R. C. (2016). "Modelling the coefficient of thermal expansion in Ni-based superalloys and bond coatings." *J. Mater. Sci.*, 51(9), 4213–4226.

Kato, H., and Komai, K. (2007). "Tribofilm formation and mild wear by tribo-sintering of nanometer-sized oxide particles on rubbing steel surfaces." *Wear*, 262(1–2), 36–41.

Kaushal, G., Singh, H., and Prakash, S. (2012). "Performance of detonation gun-sprayed Ni-20Cr coating on ASTM A213 TP347H steel in a boiler environment." *J. Therm. Spray Technol.*, 21(5), 975–986.

- KC, L. (1996). "Friction, wear, lubrication: A textbook in tribology." *Ann Arbor CRC Press. Inc, Boca Rat.*
- Khorsand Zak, A., Abd. Majid, W. H., Abrishami, M. E., and Yousefi, R. (2011). "X-ray analysis of ZnO nanoparticles by Williamson–Hall and size–strain plot methods." *Solid State Sci.*, 13(1), 251–256.
- Kim, J. H., Kim, B. K., Kim, D. I., Choi, P. P., Raabe, D., and Yi, K. W. (2015). "The role of grain boundaries in the initial oxidation behavior of austenitic stainless steel containing alloyed Cu at 700°C for advanced thermal power plant applications." *Corros. Sci.*, 96, 52–66.
- Kiryç, M., Kurumlu, D., Eggeler, G., Vaßen, R., and Marginean, G. (2023). "On the sliding wear and solid particle erosion behaviour of HVOF-sprayed CoNiCrAlY coatings and NiCrCoTi substrates in dependence of the oxidation dwell time at 900 °C." *Surf. Coatings Technol.*, 453, 129137.
- Kumar, D., Murtaza, Q., and Singh, R. C. (2016). "Sliding wear behavior of aluminum alloy coating prepared by two-wire electric arc spray process." *Int. J. Adv. Manuf. Technol.*, 85(1–4), 237–252.
- Li, B., Jia, J., Han, M., Gao, Y., Wang, W., and Li, C. (2017). "Microstructure, mechanical and tribological properties of plasma-sprayed NiCrAlY-Mo-Ag coatings from conventional and nanostructured powders." *Surf. Coatings Technol.*, 324, 552–559.
- Li, J., Lu, Y., Zhang, H., and Xin, L. (2015). "Effect of grain size and hardness on fretting wear behavior of Inconel 600 alloys." *Tribol. Int.*, 81, 215–222.
- Li, R., He, D. Y., Zhou, Z., Wang, Z. J., and Song, X. Y. (2014). "Wear and high temperature oxidation behaviour of wire arc sprayed iron based coatings." *Surf. Eng.*, 30(11), 784–790.

- Li, W., Huang, C., Yu, M., Liu, D., Feng, Y., and Liao, H. (2014). “Investigation of high temperature oxidation behavior and tribological performance on cold sprayed nickel–alumina composite coating.” *Surf. Coatings Technol.*, 239, 95–101.
- Liu, J., Jiang, D., Ma, Z., Zhang, H., Kang, G., Chen, Y., Yu, K., Ren, Y., Liu, Y., Ge, L., and Cui, L. (2022). “An in-situ study of low thermal expansion and internal stress evolution in FeMn alloys.” *Mater. Charact.*, 194, 112342.
- Liu, L., Zhou, M., Jin, L., Li, L., Mo, Y., Su, G., Li, X., Zhu, H., and Tian, Y. (2019). “Recent advances in friction and lubrication of graphene and other 2D materials: Mechanisms and applications.” *Friction*, 7(3), 199–216.
- Liu, S. H., Trelles, J. P., Li, C. J., Li, C. X., and Guo, H. B. (2022). “A review and progress of multiphase flows in atmospheric and low pressure plasma spray advanced coating.” *Mater. Today Phys.*, 27, 100832.
- Lubell, D., DellaCorte, C., and Stanford, M. (2008). “Test Evolution and Oil-Free Engine Experience of a High Temperature Foil Air Bearing Coating.” *Proc. ASME Turbo Expo*, 5 PART B, 1245–1249.
- Mahesh, R. A., Jayaganthan, R., and Prakash, S. (2008). “Oxidation behavior of HVOF sprayed Ni–5Al coatings deposited on Ni- and Fe-based superalloys under cyclic condition.” *Mater. Sci. Eng. A*, 475(1–2), 327–335.
- Maniammal, K., Madhu, G., and Biju, V. (2017). “X-ray diffraction line profile analysis of nanostructured nickel oxide: Shape factor and convolution of crystallite size and microstrain contributions.” *Phys. E Low-Dimensional Syst. Nanostructures*, 85, 214–222.
- Medabalimi, S. R., Ramesh, M. R., and Kadoli, R. (2021). “Developing partially oxidized NiCr coatings using the combined flame spray and plasma spray process for improved wear behaviour at high temperature.” *Wear*, 478–479, 203885.
- Miller, C., Field, R., and Kaufman, M. (2018). “Phase stability of γ' -Ni₂Cr and α -Cr in the Ni-Cr binary.” *Acta Mater.*, 157, 1–10.

- Molins, R., Normand, B., Rannou, G., Hannoyer, B., and Liao, H. (2003). "Interlamellar boundary characterization in Ni-based alloy thermally sprayed coating." *Mater. Sci. Eng. A*, 351(1–2), 325–333.
- Mote, V., Purushotham, Y., and Dole, B. (2012). "Williamson-Hall analysis in estimation of lattice strain in nanometer-sized ZnO particles." *J. Theor. Appl. Phys.*, 6(1), 2–9.
- Munagala, V. N. V., Torgerson, T. B., Scharf, T. W., and Chromik, R. R. (2019). "High temperature friction and wear behavior of cold-sprayed Ti6Al4V and Ti6Al4V-TiC composite coatings." *Wear*, 426–427, 357–369.
- Mussa, A., Krakhmalev, P., and Bergström, J. (2020). "Sliding wear and fatigue cracking damage mechanisms in reciprocal and unidirectional sliding of high-strength steels in dry contact." *Wear*, 444–445, 203119.
- Niu, P.-F., and Tian, B.-L. (2018). "Wear Compensation Model Based on the Theory of Archard and Definite Integral Method." *Math. Probl. Eng.*, 2018, 1–14.
- Novak, R., and Polcar, T. (2014). "Tribological analysis of thin films by pin-on-disc: Evaluation of friction and wear measurement uncertainty." *Tribol. Int.*, 74, 154–163.
- O'Flynn, J., Whitman, C. A., and Corbin, S. F. (2020). "Thermal property measurements of metal injection moulded Inconel 625 and Inconel 718 using combined thermal analysis techniques." *Powder Metall.*, 63(4), 277–287.
- Parthasarathi, N. L., Duraiselvam, M., and Borah, U. (2012). "Effect of plasma spraying parameter on wear resistance of NiCrBSiCFe plasma coatings on austenitic stainless steel at elevated temperatures at various loads." *Mater. Des.*, 36, 141–151.
- Pereira, J., Zambrano, J., Licausi, M., Tobar, M., and Amigó, V. (2015). "Tribology and high temperature friction wear behavior of MCrAlY laser cladding coatings on stainless steel." *Wear*, 330–331, 280–287.

Pham, S. T., Tieu, A. K., Wan, S., Hao, J., Zhu, H., Nguyen, H. H., and Mitchell, D. R. G. (2020). "Oxidative and Frictional Behavior of a Binary Sodium Borate-Silicate Composite in High-Temperature Lubricant Applications." *Ind. Eng. Chem. Res.*, 59(7), 2921–2933.

Pollock, T. M., and Tin, S. (2006). "Nickel-based superalloys for advanced turbine engines: Chemistry, microstructure, and properties." *J. Propuls. Power*, American Institute of Aeronautics and Astronautics Inc.

Purushotham, N., Parthasarathi, N. L., Babu, P. S., Sivakumar, G., and Rajasekaran, B. (2023). "Effect of thermal expansion on the high temperature wear resistance of Ni-20%Cr detonation spray coating on IN718 substrate." *Surf. Coatings Technol.*, 462, 129490.

Purushotham, N., Rajasekaran, B., Parthasarathi, N. L., Praveen, K., and Sivakumar, G. (2022). "Sliding wear behaviour of Ni-5 %Al coating deposited by detonation spray on IN718." *Mater. Today Proc.*, 65, 3741–3747.

Radil, K., Transactions, C. D.-T., and 2017, undefined. (2016). "The performance of PS400 subjected to sliding contact at temperatures from 260 to 927 C." *Taylor Fr.*, 60(6), 957–964.

Radu, I., and Li, D. Y. (2007). "The wear performance of yttrium-modified Stellite 712 at elevated temperatures." *Tribol. Int.*, 40(2), 254–265.

Rajasekaran, B., Raman, S. G. S., Joshi, S. V., and Sundararajan, G. (2008). "Performance of plasma sprayed and detonation gun sprayed Cu–Ni–In coatings on Ti–6Al–4V under plain fatigue and fretting fatigue loading." *Mater. Sci. Eng. A*, 479(1–2), 83–92.

Rajesh Kumar, B., and Hymavathi, B. (2017). "X-ray peak profile analysis of solid-state sintered alumina doped zinc oxide ceramics by Williamson–Hall and size-strain plot methods." *Integr. Med. Res.*, 5, 94–103.

- Raju, S., Sivasubramanian, K., Divakar, R., Panneerselvam, G., Banerjee, A., Mohandas, E., and Antony, M. P. (2004). "Thermal expansion studies on Inconel-600® by high temperature X-ray diffraction." *J. Nucl. Mater.*, 325(1), 18–25.
- Ramesh, C. S., Seshadri, S. K., and IYER, K. J. L. (1991). "A survey of aspects of wear of metals." *Indian J. Technol.*, 29(4), 179–185.
- Rong, T., and Gu, D. (2016). "Formation of novel graded interface and its function on mechanical properties of WC1-x reinforced Inconel 718 composites processed by selective laser melting." *J. Alloys Compd.*, 680, 333–342.
- Rosenberg, Y., Machavariani, S., Voronel, A., Garber, S., Rubshtein, A., Frenkel, A. I., and Stern, E. A. (2000). *Strain energy density in the x-ray powder diffraction from mixed crystals and alloys. J. Phys. Condens. Matter.*
- Roy, M. (2018). "Approaches to enhance elevated temperature erosion resistance of Ni-base superalloys." <https://doi.org/10.1080/09603409.2018.1482077>, 36(2), 142–156.
- Roy, M., Pauschitz, A., Wernisch, J., and Franek, F. (2004). "Effect of mating surface on the high temperature wear of 253 MA alloy." *Mater. Corros.*, 55(4), 259–273.
- Rynio, C., Hattendorf, H., Klöwer, J., and Eggeler, G. (2014). "The evolution of tribolayers during high temperature sliding wear." *Wear*, 315(1–2), 1–10.
- Sadeghimeresht, E., Markocsan, N., and Nylén, P. (2016). "A Comparative Study on Ni-Based Coatings Prepared by HVOF, HVOF, and APS Methods for Corrosion Protection Applications." *J. Therm. Spray Technol.*, 25(8), 1604–1616.
- Saladi, S., Menghani, J., and Prakash, S. (2014). "A Study on the Cyclic Oxidation Behavior of Detonation-Gun-Sprayed Ni-5Al Coatings on Inconel-718 at 900 °C." *J. Mater. Eng. Perform.*, 23(12), 4394–4403.
- Sampath, S., Jiang, X. Y., Matejicek, J., Prchlik, L., Kulkarni, A., and Vaidya, A. (2004). "Role of thermal spray processing method on the microstructure, residual stress and properties of coatings: an integrated study for Ni–5 wt.%Al bond coats." *Mater. Sci. Eng. A*, 364(1–2), 216–231.

- Schilke, P. W. (2004). "Advanced Gas Turbine Materials and Coatings." *Gen. Electr. Company.*, 1–30.
- Selvakumar, N., and Barshilia, H. C. (2012). "Review of physical vapor deposited (PVD) spectrally selective coatings for mid- and high-temperature solar thermal applications." *Sol. Energy Mater. Sol. Cells*, 98, 1–23.
- Shen, Z., Liu, G., Zhang, R., Dai, J., He, L., and Mu, R. (2022). "Thermal property and failure behavior of LaSmZrO thermal barrier coatings by EB-PVD." *iScience*, 25(4), 104106.
- Shi, P., Wan, S., Yi, G., Sun, H., Yu, Y., Xie, E., Wang, Q., Shen, S. Z., and Alam, N. (2020). "TiO₂–ZnO/Ni–5wt.%Al composite coatings on GH4169 superalloys by atmospheric plasma spray techniques and their elevated-temperature tribological behavior." *Ceram. Int.*, 46(9), 13527–13538.
- Shi, P., Wang, W., Wan, S., Gao, Q., Sun, H., Feng, X., Yi, G., Xie, E., and Wang, Q. (2021). "Tribological performance and high temperature oxidation behaviour of thermal sprayed Ni- and NiCrAlY-based composite coatings." *Surf. Coatings Technol.*, 405, 126615.
- Singh, L., Chawla, V., and Grewal, J. S. (2012). *A Review on Detonation Gun Sprayed Coatings. J. Miner. Mater. Charact. Eng.*
- Standard, A. (2000). "Standard test method for wear testing with a pin-on-disk apparatus." *Annu. B. ASTM Stand. G99*, 5(3).
- Stott, F. H. (2002). "High-temperature sliding wear of metals." *Tribol. Int.*, 35(8), 489–495.
- Stott, F. H., Lin, D. S., and Wood, G. C. (1973). "The structure and mechanism of formation of the 'glaze' oxide layers produced on nickel-based alloys during wear at high temperatures." *Corros. Sci.*, 13(6), 449–469.
- Stott, F. H., and Wood, G. C. (1978). "The influence of oxides on the friction and wear of alloys." *Tribol. Int.*, 11(4), 211–218.

Straffelini, G., Trabucco, D., and Molinari, A. (2001). “Oxidative wear of heat-treated steels.” *Wear*, 250(1–12), 485–491.

Sun, H., Yi, G., Wan, S., Shi, P., Yang, J., Pham, S. T., Tieu, A. K., and Ta, T. D. (2021). “Effect of adding soft Bi₂O₃ on structural modification and tribological regulation of Ni-5 wt% Al composite coating in wide temperatures range.” *Surf. Coatings Technol.*, 405(October 2020), 126517.

Sundararajan, G., Prasad, K. U. M., Rao, D. S., and Joshi, S. V. (1998). “A Comparative Study of Tribological Behavior of Plasma and D-Gun Sprayed Coatings under Different Wear Modes.” *J. Mater. Eng. Perform.*, 7(3), 343–351.

Sundaresan, C., Rajasekaran, B., Varalakshmi, S., Santhy, K., Rao, D. S., and Sivakumar, G. (2021). “Comparative hot corrosion performance of APS and Detonation sprayed CoCrAlY, NiCoCrAlY and NiCr coatings on T91 boiler steel.” *Corros. Sci.*, 189, 109556.

Szala, M., Walczak, M., Łatka, L., Gancarczyk, K., and Özkan, D. (2020). “Cavitation Erosion and Sliding Wear of MCrAlY and NiCrMo Coatings Deposited by HVOF Thermal Spraying.” *Adv. Mater. Sci.*, 20(2), 26–38.

Tang, Y., and Xu, Z. (2018). “The electrochemical dissolution characteristics of GH4169 nickel base super alloy in the condition of electrochemical machining.” *Int. J. Electrochem. Sci.*, 13(1), 1105–1119.

Texier, D., Monceau, D., Hervier, Z., and Andrieu, E. (2016). “Effect of interdiffusion on mechanical and thermal expansion properties at high temperature of a MCrAlY coated Ni-based superalloy.” *Surf. Coatings Technol.*, 307, 81–90.

Thandavan, T. M. K., Gani, S. M. A., Wong, C. S., and Nor, R. M. (2015). “Evaluation of Williamson–Hall Strain and Stress Distribution in ZnO Nanowires Prepared Using Aliphatic Alcohol.” *J. Nondestruct. Eval.*, 34(2), 1–9.

Toby, B. H. (2006). “ R factors in Rietveld analysis: How good is good enough? .” *Powder Diffr.*, 21(1), 67–70.

Torgerson, T. B., Harris, M. D., Alidokht, S. A., Scharf, T. W., Aouadi, S. M., Chromik, R. R., Zabinski, J. S., and Voevodin, A. A. (2018). "Room and elevated temperature sliding wear behavior of cold sprayed Ni-WC composite coatings." *Surf. Coatings Technol.*, 350, 136–145.

Torres, H., Varga, M., Widder, F., Cihak-Bayr, U., Viskovic, O., and Rodríguez Ripoll, M. (2016). "Experimental simulation of high temperature sliding contact of hot rolled steel." *Tribol. Int.*, 93, 745–754.

Trosch, T., Strößner, J., Völkl, R., and Glatzel, U. (2016). "Microstructure and mechanical properties of selective laser melted Inconel 718 compared to forging and casting." *Mater. Lett.*, 164, 428–431.

Ustinovshikov, Y. (2012). "Phase transformations in alloys of the Ni-Cr system." *J. Alloys Compd.*, 543, 227–232.

Varga, M., Rojacz, H., Winkelmann, H., Mayer, H., and Badisch, E. (2013). "Wear reducing effects and temperature dependence of tribolayer formation in harsh environment." *Tribol. Int.*, 65, 190–199.

Vaßen, R., Kaßner, H., Stuke, A., Hauler, F., Hathiramani, D., and Stöver, D. (2008). "Advanced thermal spray technologies for applications in energy systems." *Surf. Coatings Technol.*, 202(18), 4432–4437.

Wang, J. X., Liu, J. S., Zhang, L. Y., Sun, J. F., and Wang, Z. P. (2014). "Microstructure and mechanical properties of twin-wire arc sprayed Ni-Al composite coatings on 6061-T6 aluminum alloy sheet." *Int. J. Miner. Metall. Mater.* 2014 215, 21(5), 469–478.

Wang, L., and Li, D. Y. (2003). "Effects of yttrium on microstructure, mechanical properties and high-temperature wear behavior of cast Stellite 6 alloy." *Wear*, 255(1–6), 535–544.

Wang, T. G., Liu, Y., Wang, Q., Gong, J., Sun, C., and Kim, K. H. (2012). "Influence of residual stress on the adhesive behavior of detonation gun sprayed WC-Co coatings." *Curr. Appl. Phys.*, 12(SUPPL. 2), S59–S62.

- Wang, X., Feng, X., Lu, C., Yi, G., Jia, J., and Li, H. (2018). “Mechanical and tribological properties of plasma sprayed NiAl composite coatings with addition of nanostructured TiO₂/Bi₂O₃.” *Surf. Coatings Technol.*, 349, 157–165.
- Watson, M., and Marshall, M. (2018). “Wear mechanisms at the blade tip seal interface.” *Wear*, 404–405, 176–193.
- Winkelmann, H., Badisch, E., Varga, M., and Danninger, H. (2010). “Wear mechanisms at high temperatures. part 3: Changes of the wear mechanism in the continuous impact abrasion test with increasing testing temperature.” *Tribol. Lett.*, 37(2), 419–429.
- Xian, L., Zhao, H., Xian, G., Wang, C., and He, H. (2021). “High temperature protection of NiCrAlSiY/Al–Cr–O coatings deposited by arc ion plating on nickel-based superalloy.” *Vacuum*, 188(February), 110152.
- Yamazaki, Y., Morikawa, M., Hamaguchi, T., Habu, Y., Ohide, Y., and Takagi, K. (2022). “Relationship between the mechanical properties and structure of a suspension plasma-sprayed thermal barrier coating with columnar microstructure.” *Surf. Coatings Technol.*, 439, 128430.
- Ye, F., Lou, Z., Wang, Y., and Liu, W. (2022). “Wear mechanism of Ag as solid lubricant for wide range temperature application in micro-beam plasma cladded Ni60 coatings.” *Tribol. Int.*, 167, 107402.
- Zakeri, A. ;, Bahmani, E. ;, Ramazani, A., Zakeri, A., Bahmani, E., and Ramazani, A. (2022). “A Review on the Enhancement of Mechanical and Tribological Properties of MCrAlY Coatings Reinforced by Dispersed Micro and Nanoparticles.” *Energies 2022, Vol. 15, Page 1914*, 15(5), 1914.
- Zhang, Z., Lu, X., and Luo, J. (2007). “Tribological properties of rare earth oxide added Cr₃C₂–NiCr coatings.” *Appl. Surf. Sci.*, 253(9), 4377–4385.

Zhen, J., Li, F., Zhu, S., Ma, J., Qiao, Z., Liu, W., and Yang, J. (2014). “Friction and wear behavior of nickel-alloy-based high temperature self-lubricating composites against Si₃N₄ and Inconel 718.” *Tribol. Int.*, 75, 1–9.

Zhou, X., Xu, Z., Mu, R., He, L., Huang, G., and Cao, X. (2014). “Thermal barrier coatings with a double-layer bond coat on Ni₃Al based single-crystal superalloy.” *J. Alloys Compd.*, 591, 41–51.

Zmitrowicz, A. (1987). “A thermodynamical model of contact, friction and wear: II constitutive equations for materials and linearized theories.” *Wear*, 114(2), 169–197.

LIST OF PUBLICATIONS

N. Purushotham, N.L. Parthasarathi, P. Suresh Babu, G. Sivakumar, B. Rajasekaran, **Effect of thermal expansion on the high temperature wear resistance of Ni-20%Cr detonation spray coating on IN718 substrate**, Surface and Coatings Technology, Volume 462, 2023, 129490, ISSN 0257-8972, <https://doi.org/10.1016/j.surfcoat.2023.129490>.

Purushotham N. Parthasarathi N.L, Suresh Babu P, Sivakumar G, Rajasekaran B, **High temperature sliding wear behavior of detonation sprayed Ni-5wt%Al coating**, Wear, Volumes 530–531, 2023, 205030, ISSN 0043-1648, <https://doi.org/10.1016/j.wear.2023.205030>.

Purushotham, N., Santhy, K., Suresh Babu, P. *et al.* **In Situ High-Temperature X-ray Diffraction Study on Atmospheric Plasma and Detonation Sprayed Ni-5 wt.%Al Coatings.** *J Therm Spray Tech* **32**, 2091–2103 (2023). <https://doi.org/10.1007/s11666-023-01627-w>

N. Purushotham, B. Rajasekaran, N.L. Parthasarathi, K. Praveen, G. Sivakumar, **sliding wear behaviour of Ni-5 %Al coating deposited by detonation spray on IN718**, Materials Today: Proceedings, Volume 65, Part 8, 2022, Pages 3741-3747, ISSN 2214-7853, <https://doi.org/10.1016/j.matpr.2022.06.425>.

BIO-DATA

1. Name : N. PURUSHOTHAM
2. Father's Name : N. SANJANNA
3. Date of Birth : 10th June 1994
4. Nationality : Indian
5. Marital Status : Unmarried
6. Address : Department of Metallurgical and Materials Engg.
National Institute of Technology Karnataka
Surathkal, PO Srinivasnagar 575 025
Karnataka, India.
7. Mobile Number : +91 7981753973
8. E-mail id. : *npnaidu99@gmail.com*
9. Educational Qualification :

Qualification	University/Board	Year of Passing
Ph.D. (Metallurgical and Materials Engineering)	National Institute of Technology Karnataka	2023
M.Tech. (Metallurgical and Materials Engineering)	National Institute of Technology Jamshedpur	2019
B.Tech. (Mechanical Engineering)	Jawaharlal Nehru Technological University, Hyderabad	2016